# Microscopic Theory of Photon-Correlation Spectroscopy in Strong-Coupling Semiconductors

Dissertation
zur
Erlangung des Doktorgrades
der Naturwissenschaften
(Dr. rer. nat.)


dem Fachbereich Physik
der Philipps-Universität Marburg
vorgelegt


von
**Lukas Schneebeli**

aus Marburg

Marburg(Lahn), 2009

# Zusammenfassung

*Inhaltsangabe und Zielrichtung der Arbeit*

Während viele quantenoptische Phänomene in kalten Atomgasen gut etabliert sind, wie der Einzelphotonenemission ('photon antibunching') [1], dem gequetschten Licht ('squeezed light') [2], der Bose-Einstein Kondensation [3], und der Teleportation [4], stehen die quantenoptischen Untersuchungen in Halbleitern erst noch am Anfang [5]. Die faszinierenden Resultate, die man in den atomaren Systemen erzielt hat, inspirieren die Physiker, auch ähnliche quantenoptische Effekte in Halbleitersystemen nachzuweisen. Im Gegensatz zur Quantenoptik mit verdünnten Atomgasen hat man es im Halbleiter mit einem komplizierten Vielteilchenproblem zu tun, welches durch die Coulombwechselwirkung zwischen den Elektronen und Löchern und durch die Kopplung mit der Umgebung des Halbleitermaterials dominiert wird. Dies ist der Grund dafür, dass der experimentelle Nachweis ähnlicher quantenoptischer Effekte in Halbleitern sehr schwierig ist. Jedoch gibt es schon Experimente welche nichtklassische Effekte in Halbleitern nachgewiesen haben. Speziell hat man mit Halbleiter Quantenpunkten die Einphotonemission [6–8] und die Erzeugung von polarisations-verschränkten Photonenpaaren [9–11] gemessen. In der Tat stellen atomare- und Halbleiterquantenpunkt-Systeme innerhalb einer Mikrokavität geeignete Plattformen dar, in denen man systematische quantenoptische Untersuchungen [12, 13] als auch Pionierarbeit hinsichtlich Anwendungen in der Quanteninformation [14, 15] durchführen kann.

Ein anderes interessantes Gebiet ist das der starken Licht-Materie Kopplung, in welcher die Licht-Materie stärker ist als die Dekohärenzrate des Atoms oder des Quantenpunkts und der Kavität. Dies resultiert in eine reversible Dynamik zwischen Licht und Materieanregung. In diesem Regime der starken Licht-Materie Kopplung ist die Jaynes-Cummings Leiter vorhergesagt [16] und zeigt eine photonenzahlabhängige Aufspaltung der neuen Polariton-Zustände. Obwohl der halbklassische Effekt der Vakuum-Rabi-Aufspaltung schon experimentell beobachtet wurde in Quantenpunkten [17–20], steht der eindeutige Nachweis der quantenmechanischen Jaynes-Cummings Aufspaltung [5, 16, 21] hauptsächlich wegen Dephasierungseffekten noch aus. Es ist klar, dass die Beobachtung der Jaynes-Cummings Leiter in Quantenpunkten ein bedeutender Schritt wäre auf dem Gebiet der Quantenoptik in Halbleitern. Hier ist auch wieder zu erwähnen, dass die Anstrengungen in Quantenpunkten durch die atomaren Systeme vorangetrieben werden, in denen man nicht nur die Vakuum-Rabi-Aufspaltung [22, 23], sondern auch den Zwei-Photonen Polariton ('second rung') [24–26] gemessen hat, z.B. mittels der direkten Spektroskopie [25] und der Photonenkorrelationsmessungen [26].

Um besser mit dem Hauptthema dieser Dissertation vertraut zu werden, werden wir im Folgenden kurz die grundlegenden Resultate des Jaynes-Cummings Modells [16] zusammenfassen. Dieses Modell beschreibt die Kopplung zwischen einer einzigen Lichtmode einer Kavität und einem Zwei-Niveau System. Dazu ist in Fig. 0.1 die resultierende Jaynes-Cummings Leiter des Regimes der starken Kopplung abgebildet. Ohne Licht-
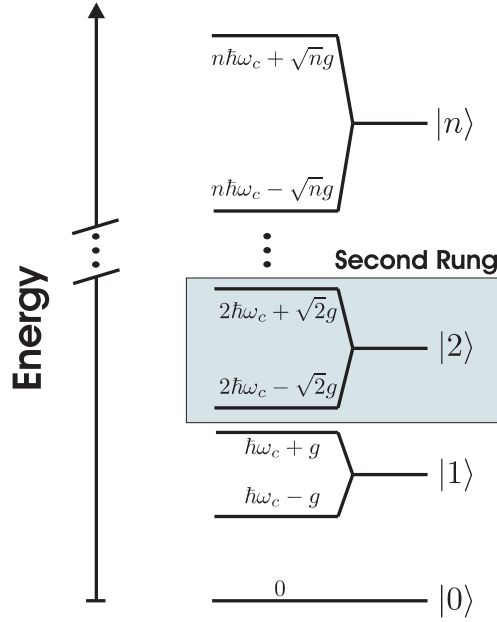
Figure 0.1: Jaynes-Cummings Leiter. Die Quantisierung des Lichtfeldes führt zu Fock-Zustände $|n\rangle$ welche durch die Licht-Materie Wechselwirkung $g$ aufspalten. Jeder Zustand $|n\rangle$ zeigt eine individuelle Kopplung $g_n = \sqrt{n}g$. In dieser Dissertation konzentrieren wir uns auf den Zwei-Photonen Polariton-Zustand ('second rung'), der durch die Schraffierung angedeutet ist.

Materie Wechselwirkung erhalten wir, wie in Fig. 0.1 dargestellt, nur die Fock-Zustände der Kavitätsmode, welche durch $|n\rangle$ mit $n = 0, 1, 2, \ldots$ beschrieben werden. Wenn wir nun die Licht-Materie Wechselwirkung einschalten, so spalten diese Zustände auf und formen neue, gekoppelte Zustände $|n\rangle|{\rm down}\rangle \pm |n-1\rangle|{\rm up}\rangle$, mit nicht angeregtem (angeregtem) Zwei-Niveau System $|{\rm down}\rangle$ ($|{\rm up}\rangle$). In der Abbildung Fig. 0.1 sehen wir deshalb, dass der Grundzustand unverändert bleibt, während die höherliegenden Leitersprossen eine Aufspaltung zeigen, die von der Photonenzahl wie $2\sqrt{n}g$ abhängt. Da die höherliegenden Leitersprossen von $n$, welches proportional zur Lichtfeldintensität ist, abhängen, betreten wir das Regime der nichtlinearen Optik, in der, vereinfacht gesprochen, die Anwesenheit oder Abwesenheit eines einzelnen Photons dramatische Auswirkungen auf den Systemzustand haben kann [5]. In dieser Dissertation befassen wir uns im Wesentlichen mit dem Zwei-Photonen Polariton, der durch die Schraffierung hervorgehoben ist. Wir betonen, dass nur eine voll quantenmechanische Theorie die Existenz des Zwei-Photonen Polaritons der Jaynes-Cummings Leiter erklären kann. In einer halbklassischen Theorie, welche nur die Materie quantisiert, nicht aber das Licht welches klassisch behandelt wird, kann man den Zwei-Photonen Polariton nicht erklären. Deswegen ist der experimentelle Nachweis des Zwei-Photonen Polaritons eine eindeutige Signatur des quantenmechanischen, starken Kopplungs-Regimes.

In dieser Dissertation verwenden wir extensiv die so genannte Cluster Entwicklungsmethode [27–29]. Diese Methode wurde schon erfolgreich in der Untersuchung verschiedenster
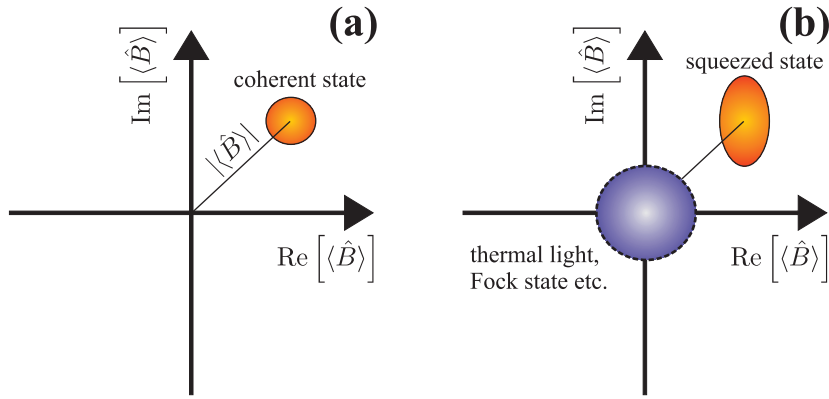
Figure 0.2: Phasenraum-Darstellung einiger Lichtfelder. (a) Klassische Optik welche anhand des kohärenten Zustandes ('coherent state') verdeutlicht wird. Hier spielen Amplitude und Phase die wesentliche Rolle. (b) Quantenoptik. Abgebildete Beispiele sind gequetschter Zustand ('squeezed state'), Fock-Zustand ('Fock state'), und thermisches Licht ('thermal light'), welche alle eine nicht verschwindende Quantenfluktuation aufweisen.

Vielteilchen- und quantenoptischen Systemen eingesetzt [30–33], wie der Exzitonbildung in Halbleiter Heterostrukturen [34], der konsistenten Beschreibung der Wechselwirkung zwischen Licht und Elektron-Loch Anregungen in Halbleiter Nanostrukturen [28, 35], und der Quasiteilchen- und quantenoptischen Spektroskopie zur direkten Kontrolle und Bildung von Exzitonenpopulation [36, 37]. Während eine Lösung der Dichtematrix für generische Multimoden- und Vielteilchen-Systeme sehr schwierig, wenn nicht gar unmöglich ist, stellt doch die Clusterentwicklung eine geeignete Methode dar, um konsistente Näherungslösungen zu entwickeln, welche systematisch verbessert werden können. Diese Näherungen sind meistens sehr genau, da wir oft nur an einer Teilmenge aller Erwartungswerte interessiert sind, die das System gut beschreiben.

Es gibt auch alternative Methoden, um Vielteilcheneffekte zu beschreiben, wie z.B. die Green-Funktions Methode [38], die Dichtefunktionaltheorie [39], und Monte-Carlo Methoden [40]. Für jeden Problemfall muß man die geeignete Methode wählen. Wir entscheiden uns für die Clusterentwicklung, da diese eine nützliche Methode darstellt, mit der man die Emissionseigenschaften eines Materialsystems berechnen kann. Zudem bietet die Cluster Entwicklungsmethode auch einen ansprechenden Formalismus, mit dem man die wesentlichen Mechanismen eines gegebenen Phänomens herausarbeiten kann.

Mit Hilfe dieser Theorie können wir das Lichtfeld und die Materialanregung auf der gleichen Näherungsstufe lösen, was zu einer selbstkonsistenten Theorie führt. Die Theorie ist auch flexibel, um verschiedene Lichtfelder zu beschreiben. Das bedeutet, dass wir klassische als auch quantenmechanische Lichtfelder beschreiben können. Um den Unterschied zwischen der klassischen Optik und der Quantenoptik zu wiederholen, ist in Fig. 0.2 die Phasenraum-Darstellung einiger einmodigen Lichtfelder dargestellt. Genauer ausgedrückt ist hier ein Schema der Wignerfunktion [41, 42] als Contour-

Graphik skizziert. Das Symbol $\hat{B}$ bedeutet hier der bosonische Photonenoperator. Die Abbildung 0.2(a) demonstriert das Regime der klassischen Optik und zeigt als Beispiel die Phasenraumverteilung des kohärenten Zustands. Der kohärente Zustand ist ein klassisches Lichtfeld, mit einer gut definierbaren Phase, niedriger Fluktuation in der Photonenzahl, und beschreibt in guter Näherung einen Laser oberhalb der Laserschwelle. Die Abbildung 0.2(a) zeigt, dass das kohärente Lichtfeld vollständig durch Amplitude $|\langle\hat{B}\rangle|$ und Phase $\langle\hat{B}\rangle/|\langle\hat{B}\rangle|$ festgelegt ist.

Im Gegensatz dazu zeigt die Abbildung 0.2(b) das Regime der Quantenoptik. Die Phasenraumverteilungen des thermischen Lichts, des Fock-Zustands, und des gequetschten Lichts sind dargestellt. Der Fock-Zustand und der gequetschte Zustand gelten als sehr quantenmechanische Zustände, da der Fock-Zustand keine Fluktuation in der Photonenzahl und der gequetschte Zustand eine Fluktuation in einer Quadraturrichtung unterhalb der minimalen Unschärfegrenze [43] aufweist. Das thermische Licht ist ein inkohärentes Lichtfeld ohne Amplitude und Phase, und weist eine große Fluktuation in der Photonenzahl auf. Das thermische Licht beschreibt einen Laser unterhalb der Laserschwelle. In der Abbildung 0.2(b) sehen wir, dass das thermische Licht und der Fock-Zustand weder Amplitude noch Phase besitzen, jedoch nicht verschwindende Quantenfluktuationen aufweisen. *Somit kann das Licht nicht nur eine Amplitude und Phase aufweisen, sondern auch Quantenfluktuationen.* Dies ist das Regime der Quantenoptik, welche mittels Korrelationen [43] beschrieben werden kann. Als Beispiel für solch eine Korrelation führen wir $\Delta\langle\hat{B}\hat{B}\rangle \equiv \langle\hat{B}\hat{B}\rangle - \langle\hat{B}\rangle\langle\hat{B}\rangle$ auf, welches den vollen Erwartungswert abzüglich der klassischen Faktorisierung darstellt.

Formal sind die Korrelationen durch die Notation $\Delta\langle\hat{O}\rangle$ in dieser Dissertation hervorgehoben, wobei $\hat{O}$ eine allgemeine Operatorkombination sein kann. Als Beispiel zeigt der gequetschte Zustand eine nicht verschwindende Zwei-Photonen Korrelation $\Delta\langle\hat{B}\hat{B}\rangle$ [43–46], welche den Grad der Quetschung entlang einer Richtung im Phasenraum angibt. Um dies zu verdeutlichen, haben wir die Phasenraumverteilung eines gequetschten Zustands in Abbildung 0.2(b) gezeigt. Wir sehen, dass dieses Beispiel eine Quetschung entlang der $\mathrm{Re}[\langle\hat{B}\rangle]$ Richtung zeigt.

Wie bereits in Ref. [5] betont sind die nicht verschwindenden Korrelationen, z.B. $\Delta\langle\hat{B}\hat{c}^\dagger\hat{c}\rangle$ mit Lichtfeldoperator $\hat{B}$ und elektronischem Operator $\hat{c}$, wichtig für jegliche quantenoptische Beschreibung. Hierbei stellt das Kriterium $\Delta\langle\hat{B}\hat{c}^\dagger\hat{c}\rangle \neq 0$ eine eindeutige Unterscheidung zwischen halbklassischen und quantenoptischen Verfahren dar. Wir erwähnen, dass die Korrelationen die volle Quantenstatistik des Lichtes darstellen und dass diese äquivalent sind zu anderen Darstellungen mittels Erwartungswerten [43], Dichtematrix, reduzierten Verteilungen ('marginal distributions') [43], und mittels Phasenraumverteilungen wie z.B. Glauber-Sudarshan-Funktion [47–49], Wignerfunktion [41, 42], und Husimi Q Funktion [41, 50]. In dieser Dissertation verwenden wir die Erwartungswerte und Korrelationen zur theoretischen Beschreibung der Licht-Materie Kopplung.

In diesem theoretischen Rahmen können die Halbleiter-Blochgleichungen und Halbleiter-Lumineszenz-Gleichungen aufgestellt werden, welche die Licht-Materie Wechselwirkung und das reemittierte Lichtfeld beschreiben. Überdies können die Bewegungsgleichungen zur Bildung des gequetschten Lichtes aufstellt werden. Diese Gleichungen werden auch

in dieser Dissertation diskutiert.

Die Dissertation ist wie folgt gegliedert. Kapitel 2 führt den Modellhamiltonian ein, welcher das starke Kopplungs-Regime beschreibt, und faßt die charakteristischen Modellparameter für die verschiedenen, betrachteten Systeme zusammen. In Kapitel 3 leiten wir die Heisenberg Bewegungsgleichungen her, die alle Korrelationen bis zur Drei-Teilchen Ebene enthalten. Als Nächstes wenden wir in Kapitel 4 die aufgebaute Theorie auf Quantenpunkten als auch auf atomare Systeme an und studieren die Eigenschaften der Emission des Zwei-Photonen Polaritons. In Kapitel 5 diskutieren wir das Konzept der Zwei-Photonen Korrelationsmessung und heben seine Vorteile hervor. Diese Diskussion wird erweitert in Kapitel 6, in dem wir auch die mikroskopische Theorie der gequetschten Lichtemission behandeln.

### *Bedeutung der erzielten Resultate*

In dieser Dissertation haben wir eine voll quantisierte Theorie entwickelt, um die Resonanzfluoreszenz von Halbleiter Nanostrukturen zu untersuchen. Hierbei ist das Materialsystem optisch mit einem externen Laser angeregt während das reemittierte Lichtspektrum detektiert wird. Wir haben die Erscheinung des Zwei-Photonen Polaritons der Jaynes-Cummings Leiter in den stark gekoppelten Halbleiter Quantenpunkten analysiert und geeignete experimentelle Methoden zur Detektierung dieser Signaturen vorgeschlagen. Wir haben herausgestellt, dass der Zwei-Photonen Polariton ein wahrer quantenoptischer Effekt ist. Die entwickelte Theorie haben wir auf aktuelle Quantenpunkte angewendet, die die halbklassische Vakuum-Rabi-Aufspaltung gezeigt haben. Überdies haben wir experimentelle Daten eines atomaren Systems, welches den Zwei-Photonen Polariton im Intensitätsspektrum aufgezeigt hat, theoretisch untersucht und gute Übereinstimmung zwischen Experiment und unserer Theorie gefunden. Unsere Ergebnisse für die Quantenpunkte haben noch vorhersagenden Charakter, da die experimentelle Arbeit noch im Prozess ist.

Um diese Ergebnisse zu erzielen, haben wir ein voll quantenmechanisches Modell aufgestellt, welches die Wechselwirkung zwischen vielen Quantenpunkten innerhalb einer Kavität und vielen quantisierten Lichtmoden beschreibt. Es stellt sich heraus, dass dieses Modell sehr gut geeignet ist, da es uns erlaubt, die, z.B., Lichtpropagation und Licht-Materie Kopplung ohne phänomenologische Parameter zu erhalten. Dazu genügt es, für ein gegebenes Resonatormodell die Lichtmoden-Funktionen mit der Helmholtz-Gleichung und der Transfermatrix-Methode zu lösen. Die experimentellen Parameter, wie z.B. die Qualität der Kavität und die Vakuum-Rabi-Aufspaltung, werden dabei den jeweiligen experimentellen Gegebenheiten angepaßt.

Als nächsten Schritt haben wir die Methode der Heisenberg Bewegungsgleichungen verfolgt, um die relevanten Operatorkombinationen auszuwerten. Wir sind auf das bekannte Hierarchieproblem gestoßen, das ihren Ursprung im quantisierten Wechselwirkungshamiltonian hat. Um diese Hierarchie zu durchbrechen, haben wir die Cluster Entwicklungsmethode angewendet, die konsistente Näherungslösungen produziert. Diese Methode erlaubt es uns alle Korrelationen bis zu einer gewünschten Ordnung

mitzunehmen. Wir haben sorgfältig die Genauigkeit der erhaltenen Gleichungen unter-
sucht, indem wir die dazugehörigen numerischen Resultate mit den exakten Lösungen,
für den Fall eines Quantenpunktes und einer einzelnen Lichtmode, verglichen haben.
Diese Untersuchungen sind im Anhang detailliert dargestellt. Wir haben gezeigt, dass
der Zwei-Photonen Polariton im Intensitätsspektrum in einer Dreiteilchen Theorie und
im gequetschten Spektrum in einer Zweiteilchen Theorie erhalten werden kann. Somit
haben wir gerechtfertigt, dass wir eine Theorie verwenden können, welche alle Kor-
relationen bis zur Drei-Teilchen Ebene beinhaltet. Die resultierenden Gleichungen
werden Maxwell-Blochgleichungen, Lumineszenz-Gleichungen, 'squeezing'-Gleichungen,
und 'triplet'-Gleichungen genannt.

Wir haben gezeigt, dass die Emission des Zwei-Photonen Polaritons bestimmt ist durch
die Besetzung des Zwei-Photonen Zustandes des anregenden Lichtpulses. In diesem
Zusammenhang haben wir die optimalen Anregungsbedingungen herausgearbeitet. Wir
haben zudem ein erst kürzlich betrachtetes atomares Experiment analysiert, das den
Zwei-Photonen Polariton direkt im Intensitätsspektrum gemessen hat. Unsere Theo-
rie stimmt gut mit den experimentellen Ergebnissen überein. Zudem finden wir, dass
derselbe Mechanismus zur Erzeugung des Zwei-Photonen Polaritons in atomaren- und
Halbleiter Quantenpunkt-Systemen angewendet werden kann.

Da die realistische Dephasierung aktueller Quantenpunktproben die wesentlichen,
interessanten Effekte im Intensitätsspektrum ausschmieren, haben wir vorgeschlagen,
die Zwei-Photonen Korrelationsmessungen zu verwenden. Im Gegensatz zum Inten-
sitätsspektrum finden wir, dass die Vakuum-Rabi Resonanzen abwesend sind im Zwei-
Photonen Korrelationsspektrum. Dies eliminiert den störenden Hintergrundbeitrag. Zu-
dem finden wir eine verstärkte Resonanz an der Emissionsfrequenz des Zwei-Photonen
Polaritons, welche wir auf den gequetschten Charakter des emittierten Lichtfeldes
zurückführen, das im Pumpprozess des Zwei-Photonen Polaritons generiert wird. Wir
haben gezeigt, dass diese verstärkte Resonanz genügend robust ist gegenüber
Dephasierung. Da diese große Resonanz der Zwei-Photonen Korrelation in einem Exper-
iment mit Atomen schon beobachtet wurde, als Nachweis des Zwei-Photonen Polaritons,
sind wir überzeugt, dass diese Methode auch anwendbar sein sollte in den Quantenpunk-
tsystemen.

Wir haben diese Diskussion erweitert und auch die Kreuzkorrelationen der Zwei-
Photonen Korrelationen untersucht. Wir haben vorgeschlagen, dass sich die exper-
imentellen Anstrengungen auf die Kreuzkorrelationen konzentrieren sollten, da diese
unter stationären Bedingungen beobachtet werden können und eine größere Resonanz
als die einfachen Autokorrelationen aufweisen. Wir haben diese Ergebnisse mittels eines
reduzierten Modells überprüft, das wir analytisch gelöst haben. Die explizite Her-
leitung der analytischen Lösung ist im Anhang detailliert dargestellt. Wir haben gezeigt,
dass das reduzierte Modell unter typischen starken Kopplungsbedingungen sehr genaue
Ergebnisse erzielt. Im Einzelnen haben wir eine sehr gute Übereinstimmung zwischen
Numerik und Analytik gefunden.

Wir haben den entwickelten Formalismus verwendet, um den physikalischen Ursprung
der gequetschten Lichtemission zu erklären. Dazu haben wir den generischen Fall der
Licht-Materie Kopplung betrachtet und geschlossen, dass die Materie eine fermionische

Statistik aufweisen muß, um gequetschtes Licht produzieren zu können. Zum Schluss haben wir eine exakte Beziehung zwischen dem generierten, gequetschten Licht und der Zwei-Photonen Korrelationen präsentiert.

Als Ausblick werde ich die verbleibenden Artikel fertig stellen, welche noch in der Bearbeitung sind, siehe 'Author's Contributions' am Anfang dieser Dissertation. Speziell wird das Thema der Verschränkung ('entanglement'), der theoretische Vorschlag zur Exziton-Biexziton Anregung in CdSe-basierenden Quantenpunkten in Zeno-Logik Anwendungen, und die starke Kopplung in atomaren Systemen gegenüber Quantenpunkten in verschiedenen Artikeln zusammengefasst.

# Danksagung

Mein Dank gilt Prof. Dr. Mackillo Kira und Prof. Dr. Stephan W. Koch für die langjährige konstruktive Zusammenarbeit und intensive Betreuung. Prof. Dr. Dr. h.c. Peter Thomas danke ich für die Organisation der gemeinsamen Wanderungen.

Ich bedanke mich bei Dr. Martin Schäfer und Marco Werchner für die stets hilfsbereite Beantwortung meiner Fragen zu Transfermatrixmethode und Lumineszenzgleichungen, bei Dr. Walter Hoyer für tiefere Einsichten in die Clusterentwicklung und bei Thomas Feldtmann für die gute und humorvolle Zusammenarbeit.

Bedanken möchte ich mich bei Dr. Bernhard Pasenow für die gute Atmosphäre in unserem gemeinsamen Büro und für seine praktischen Tipps in der alltäglichen Arbeit.

# Author's Contributions

## Publications

### Papers

(I) T. Feldtmann, L. Schneebeli, M. Kira, and S.W. Koch, *Quantum theory of light emission from a semiconductor quantum dot*, Phys. Rev. B **73**, 155319 (2006).

(II) L. Schneebeli, M. Kira, and S.W. Koch, *Characterization of strong light-matter coupling in semiconductor quantum-dot microcavities via photon-statistics spectroscopy*, Phys. Rev. Lett. **101**, 097401 (2008).

(III) L. Schneebeli, M. Kira, and S.W. Koch, *Characterization of strong light-matter coupling in semiconductor quantum-dot microcavities*, Proceedings of the International Workshop NOEKS-9, Phys. Status Solidi C **6**, 407-410 (2009).

(IV) L. Schneebeli, M. Kira, and S.W. Koch, *Microscopic Theory of Squeezed-Light Emission in Strong-Coupling Semiconductor Quantum-Dot Systems*, Phys. Rev. A **80**, 033843 (2009).

(V) L. Schneebeli, M. Kira, and S.W. Koch, *Atomic vs. quantum-dot strong coupling*, In preparation (2009).

(VI) L. Schneebeli, T. Feldtmann, M. Kira, and S.W. Koch, *Exciton-Biexciton Pumping in Zeno-Logic Applications*, In preparation (2009).

(VII) L. Schneebeli, M. Kira, and S.W. Koch, *Nature of Entanglement and Coherence in Resonance Fluorescence*, In preparation (2009).

### Poster and Talks

(i) L. Schneebeli, T. Feldtmann, M. Kira, and S.W. Koch, Talk: *Quantum Theory of Quantum Dot Emission*, DPG spring meeting Dresden, Germany (March 26-31, 2006).

(ii) L. Schneebeli, M. Kira, and S.W. Koch, Talk: *Jaynes-Cummings Ladder in Quantum-Dot Microcavities*, DPG spring meeting Darmstadt, Germany (March 10-14, 2008).

(iii) L. Schneebeli, M. Kira, and S.W. Koch, Poster: *Characterization of strong light-matter coupling in semiconductor quantum-dot microcavities via photon-statistics spectroscopy*, International Workshop NOEKS-9 Klink/Müritz, Germany (May 26-29, 2008).

(iv) L. Schneebeli, M. Kira, and S.W. Koch, Invited Talk: *Strong light-matter coupling in semiconductor quantum-dot microcavities*, joint group seminar Förstner/Meier Paderborn, Germany (September 23, 2008).

(v) L. Schneebeli, M. Kira, and S.W. Koch, Talk: *Photon Correlations in Systems with Strong Light-Matter Coupling*, International Conference CLEO/IQEC 2009 Baltimore, USA (May 31 - June 5, 2009).

(vi) L. Schneebeli, M. Kira, and S.W. Koch, Invited Talk: *Photon Correlations and Squeezing in Strong-Coupling Semiconductors*, group seminar A. Knorr Technische Universität Berlin, Germany (October 27, 2009).

# Original Contributions

In my first studies, I developed a consistent theory which treats the quantum dynamics of the interacting charge carriers in a semiconductor quantum dot. We used the cluster-expansion approach which was applied earlier in our group to quantum wells and quantum wires. The aim was to analyze the convergence of the theory of isolated quantum dots and to extend the theory to open quantum dot systems which exhibit coupling to the delocalized wetting-layer states, phonons, and photons. In this context, we collaborated with Frank Jahnke's group in Bremen and discussed the single-particle wavefunctions and corresponding matrix elements. The results are summarized in Paper [I] to which I made significant contributions. I also presented the material as a talk at the DPG conference in Dresden [i].

When the interesting effect of the vacuum Rabi splitting was measured in 2004 with semiconductor quantum dots embedded in microcavities, it was motivating to ask whether these systems can also show the climbing of the so-called Jaynes-Cummings ladder. Such an observation would clearly prove that the emission has true quantum characteristics. We decided to study this issue because we had already developed the theoretical framework which can treat the semiconductor quantum dot. I then included into the theory the coupling to the quantized multimode light field and the resonator model of the cavity. For this, it was necessary for me to derive many equations of motion to include all relevant correlations. Furthermore, I programmed the numerical code to simulate the corresponding resonance fluorescence from the strong-coupling semiconductor quantum dots inside the cavity. Moreover, I carried out many analytical derivations to thoroughly test the numerical results and to obtain deep insights, e.g., into the second-rung pumping process [II-III] and the squeezed-light emission [IV].

During my analysis of the resonance fluorescence spectrum, I confirmed the difficulties in the semiconductor quantum dots to observe the second rung, i.e. the first quantum-mechanical contribution, of the Jaynes-Cummings ladder. I then investigated the buildup of the squeezing and two-photon correlations. This lead to the concept of the photon-statistics spectroscopy which we published in Papers [II-III]. These results were presented by me as a talk at the DPG meeting in Darmstadt [ii] and as a poster at the NOEKS 9 meeting in Klink/Müritz [iii]. I also gave an invited talk in the joint group seminar of Jens Förstner and Torsten Meier at the University Paderborn [iv].

I extended the simple photon-statistics spectroscopy to analyze also the cross correlations. This lead to a deep understanding of the temporal dynamics and spectral

properties of the full two-photon emission spectrum. I developed a microscopic theory of the squeezed-light emission and worked out the connection to the two-photon correlations. These results are given in Paper [IV]. During that time, I also collaborated with P. Michler's group in Stuttgart and we discussed the experimental techniques to detect the second-rung resonance with the semiconductor quantum dots. Unfortunately, the limitation of the detection resolution prevented fast success and the experiment was postponed.

It is interesting to note that the efforts done in atomic systems to measure the second rung were quite at the same time when I was working on the dot problem, in 2008. This gave me the chance to learn also about the atomic systems. I had discussions with Gerhard Rempe's group in Garching and I tried to explain their experimental data which they had already published in a Nature article. The results of this comparison are summarized in this Thesis. It is also remarkable that in the same year, Rempe's group confirmed in their atomic system that the photon-statistics scheme is a reliable method to detect the second rung. I also had the possibility to give a talk about these observations at an international conference in Baltimore [v]. Furthermore, I am working on a Paper which treats the comparison between atomic- vs. quantum-dot strong coupling [V].

During February 2009, I worked on an elementary model which describes the exciton-to-biexciton transition in CdSe-based quantum dots. We worked out a theoretical proposal for a device design for Zeno-based optoelectronics. These results will be summarized in Paper [VI].

I also worked on developing a theory which treats fundamental aspects of entanglement. I learned different entanglement measures and analyzed the entanglement dynamics for a special class of interaction Hamiltonians. This work will be summarized in Paper [VII].

I also had the pleasure to give an invited talk in the group seminar of Andreas Knorr at the Technische Universität Berlin [vi].

# Contents

*Contents*

# 1 Introduction

While many quantum-optical phenomena are already well established in the atomic systems, like the photon antibunching [1], squeezing [2], Bose-Einstein condensation [3], teleportation [4], the quantum-optical investigations in semiconductors are still at their beginning [5]. The fascinating results observed in the atomic systems inspire physicists to demonstrate similar quantum-optical effects also in the semiconductor systems. In contrast to quantum optics with dilute atomic gases, the semiconductors exhibit a complicated many-body problem which is dominated by the Coulomb interaction between the electrons and holes and by coupling with the semiconductor environment. This makes the experimental observation of similar quantum-optical effects in semiconductors demanding. However, there are already experiments which have verified nonclassical effects in semiconductors. In particular, experiments have demonstrated that semiconductor quantum dots (QDs) can exhibit the single-photon emission [6–8] and generation of polarization-entangled photon pairs [9–11]. In fact, both atom and QD systems, embedded within a microcavity, have become versatile platforms where one can perform systematic quantum-optics investigations [12, 13] as well as development work toward quantum-information applications [14, 15].

Another interesting field is the strong-coupling regime in which the light-matter coupling exceeds both the decoherence rate of the atom or QD and the cavity resulting in a reversible dynamics between light and matter excitations. In the strong-coupling regime, the Jaynes-Cummings ladder [16] is predicted and shows a photon-number dependent splitting of the new dressed strong-coupling states which are the polariton states of the coupled light-matter system. Although the semiclassical effect of the vacuum Rabi splitting has already been observed in QDs [17–20], the verification of the quantum-mechanical Jaynes-Cummings splitting [5, 16, 21] is still missing mainly due to the dephasing. Clearly, the observation of the Jaynes-Cummings ladder in QDs would be a great contribution in the growing field of quantum optics in semiconductors. The efforts in QD systems are again driven by the atomic systems which not only have shown the vacuum Rabi splitting [22, 23], but also the second rung [24–26], e.g. via direct spectroscopy [25] and via photon-correlation measurements [26].

In order to get already some insights into the main discussion of this Thesis, we briefly review now the basic results of the Jaynes-Cummings model [16] which describes the coupling between a single light mode and a two-level emitter. For this, we present in Fig. 1.1 the resulting Jaynes-Cummings ladder in the strong-coupling regime. Without light-matter coupling, we obtain the Fock number states of the cavity light mode, denoted as $|n\rangle$ where $n$ can be $0, 1, 2, \ldots$, as depicted in Fig. 1.1. If we switch on the light-matter coupling, these states split and form new dressed states of the format $|n\rangle|\text{down}\rangle \pm |n-1\rangle|\text{up}\rangle$ with unexcited (excited) two-level system $|\text{down}\rangle$ ($|\text{up}\rangle$). In
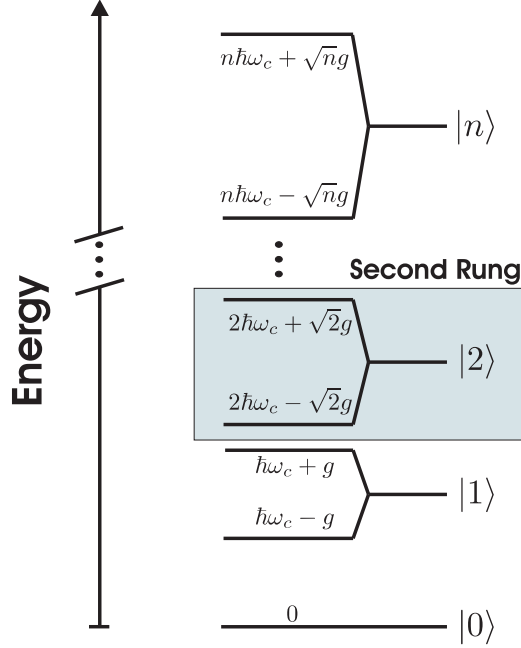
Figure 1.1: Jaynes-Cummings ladder. The quantized nature of light introduces the Fock number states $|n\rangle$ which split due to the light-matter coupling $g$. Each state $|n\rangle$ shows an individual coupling of $g_n = \sqrt{n}g$. In this Thesis, we mainly focus on the second rung which is highlighted by the shaded area.

Fig. 1.1, we thus observe that the ground state is unsplit while the higher-lying rungs show a photon-number dependent splitting of $2\sqrt{n}g$. Since the higher-lying rungs depend on $n$ which is proportional to the light-field intensity, we enter the regime of the nonlinear optics where the presence or absence of a single photon can change the state of the system dramatically [5]. In this Thesis, we mainly focus on the second rung which is highlighted by the shaded area. We point out that only a fully quantized theory can explain the existence of the second rung of the Jaynes-Cummings ladder. In a semiclassical theory which quantizes only the matter but treats the light classically, the second rung cannot be obtained. Thus, the experimental verification of the second rung provides a clear signature of the true strong-coupling regime.

In this Thesis, we strongly make use of the so-called cluster-expansion approach [27–29]. This method has already been successfully applied to various phenomena in many-body and quantum-optical systems [30–33], such as the exciton formation in semiconductor heterostructures [34], the consistent treatment of interaction of light and electron-hole excitations in semiconductor nanostructures [28, 35], and the quasi-particle and quantum-optical spectroscopy for the direct access and generation of exciton population [36, 37]. While it becomes very tedious if not impossible to solve the density matrix for genuine multi-mode and many-particle systems, the cluster expansion provides a convenient method to generate consistent approximations which can be systematically improved. These approximations are usually very accurate since we are interested only in a subset of expectation values which often describe the system already very well.
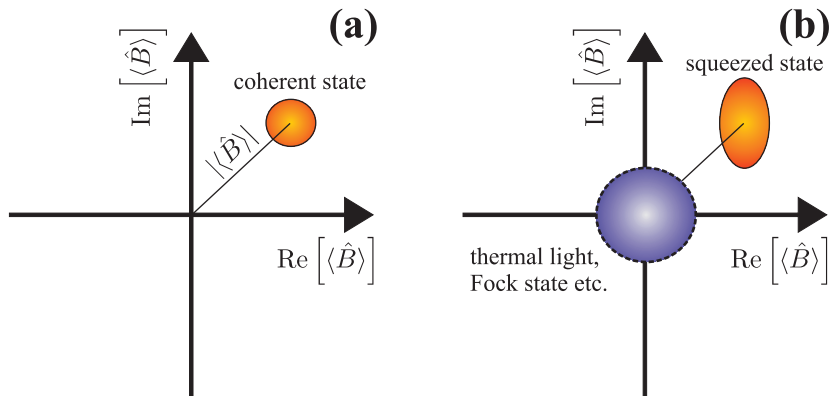
Figure 1.2: Phase-space representation of special light fields. (a) Classical optics, characterized through coherent state with amplitude and phase. (b) Quantum optics, e.g. squeezed state, Fock state, thermal light all of which exhibit nonvanishing quantum fluctuations.

To describe many-particle effects, there are also alternative approaches, like the Green's function approach [38], density functional theory [39], and Monte Carlo methods [40]. One has to choose the appropriate method to solve the problem at hand. We apply the cluster expansion because it is a very powerful tool to compute the emission properties of a material system. Moreover, the cluster-expansion approach provides a convenient formalism which allows us to find the relevant mechanisms of a given phenomena. This makes the theoretical treatment of many-body quantum-optical systems very appealing.

We can describe the light field and the excitation of the matter system at the same level of approximation, leading to a self-consistent solution. The theory is also flexible to describe various states of the light field. That means that we can describe classical fields as well as quantum fields. To remind of the difference between the classical and quantum optics, Fig. 1.2 shows the phase-space representation of a few single-mode light fields. More precisely, we have shown a schematic picture of the Wigner function [41, 42] as a contour plot. Here, the bosonic photon operator is denoted by $\hat{B}$. Figure 1.2(a) demonstrates the regime of the classical optics and presents as an example the phase-space distribution of the coherent state. The coherent state is closest to a classical field, with a well-defined phase, low photon-number fluctuations, and accurately describes a laser above threshold. Figure 1.2(a) demonstrates that the coherent light field is fully determined by its amplitude $|\langle\hat{B}\rangle|$ and phase $\langle\hat{B}\rangle/|\langle\hat{B}\rangle|$.

In contrast to that, Fig. 1.2(b) demonstrates the regime of the quantum optics. The phase-space distributions of the thermal light, Fock state, and squeezed state are shown. The Fock state and squeezed state are considered to be very quantum in that the Fock state has vanishing photon-number fluctuations and the squeezed state can have quadrature fluctuations below the minimum uncertainty limit [43]. The thermal light is an incoherent light field which does not have any amplitude or phase and which exhibits large photon-number fluctuations. The thermal light describes a laser below threshold. In Fig. 1.2(b), we can see that the thermal light and Fock state have vanishing ampli-

tude and phase, but exhibit nonvanishing quantum fluctuations. *Thus, the light can not only have amplitude and phase, but also quantum fluctuations.* This is the regime of the quantum optics which can be described via the correlations [43]. As an example for such a correlation, we can take $\Delta\langle\hat{B}\hat{B}\rangle \equiv \langle\hat{B}\hat{B}\rangle - \langle\hat{B}\rangle\langle\hat{B}\rangle$ which describes the full expectation value minus its classical factorization.

Formally, the correlations are highlighted in the Thesis via the notation $\Delta\langle\hat{O}\rangle$ for general operator combinations $\hat{O}$. As an example, the squeezed light shows a nonvanishing two-photon correlation $\Delta\langle\hat{B}\hat{B}\rangle$ [43–46] which describes the amount of the squeezing in one quadrature direction in the phase-space distribution. To visualize this, we have schematically shown in Fig. 1.2(b) the phase-space distribution of a squeezed state. We observe that this example shows a squeezing along the $\text{Re}[\langle\hat{B}\rangle]$ direction.

As pointed out in Ref. [5], the nonvanishing correlations, e.g. $\Delta\langle\hat{B}\hat{c}^\dagger\hat{c}\rangle$ for a combined field $\hat{B}$ and electronic operator $\hat{c}$, are important for any quantum-optical description. Especially, the criterion $\Delta\langle\hat{B}\hat{c}^\dagger\hat{c}\rangle \neq 0$ clearly distinguishes between the semiclassical and quantum-optical approaches. We note that the correlations describe the full quantum statistics of the light and are equivalent to the alternative representations via the expectation values [43], density matrix, marginal distributions [43], and via the phase-space distributions Glauber-Sudarshan function [47–49], Wigner function [41, 42], and Husimi Q function [41, 50]. In this Thesis, we use the expectation-value and correlation picture for the theoretical treatment of the light-matter coupling.

Within this theoretical framework, the semiconductor Bloch and luminescence equations can be developed which describe the interaction between the light and matter and the re-emitted light field. Moreover, the equations of motion for the generation of the squeezing can be derived, which is also presented in this Thesis.

The Thesis is organized as follows. Chapter 2 introduces the model Hamiltonian which describes the strong-coupling regime and summarizes the characteristic model parameters for the various systems. In Chapter 3, we derive the Heisenberg equations of motion which includes all correlations up to the three-particle level. Next, in Chapter 4, we apply the developed theory to the QD as well as to the atomic systems and study the properties of the second-rung emission. In Chapter 5, we discuss the concept of the two-photon correlation measurement and highlight its convenience. This discussion is expanded in Chapter 6 which also covers the microscopic theory of the squeezed-light emission.

# 2 Model Hamiltonian

In this Chapter, we discuss the basic model to describe the QD-cavity systems in the strong-coupling regime. As a starting point, we present the fully quantized system Hamiltonian which describes the interaction of multiple QDs inside a cavity with a multi-mode quantized light field. This model is fundamental but also useful at the same time. We also implement a dephasing model which enables us to study the resonance fluorescence from the QD-cavity systems under realistic dephasing conditions. The explicit application of the model is worked out step by step in the subsequent Chapters. Here, we focus on the model system, its simplifications and the characteristic model parameters for the various systems.

Methodically, we use a multi-mode generalization of the original Jaynes-Cummings Hamiltonian [16] which describes the interaction of one two-level emitter and one cavity mode. As we aim to describe the strong-coupling experiments which always contain a multitude of QDs inside a cavity, we have to use a generalized model. We therefore include into the model many QDs and also many light modes. The advantage of having a multi-mode system is that we can describe the propagation of the light field into the cavity and the interaction between the light and QDs without additional phenomenological parameters. The light propagation is obtained by solving the Helmholtz equation [35, 51] for a given dielectric structure. This dielectric structure consists of distributed Bragg reflector (DBR) mirrors which enclose a cavity region. We use the transfer-matrix method [52, 53] to compute the light-mode functions within this structure and obtain a Lorentzian-like cavity resonance at the position of the QDs. We can thus describe strong-coupling situations and fix the system parameters to experimental configurations, like the quality of the cavity and the resulting vacuum Rabi splitting.

Another ingredient of the model is that we consider strongly-confined QDs which act as effective two-level emitters. This simplification is justified in most strong-coupling considerations. Even though we have also considered QDs with more shells in another context where we investigate the luminescence from stable QD states [29], we do not repeat these results - for a review, see Ref. [54]. However, the reader can well understand all the material presented in the following Chapters which are self-contained and include all the necessary ingredients.

## 2.1 Quantum-Dot Configuration

We introduce a microscopic model which describes the interaction between QDs and a semiconductor microcavity. The theoretical description of such a dot-cavity system represents a complicated many-body problem [29, 55–57] since the localized dot states
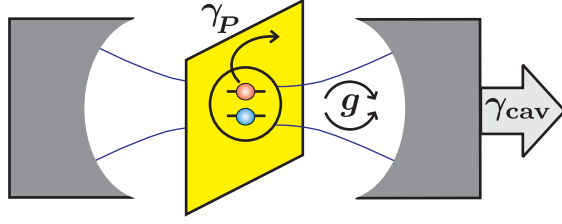
Figure 2.1: Schematic setup. The quantum dot inside the cavity is placed on a quantum well with dephasing coupling $\gamma_P$ to a reservoir of continuum electron states and phonons. The light-matter coupling constant is denoted by $g$ and the loss rate of the cavity is given by $\gamma_{\text{cav}}$. See also Ref. [21], Fig. 1.

couple to each other and also to the continuum states of the surrounding semiconductor material via the Coulomb interaction. Moreover, the dots couple to phonons and to the quantized light field.

As in most strong-coupling investigations, we study strongly confined QDs where only one discrete electron and hole level – constituting an effective two-level system – is energetically close to the cavity resonance. We neglect further level-splitting effects which can be caused by, e.g., the shape anisotropy of the QDs, such that no spectrally close other resonances should exist in the system. We thus use a formal two-level system where all Coulomb effects are included into the levels themselves. Since the recent strong-coupling QD experiments [17–21] are able to realize this situation, we can demonstrate quantum-optical effects based on the theoretical model, introduced in the following via the system Hamiltonian (2.2), which isolates quantum-optical effects from Coulomb-correlation effects which we do not expect to be observed under these conditions. This scenario allows us to simplify the analysis considerably because the remaining WL electrons and the phonon interaction can be included via a dephasing model which describes coupling of noise reservoirs to the isolated two-level system.

Figure. 2.1 visualizes this scenario in which the QDs are placed on a quantum well with dephasing $\gamma_P$ coupling to the semiconductor environment. The QDs are placed within a cavity which introduces the light-matter coupling $g$ and cavity loss $\gamma_{\text{cav}}$, as depicted in Fig. 2.1. If the QDs are optimally placed within the cavity, one can reach the strong-coupling regime with potential access to the introduced Jaynes-Cummings ladder Fig. 1.1.

## 2.2  System Hamiltonian

As in real semiconductor cavities, we introduce a variable number of dots, labeled $j$, within the cavity, with eigen energy $E^c$ ($E^v$) for conduction (valence) electrons which are described via fermionic operators $\hat{c}_j$ ($\hat{v}_j$). The quantization of the light field is

introduced via the field operators $\hat{B}_q$ [58] which obey bosonic commutation relations

$$\left[\hat{B}_q, \hat{B}_{q'}^\dagger\right]_- = \delta_{qq'}, \tag{2.1a}$$

$$\left[\hat{B}_q, \hat{B}_{q'}\right]_- = \left[\hat{B}_q^\dagger, \hat{B}_{q'}^\dagger\right]_- = 0, \tag{2.1b}$$

and correspond to light modes $u_q(\mathrm{r})$ with free space wave vector $q$. The total system Hamiltonian [28, 29] then reads

$$\begin{aligned}
\hat{H} &= \sum_j \left(E^c \hat{c}_j^\dagger \hat{c}_j + E^v \hat{v}_j^\dagger \hat{v}_j\right) + \sum_q \hbar\omega_q \left(\hat{B}_q^\dagger \hat{B}_q + \frac{1}{2}\right) \\
&+ \sum_{qj} \left(\mathcal{F}_q^\star \hat{B}_q^\dagger \hat{v}_j^\dagger \hat{c}_j + \text{h.c.}\right).
\end{aligned} \tag{2.2}$$

The photon energy is defined by $\hbar\omega_q = \hbar|q|c$ and the dipole-coupling constants are given by

$$\mathcal{F}_q = -id\mathcal{E}_q u_q(\mathbf{r}_j), \tag{2.3}$$

which contain the dipole-matrix element $d$, the vacuum-field amplitude

$$\mathcal{E}_q \equiv \sqrt{\hbar\omega_q/(2\varepsilon_0)}, \tag{2.4}$$

and the position of the dot $\mathbf{r}_j$. The first part in Eq. (2.2) represents the free kinetic energy of the QDs, the second part is the free field energy of the quantized light field, and the last part constitutes the dipole-interaction Hamiltonian of the light-matter coupling in the rotating wave approximation. The system Hamiltonian Eq. (2.2) is the starting point for the quantum-optical investigation.

## 2.3 System Parameters

It is convenient to introduce the multi-mode description of the light field in the system Hamiltonian Eq. (2.2). This description enables us to treat light propagation effects, coupling of external pulses to the cavity, and the finite linewidth of the cavity without additional phenomenological parameters. For the light propagation, we have to solve the light mode functions $u_q(\mathrm{r})$ which obey the Helmholtz equation [35, 51]

$$\left[\nabla^2 + q^2 n^2(\mathrm{r})\right] u_q(\mathrm{r}) = 0, \tag{2.5}$$

where $n(\mathrm{r})$ denotes the position-dependent background refractive index and defines the dielectric environment.

Figure 2.2 shows characteristic features of the cavity model used in our investigations. Figure 2.2(a) presents the position-dependent background refractive index $n(z)$ as grey shaded area where the direction of the pump pulse is chosen to be the $z$ axis. We model the cavity via distributed Bragg reflector (DBR) mirrors on each side of the cavity
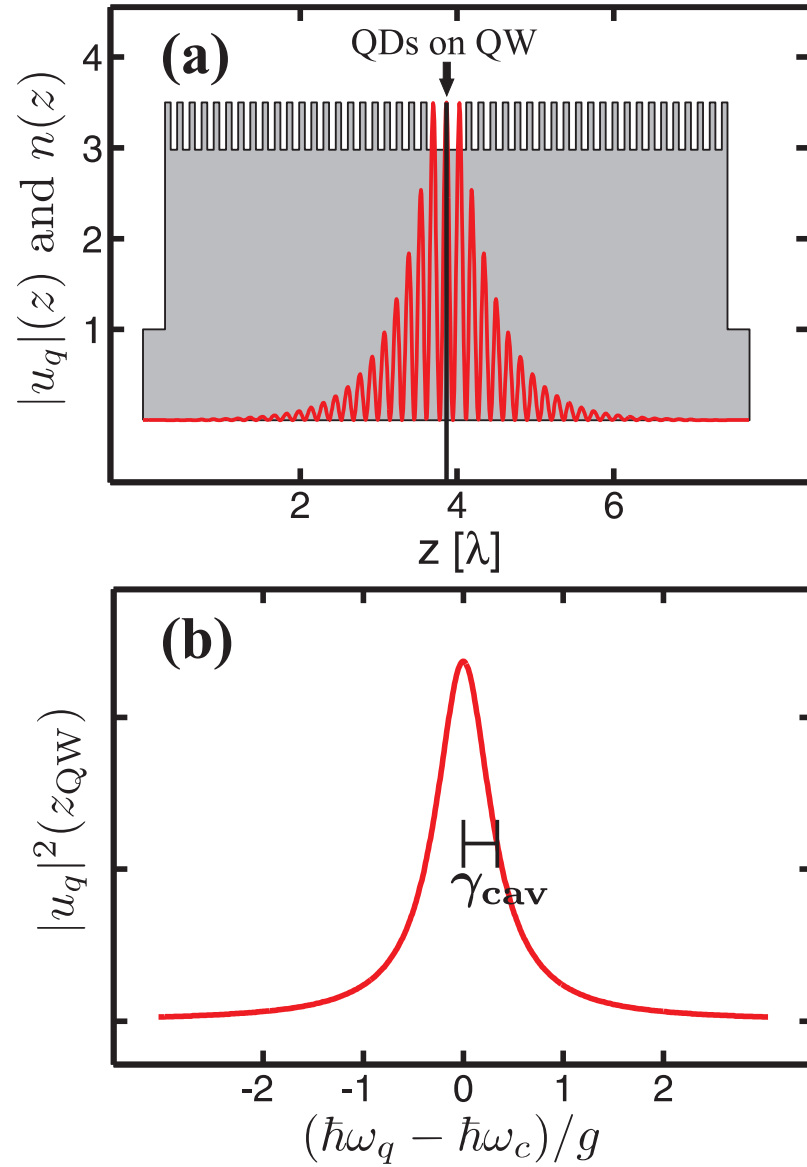
Figure 2.2: Cavity model. (a) The quantum well (QW), indicated by the vertical line, is placed in between distributed Bragg reflector (DBR) mirrors with varying background refractive index (grey shaded area), as function of position $z$ in units of light wavelength $\lambda$. The calculated light-mode function is given by the oscillating solid line. (b) Light-mode function at QW position $z_{\mathrm{QW}}$ shows a Lorentzian resonance with cavity frequency $\omega_c$ and half width $\gamma_{\mathrm{cav}}$. According to Paper [IV].

region with quantum well (QW) placed in-between (vertical line). The resulting light-mode function $u_q(z)$ are computed via a transfer-matrix method [52, 53]. An example is shown by the oscillating solid line in Fig. 2.2(a) while the shaded area represents the dielectric structure. The QDs on the QW are placed at the position of the maximum light field to guarantee strong light-matter coupling. In Fig. 2.2(b), the resulting light-mode function $|u_q(z_{\mathrm{QW}})|^2$ at the QW position is presented as function of momentum $q$. We observe that the identified $|\mathcal{F}_{q,j}|^2$ in Eq. (2.3), proportional to $|u_q(z_j)|^2$, displays a Lorentzian resonance [35] having a width $\gamma_{\mathrm{cav}}$ around the cavity frequency $\omega_c$.

Even though we have specified a particular resonator system, our model is well suited to describe different types of cavities with Lorentzian resonances. For this purpose, it is sufficient to specify only $\omega_c$, $\gamma_{\mathrm{cav}}$, and the so-called cavity-quality factor

$$Q \equiv \frac{\hbar\omega_c}{2\gamma_{\mathrm{cav}}}, \tag{2.6}$$

for the given cavity system. Furthermore, we can also adjust the vacuum Rabi splitting $2g$ to the experiment since the vacuum Rabi splitting is proportional to the dipole-matrix element $d$ and the square of the number of dots $N_{\mathrm{dot}}$ inside the cavity, giving [59]

$$2g = 2d\mathcal{E}_c \sqrt{N_{\mathrm{dot}} \sum_q |u_q(\mathbf{r}_j)|^2}. \tag{2.7}$$

In Ref. [60], we apply the developed theory to three recently published experiments with semiconductor QDs which have shown the vacuum Rabi splitting. The QD-pillar investigations [17, 61] have $n_{\mathrm{dot}} = 1.3 \cdot 10^9\,\mathrm{cm}^{-2}$ within DBR mirrors yielding a quality factor of $Q = 2.4 \cdot 10^4$ with cavity frequency $\hbar\omega_c = 1.33$ eV. The effective cavity area is $S = 3.0\,\mu\mathrm{m}^2$ yielding $N_{\mathrm{dot}} = 39$ and $g = 20$ GHz. In another QD-crystal experiment [18], $n_{\mathrm{dot}} = 6.0 \cdot 10^9\,\mathrm{cm}^{-2}$ QDs were placed within a photonic crystal providing $Q = 2.2 \cdot 10^4$, $\hbar\omega_c = 1.0$ eV, $S = 10\,\mu\mathrm{m}^2$, $N_{\mathrm{dot}} = 600$, and $g = 22$ GHz. In the QD-disk example [62], $n_{\mathrm{dot}} = 10^{10}\,\mathrm{cm}^{-2}$ QDs were positioned within a microdisk giving $\hbar\omega_c = 1.0$ eV, $Q = 4 \cdot 10^5$, $S = 2.5\,\mu\mathrm{m}^2$, $N_{\mathrm{dot}} = 250$, and $g = 11$ GHz. The dot dipole moment is $d = 5.3$ Åe in all these systems. In the Thesis, we refer to these QD-cavity systems as *QD-pillar*, *QD-crystal*, and *QD-disk* system, respectively.

# 3 Equation-of-Motion Approach

In Chapter 2, we have presented the model system and we have given the corresponding system Hamiltonian (2.2). In this Chapter, we expand the theory to its practical usage. Here, our aim is to develop a theory which provides a consistent description of the light-matter interaction and which is also able to describe the quantum rungs of the JC ladder. The outcome of this are resonance fluorescence equations which we solve explicitly in the following Chapters. These equations are very powerful and allow us to gain deep insights into the interplay between the excitation and quantum statistics of the re-emitted light.

Technically, we apply the Heisenberg equation of motion [63] for the relevant expectation values to describe the temporal dynamics of the system. The result is an infinite hierarchy of coupled differential equations. This hierarchy has to be truncated consistently in order to get a physical correct and computable solution. To reach this goal, we apply the cluster expansion [27–29] to truncate the hierarchy and finally obtain a closed and finite set of differential equations which we can solve.

The obtained equations are called *Maxwell-Bloch equations*, *luminescence equations*, *squeezing equations*, and *triplet equations*. They are all coupled to each other and we solve them numerically via the standard Runge-Kutta method [64]. In some cases, we can solve them analytically. Especially, in Chapter 6, we solve the squeezing equations analytically and obtain a remarkable good agreement with the full numerical calculation.

Each of these subsets of equations have a special physical meaning. Namely, the Maxwell-Bloch equations self-consistently describe the excitation of the QDs and the backcoupling to the light field. The luminescence equations yield the intensity spectrum while the squeezing equations yield the amount of the squeezing present in the re-emitted light. Finally, the triplet equations describe the dynamics of the higher-order correlations up to the three-particle level. In Chapter 3, we explain the different terms appearing in these equations and highlight their physical interpretation. We will learn that the cluster expansion provides us with an intuitive picture.

## 3.1 Cluster Expansion

We start from the system Hamiltonian (2.2) and follow the Heisenberg equation-of-motion technique to set up the dynamical equations for the relevant expectation values. This approach is very suitable to solve the emission properties of a system which contains infinitely many light modes. The Heisenberg equation of motion is given by [63]

$$\mathrm{i}\hbar \frac{\partial}{\partial t}\hat{O} = \left[\hat{O}, \hat{H}\right]_{-},\tag{3.1}$$
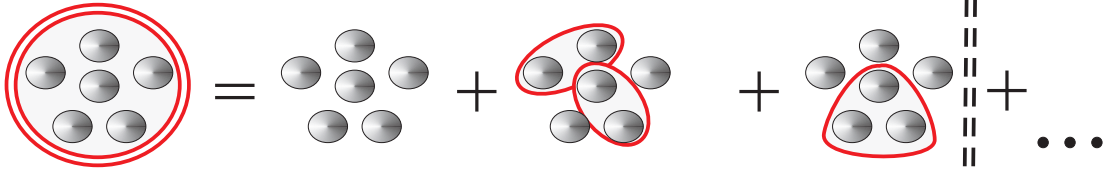
Figure 3.1: Diagrammatic presentation of the cluster expansion. The general N-particle expectation value can be expanded into the singlets (Hartree-Fock truncation), doublets (two-particle correlations), triplets (three-particle correlations), up to pure N-particle correlations. In our truncation scheme, we explicitly include all the singlets, doublets, and triplets.

where $\hat{O}$ is a time-dependent operator in the Heisenberg picture and $\hat{H}$ denotes the system Hamiltonian (2.2). We have then access to the expectation values via

$$\langle \hat{O} \rangle = \mathrm{Tr}\left[ \hat{\rho}\hat{O} \right], \tag{3.2}$$

where $\hat{\rho}$ is the system's density matrix.

Due to the quantum-optical light-matter coupling within $\hat{H}$, we formally obtain an infinite hierarchy structure of equations. We apply the cluster expansion [27–29] to systematically truncate this hierarchy problem. At the lowest level of approximation which is equal to the Hartree-Fock approximation, we obtain the singlet equations which describe the time evolution of the single-particle expectation values $\langle 1 \rangle$ (singlets). They are covered by the Maxwell-Bloch equations in Sec. 3.2. At the next level, we obtain the two-particle correlations $\Delta\langle 2 \rangle$ (doublets) which are defined by

$$\Delta\langle 2 \rangle \equiv \langle 2 \rangle - \langle 1 \rangle\langle 1 \rangle, \tag{3.3}$$

where $\langle 2 \rangle$ refers symbolically to a two-particle expectation value. The two-particle correlations $\Delta\langle 2 \rangle$ are described by the luminescence and squeezing equations (Secs. 3.3 and 3.4) and are relevant for solving the emission properties of the QD-cavity system. If we increase the truncation level further, we obtain the three-particle correlations $\Delta\langle 3 \rangle$ (triplets) which are given by

$$\Delta\langle 3 \rangle \equiv \langle 3 \rangle - \langle 1 \rangle\langle 1 \rangle\langle 1 \rangle - \langle 1 \rangle\Delta\langle 2 \rangle, \tag{3.4}$$

where $\langle 3 \rangle$ denotes a three-particle expectation value. In the theoretical description, we explicitly include the three-particle correlations and present the corresponding triplet equations in Sec. 3.5 and App. D.

Figure 3.1 is a diagrammatic presentation of the cluster expansion. Any N-particle expectation value can be expanded into the singlets, doublets, triplets, up to pure N-particle correlations. In order to obtain a closed set of equations, we truncate the hierarchy of equations at the singlet-doublet-triplet level, as depicted in Fig. 3.1. In some studies, we also include the four-particle correlations (quadrupolets) to investigate the role of the higher-order clusters, see Apps. B and C.

## 3.2 Maxwell-Bloch Equations

In order to self-consistently treat the interaction between the classical light field and the dot-cavity system, we have to set up the Maxwell-Bloch equations. They describe the time evolution of the field

$$\langle \hat{E}(r) \rangle = \sum_q i\mathcal{E}_q u_q(r) \langle \hat{B}_q \rangle + \text{c.c.}, \tag{3.5}$$

(c.c. = complex conjugate) the QD polarization $P_j = \langle \hat{v}_j^\dagger \hat{c}_j \rangle$, and the QD conduction (valence) electron densities $f_j^c = \langle \hat{c}_j^\dagger \hat{c}_j \rangle$ ($f_j^v = \langle \hat{v}_j^\dagger \hat{v}_j \rangle$). In this connection, it is also convenient to introduce the QD hole densities $f_j^h \equiv 1 - f_j^v$ and a density operator $\hat{f}_j^{cv} \equiv \hat{c}_j^\dagger \hat{c}_j - \hat{v}_j^\dagger \hat{v}_j$. Then, the *Maxwell-Bloch equations* read [28, 65]

$$\begin{aligned} i\hbar \frac{\partial}{\partial t} P_j &= (E^{cv} - i\gamma_P) P_j - \left(1 - f_j^c - f_j^h\right) \Omega_j \\ &\quad - \sum_q \mathcal{F}_q \Delta \langle \hat{B}_q \hat{f}_j^{cv} \rangle, \end{aligned} \tag{3.6}$$

$$i\hbar \frac{\partial}{\partial t} f_j^{c,h} = 2i\text{Im}\left[\Omega_j^\star P_j\right] - \sum_q 2i\text{Im}\left[\mathcal{F}_q^\star \Pi_{qj}\right], \tag{3.7}$$

$$i\hbar \frac{\partial}{\partial t} \langle \hat{B}_q \rangle = \hbar\omega_q \langle \hat{B}_q \rangle + \sum_j \mathcal{F}_q^\star P_j. \tag{3.8}$$

Here, we have defined the energy difference $E^{cv} \equiv E^c - E^v$, the QD polarization operator $\hat{P}_j \equiv \hat{v}_j^\dagger \hat{c}_j$ and the photon-assisted polarization $\Pi_{qj} \equiv \Delta \langle \hat{B}_q^\dagger \hat{P}_j \rangle$ where $\Delta \langle \hat{O} \rangle$ denotes again the correlated part of the full expectation value $\langle \hat{O} \rangle$. Furthermore, the classical Rabi frequency at the QD position is defined by $\Omega_j \equiv d\langle \hat{E}(\mathbf{r}_j) \rangle$. The dissipative coupling to the reservoir of continuum electron states and phonons introduces the dephasing $\gamma_P$ for all polarization-dependent quantities, included phenomenologically in the homogeneous part of Eq. (3.6).

We observe that the classical field, which is initially outside the cavity, produces the QD polarization $P_j$ as soon as it enters the cavity. The QD polarization is generated via the term $\left(1 - f_j^c - f_j^h\right)\Omega_j$ in Eq. (3.6) where $\left(1 - f_j^c - f_j^h\right)$ is called the phase-space filling factor which originates from the fermionic nature of the QD carriers. The generated polarization then creates densities, as can be seen in Eq. (3.7) from the term $\text{Im}\left[\Omega_j^\star P_j\right]$. Moreover, the polarization couples back to the classical field in Eq. (3.8) via the term $\sum_j \mathcal{F}_q^\star P_j$. Hence, the coupling between the light field and QD-cavity system is self-consistently described via the Maxwell-Bloch equations.

Additional to the classical Maxwell-Bloch equations, we obtain the quantum corrections in Eqs. (3.6) and (3.7) in terms of the photon-density correlations $\Delta \langle \hat{B}_q \hat{f}_j^{cv} \rangle \equiv \langle \hat{B}_q \hat{f}_j^{cv} \rangle - \langle \hat{B}_q \rangle \langle \hat{f}_j^{cv} \rangle$ and photon-assisted polarization $\Pi_{qj} \equiv \langle \hat{B}_q^\dagger \hat{P}_j \rangle - \langle \hat{B}_q^\dagger \rangle \langle \hat{P}_j \rangle$. They represent the quantum-optical two-particle correlations and are covered by the luminescence and squeezing equations which enable us to investigate the fluorescent light.

## 3.3 Luminescence Equations

In the resonance fluorescence setup, an external laser pump excites the QD-cavity system while the re-emitted light in the directions different from the excitation is detected. We can describe this scenario with the Maxwell-Bloch equations together with the luminescence equations. As the exciting pump pulse enters the cavity, the QD polarization and densities are generated according to the Maxwell-Bloch equations. Moreover, the quantum-optical correlations are induced and lead to the re-emission which is determined by the photon-number like correlations $\Delta\langle \hat{B}_q^\dagger \hat{B}_q \rangle$. The re-emission then follows from the *luminescence equations* which are given by

$$
\begin{aligned}
i\hbar \frac{\partial}{\partial t} \Delta\langle \hat{B}_q^\dagger \hat{B}_{q'} \rangle &= \hbar \left( \omega_{q'} - \omega_q \right) \Delta\langle \hat{B}_q^\dagger \hat{B}_{q'} \rangle \\
&\quad + \sum_j \left( \mathcal{F}_{q'}^\star \Pi_{qj} - \mathcal{F}_q \Pi_{q'j}^\star \right),
\end{aligned}
\tag{3.9}
$$

$$
\begin{aligned}
i\hbar \frac{\partial}{\partial t} \Pi_{qj} &= \left( E^{cv} - \hbar\omega_q - i\gamma_P \right) \Pi_{qj} \\
&\quad + \left( 1 - f_j^c - f_j^h \right) \sum_{q'} \mathcal{F}_{q'} \Delta\langle \hat{B}_q^\dagger \hat{B}_{q'} \rangle \\
&\quad + \Omega_j \Delta\langle \hat{B}_q \hat{f}_j^{cv} \rangle^\star - \mathcal{F}_q \left( f_j^c - |P_j|^2 \right) \\
&\quad - \sum_{q'} \mathcal{F}_{q'} \Delta\langle \hat{B}_q^\dagger \hat{B}_{q'} \hat{f}_j^{cv} \rangle.
\end{aligned}
\tag{3.10}
$$

We observe from Eq. (3.9) that the emission $\Delta\langle \hat{B}^\dagger \hat{B} \rangle$ couples to the photon-assisted polarization $\Pi_{qj} = \Delta\langle \hat{B}_q^\dagger \hat{v}_j^\dagger \hat{c}_j \rangle$ which presents the correlated creation of a photon and destruction of an electron-hole pair. Hence, these processes are crucial for the physically correct description of the emission. The correlations $\Pi_{qj}$ are built up spontaneously via the source term $\left( f_j^c - |P_j|^2 \right)$ in Eq. (3.10) and produce the nonvanishing emission in Eq. (3.9). The created emission then couples back to $\Pi_{qj}$ via the stimulated term $\sum \Delta\langle \hat{B}^\dagger \hat{B} \rangle$ in Eq. (3.10) and eventually leads to the vacuum Rabi splitting. Equation (3.10) also contains the photon-density correlations $\Delta\langle \hat{B}_q \hat{f}_j^{cv} \rangle$ and the three-particle correlations $\Delta\langle \hat{B}_q^\dagger \hat{B}_{q'} \hat{f}_j^{cv} \rangle$ which both contribute to the generation of the higher rungs of the JC ladder.

## 3.4 Squeezing Equations

We are also interested in the generation of the squeezing which is described by the two-photon correlations $\Delta\langle \hat{B}\hat{B} \rangle$ [43]. The squeezing in the fluorescent light then follows

from

$$
\begin{aligned}
\mathrm{i}\hbar \frac{\partial}{\partial t}\Delta\langle \hat{B}_q \hat{B}_{q'}\rangle ={}& \hbar\left(\omega_q + \omega_{q'}\right)\Delta\langle \hat{B}_q \hat{B}_{q'}\rangle \\
&+ \sum_j \Delta\langle\left(\mathcal{F}_{q'}^{\star}\hat{B}_q + \mathcal{F}_q^{\star}\hat{B}_{q'}\right)\hat{P}_j\rangle,
\end{aligned}
\tag{3.11}
$$

$$
\begin{aligned}
\mathrm{i}\hbar \frac{\partial}{\partial t}\Delta\langle \hat{B}_q \hat{P}_j\rangle ={}& \left(\hbar\omega_q + E^{cv} - i\gamma_P\right)\Delta\langle \hat{B}_q \hat{P}_j\rangle \\
&+ \left(1 - f_j^c - f_j^h\right)\sum_{q'}\mathcal{F}_{q'}\Delta\langle \hat{B}_q \hat{B}_{q'}\rangle \\
&+ \Omega_j\,\Delta\langle \hat{B}_q \hat{f}_j^{cv}\rangle - \mathcal{F}_q^{\star}P_j^2 \\
&- \sum_{q'}\mathcal{F}_{q'}\Delta\langle \hat{B}_q \hat{B}_{q'}\hat{f}_j^{cv}\rangle.
\end{aligned}
\tag{3.12}
$$

To get a closed set of the singlet-doublet equations, we finally present the dynamical equation for the photon-density correlations

$$
\begin{aligned}
\mathrm{i}\hbar \frac{\partial}{\partial t}&\Delta\langle \hat{B}_q \hat{f}_j^{cv}\rangle \\
={}& \hbar\omega_q\Delta\langle \hat{B}_q \hat{f}_j^{cv}\rangle \\
&+ 2P_j^{\star}\sum_{q'}\mathcal{F}_{q'}\Delta\langle \hat{B}_q \hat{B}_{q'}\rangle - 2P_j\sum_{q'}\mathcal{F}_{q'}^{\star}\Delta\langle \hat{B}_{q'}^{\dagger}\hat{B}_q\rangle \\
&+ 2\Omega_j^{\star}\Delta\langle \hat{B}_q \hat{P}_j\rangle - 2\Omega_j\Pi_{qj}^{\star} - \mathcal{F}_q^{\star}\left(f_j^c + f_j^h\right)P_j \\
&+ \sum_{q'}2\left(\mathcal{F}_{q'}\Delta\langle \hat{B}_q \hat{B}_{q'}\hat{P}_j^{\dagger}\rangle - \mathcal{F}_{q'}^{\star}\Delta\langle \hat{B}_{q'}^{\dagger}\hat{B}_q \hat{P}_j\rangle\right).
\end{aligned}
\tag{3.13}
$$

Equations (3.11),(3.12), and (3.13) constitute the *squeezing equations* which are very similar to the luminescence equations. Again, we can identify the spontaneous source terms which are proportional to the QD polarization and densities, and the stimulated terms $\sum\Delta\langle\hat{B}^{(\dagger)}\hat{B}\rangle$ which lead to the vacuum Rabi splitting. Furthermore, like the photon-assisted polarization $\Pi_{qj}$ in Eq. (3.10), the photon-polarization correlations $\Delta\langle\hat{B}\hat{P}\rangle$ in Eq. (3.12) and photon-density correlations $\Delta\langle\hat{B}\hat{f}_j^{cv}\rangle$ in Eq. (3.13) show the coupling to the triplets.

To summarize the equation structure, we obtain a closed set of Maxwell-Bloch, luminescence and squeezing equations which describe a consistent and physical solution at the singlet-doublet level which includes all the one-particle expectation values and two-particle quantum-optical correlations. They form the basis for the investigation of the resonance fluorescence in the QD-cavity systems and yield the information about the QD excitation and the fluorescent light.

## 3.5 Triplet Equations

In order to reproduce the strong-coupling rungs in the emission spectrum, discussed in more detail in Sec. 4.1, we have to include the higher-order correlations. Formally,

the higher-order correlations are already included in the luminescence and squeezing equations in terms of the triplet quantities. If we additionally set up the dynamical equations for the triplets, we obtain a closed set of equations at the singlet-doublet-triplet level. As an example, we present here the equation of motion for the photon-number-density triplet which reads

$$
\begin{aligned}
i\hbar \frac{\partial}{\partial t} & \Delta\langle \hat{B}_q^\dagger \hat{B}_{q'} \hat{f}_j^{cv}\rangle \\
= \ & \hbar\left(\omega_{q'} - \omega_q\right) \Delta\langle \hat{B}_q^\dagger \hat{B}_{q'} \hat{f}_j^{cv}\rangle \\
& + \ 2\sum_{q''}\Big[\mathcal{F}_{q''}\Pi_{q'j}^\star \Delta\langle \hat{B}_q^\dagger \hat{B}_{q''}\rangle - \mathcal{F}_{q''}^\star \Pi_{qj} \Delta\langle \hat{B}_{q''}^\dagger \hat{B}_{q'}\rangle \\
& + \ \mathcal{F}_{q''}\Delta\langle \hat{B}_q\hat{P}_j\rangle^\star \Delta\langle \hat{B}_{q'}\hat{B}_{q''}\rangle - \mathcal{F}_{q''}^\star \Delta\langle \hat{B}_{q'}\hat{P}_j\rangle \Delta\langle \hat{B}_q\hat{B}_{q''}\rangle^\star \\
& + \ \mathcal{F}_{q''}P_j^\star \Delta\langle \hat{B}_q^\dagger \hat{B}_{q'}\hat{B}_{q''}\rangle - \mathcal{F}_{q''}^\star P_j \Delta\langle \hat{B}_{q'}^\dagger \hat{B}_q\hat{B}_{q''}\rangle^\star \Big] \\
& + \ 2\Omega_j^\star \Delta\langle \hat{B}_q^\dagger \hat{B}_{q'}\hat{P}_j\rangle - 2\Omega_j \Delta\langle \hat{B}_{q'}^\dagger \hat{B}_q\hat{P}_j\rangle^\star \\
& + \ \left(f_j^c + f_j^h\right)\left(\mathcal{F}_q\Pi_{q'j}^\star - \mathcal{F}_{q'}^\star \Pi_{qj}\right) \\
& - \ 2\sum_{q''}\mathcal{F}_{q''}^\star \Delta\langle \hat{B}_{q''}^\dagger \hat{B}_q^\dagger \hat{B}_{q'}\hat{P}_j\rangle + 2\sum_{q''}\mathcal{F}_{q''}\Delta\langle \hat{B}_{q''}^\dagger \hat{B}_{q'}^\dagger \hat{B}_q\hat{P}_j\rangle^\star \\
& + \ \mathcal{F}_q P_j^\star \Delta\langle \hat{B}_{q'}\hat{f}_j^{cv}\rangle - \mathcal{F}_{q'}^\star P_j \Delta\langle \hat{B}_q\hat{f}_j^{cv}\rangle^\star.
\end{aligned}
\tag{3.14}
$$

Analogous to the luminescence and squeezing equations, Eq. (3.14) shows the spontaneous source and stimulated terms. Additionally, we notice that also the four-particle correlations $\Delta\langle \hat{B}_{q''}^\dagger \hat{B}_q^\dagger \hat{B}_{q'}\hat{P}_j\rangle$ and $\Delta\langle \hat{B}_{q''}^\dagger \hat{B}_{q'}^\dagger \hat{B}_q\hat{P}_j\rangle$ enter the equation of motion. The four-particle correlations are explicitly analyzed in Apps. B and C. We note that Eq. (3.14) presents only one of the several triplet equations. To close the set of equations at the singlet-doublet-triplet level, we present the remaining triplet equations in App. D. We find that the remaining triplet equations exhibit a very similar structure.

# 4 Second-Rung Emission

In Chapters 2 and 3, we have developed the theory for the resonance fluorescence of the QD-cavity systems. In this Chapter, we apply the theory to study the second-rung emission from the strongly-coupled semiconductor QDs for different excitation conditions. We are interested in determining the best excitation conditions with an external coherent light pulse to obtain the maximum second-rung emission intensity. These results are important for any strong-coupling experiment which tries to access the two-photon strong-coupling states.

Methodically, we numerically solve the full coupled set of Maxwell-Bloch equations, luminescence equations, squeezing equations, and triplet equations presented in Secs. 3.2-3.5. We evaluate the intensity spectrum by using the photon correlations $\Delta \langle \hat{B}_q^\dagger \hat{B}_q \rangle$ and sweep the pump frequency and pump intensity of the exciting coherent light pulse. This way, we can analyze the second-rung response as a function of the excitation properties. Another aspect of our analysis in this Chapter addresses a more theoretical issue and answers the question which correlations are important for the description of the second-rung emission. For this purpose, we carry out a switch on and off analysis of the triplet correlations.

We find that the second-rung emission is determined by the occupation of the two-photon state $|2\rangle$ in the pump pulse. This has clear consequences on the optimum excitation conditions. In particular, we obtain an optimum pump frequency and also an optimum pump intensity for the second-rung emission intensity. For low excitation intensities, the second-rung emission scales like the square of the input intensity, i.e. we obtain an $I^2$ dependence. This property has already been verified experimentally with atoms in high-quality cavities [25]. We also apply our theory to this atomic experiment and find a good agreement between the experiment and our theory. Furthermore, we demonstrate that we obtain the same second-rung pumping mechanism in the atomic and semiconductor QD systems. Finally, the more theoretical analysis of the role of correlations shows that the triplet correlations are important for an accurate theoretical description of the second rung in the intensity spectrum.

*Most of the results that we discuss in this Chapter are based on Papers [II-III].*

## 4.1 Intensity Spectrum

In this Section, we solve the full set of the singlet-doublet-triplet (sdt) equations presented in Sec. 3 and investigate the light emission from the optically excited QD-cavity system. We restrict the analysis to the QD-disk system Ref. [62]. As an initial condition for the fluorescence computation, we assume the QD to be unexcited. Furthermore, we
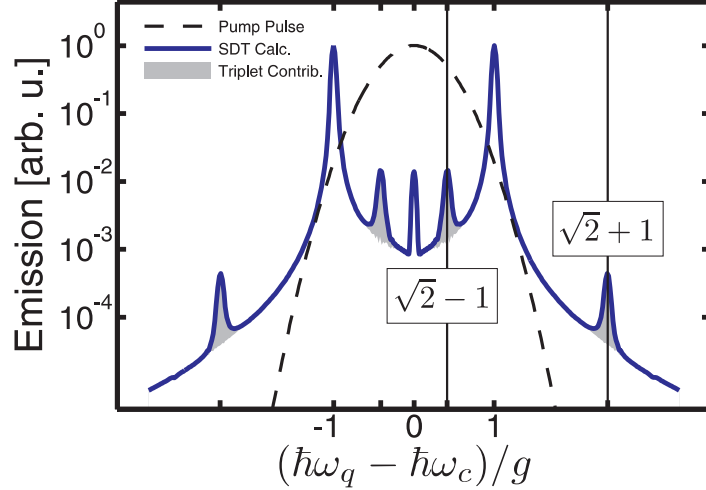
Figure 4.1: Resonance fluorescence spectrum of the QD-disk system ($\Delta = 0$). The dashed line is the mode distribution of the exciting pump pulse while the solid line is the resulting emission in the singlet-doublet-triplet (sdt) approximation. The triplet contributions are given by the grey shaded area. The emission from the second rung at $(\hbar\omega_q - \hbar\omega_c)/g = \sqrt{2} \pm 1$ is indicated by the vertical lines.

introduce an exciting pump pulse which is initially placed outside the cavity and which propagates perpendicularly to the quantum well. According to the Maxwell-Bloch equations Sec. 3.2, the QD polarization and population are built up. At the same time, the quantum-optical correlations are generated according to the luminescence equations Sec. 3.3 and lead to the re-emission. We can determine the emission intensity by the photon-number like two-photon correlations

$$I(\omega_q) \equiv \Delta\langle \hat{B}_q^\dagger \hat{B}_q \rangle. \tag{4.1}$$

Figure 4.1 presents the emission spectrum (solid line) for the zero dot-cavity detuning $\Delta \equiv E^{cv} - \hbar\omega_c$ after the excitation with a coherent pump pulse (dashed line) which is centered at the cavity frequency. The grey shaded area shows the triplet contributions of Sec. 3.5. We observe two main peaks at $(\hbar\omega_q - \hbar\omega_c)/g = \pm 1$ which are the usual vacuum Rabi peaks of the strong coupling [21]. Additionally, we obtain two peaks at $(\hbar\omega_q - \hbar\omega_c)/g = -(\sqrt{2} \pm 1)$ and another two peaks at $(\hbar\omega_q - \hbar\omega_c)/g = (\sqrt{2} \pm 1)$ which are marked by the vertical lines. These four additional resonances are attributed to the emission from the second rung of the Jaynes-Cummings ladder and are a clear signature for the true quantum emission [66, 67]. For the non-zero dot-cavity detuning, the general expression for the *second-rung emission frequencies* reads

$$\hbar\omega_{2\text{nd}} = \hbar\omega_c + (\sqrt{\Delta^2 + 8g^2} \pm \sqrt{\Delta^2 + 4g^2})/2. \tag{4.2}$$

In Fig. 4.1, we have also shown the contributions of the triplets to the emission spectrum, as shown by the grey shaded area. *We can clearly see that the second rung in the intensity spectrum needs a singlet-doublet-triplet description.*
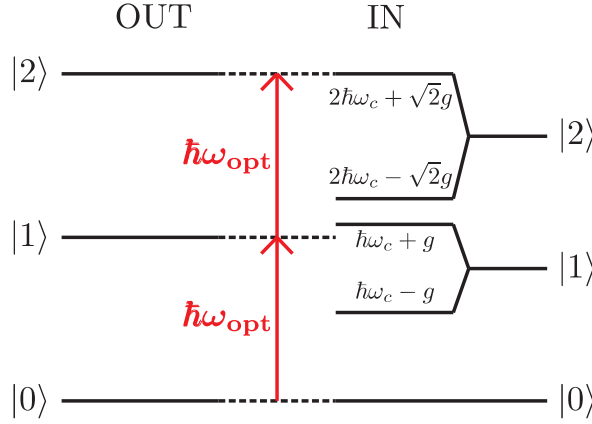
Figure 4.2: Second-rung pumping scheme. The dressed states of the strongly-coupled dot-cavity system are shown on the right while the Fock states within the pump field are shown on the left. The Fock-state $|2\rangle$ component within the pump is converted into the second-rung dressed state, leading to an optimum pumping frequency $\omega_{\text{opt}}$. According to Paper [III].

In Apps. B and C, we further analyze the role of the different clusters. There, we confirm that the second rung can be accurately described at the singlet-doublet-triplet level in the intensity spectrum while the second rung in the squeezing spectrum is already well reproduced at the singlet-doublet level. This is already a hint that the squeezing spectrum and also the related two-photon correlation spectrum $g^{(2)}$, introduced in Chapters 5 and 6, can show the second rung more clearly than the intensity spectrum.

## 4.2 Optimum Excitation Conditions

In the Jaynes-Cummings model [16], we obtain the second-rung wave function $|\psi_\pm\rangle \sim |1\rangle|\text{up}\rangle \pm |2\rangle|\text{down}\rangle$ where $|\text{up}\rangle$ ($|\text{down}\rangle$) denotes the excited (unexcited) dot and $|n\rangle$ denotes the Fock state with the photon number $n$. Thus, one can reach this state either by having an initially excited state and providing sufficient occupation of the $|1\rangle$ photon state or having an initially unexcited state while the light has a strong occupation of the state $|2\rangle$. Hence, as in the resonance fluorescence setup which we study here, the second-rung state can be reached by bringing the cavity directly into the Fock state $|2\rangle$ for an initially unexcited dot ($|\text{down}\rangle$). A resonant excitation of the dot-cavity system with a coherent laser, described by [68]

$$|\alpha\rangle = \sum_{n=0}^{\infty} \alpha^n/\sqrt{n!} \exp\left[-|\alpha|^2/2\right] |n\rangle \qquad (4.3)$$

with photon-number distribution

$$P_n = |\alpha|^{2n}\exp[-|\alpha|^2]/n!, \qquad (4.4)$$

always shows some occupation at $|2\rangle$. Especially, the $|2\rangle$ component of the external pump is selectively converted to the second-rung state $|\psi_+\rangle$ if its energy $E_{\text{pump}} = 2\hbar\omega$ matches the energy of the dressed dot-cavity state $E_{\text{dress}} = 2\hbar\omega_c + \sqrt{2}g$, leading to the condition $\hbar\omega = \hbar\omega_c + \frac{g}{\sqrt{2}}$ for zero dot-cavity detuning $\Delta$.

Figure 4.2 visualizes this second-rung pumping mechanism. Here, the light modes of the uncoupled light field are shown on the left hand side ('OUT') while the dressed states of the coupled system are depicted on the right hand side ('IN'). When the light propagates from the outside to inside of the cavity, the energy is essentially transferred from the 'OUT' modes to the dressed-states 'IN' modes. A perfect transfer follows only when the Fock state $|2\rangle$ in the pump is converted to the second-rung state. The transfer of the other $|n\rangle$ states is suppressed. For non-zero $\Delta$, the *optimum pump energy* is defined by

$$\hbar\omega_{\text{opt}} = \hbar\omega_c + (\Delta + \sqrt{\Delta^2 + 8g^2})/4. \tag{4.5}$$

This condition guarantees the selective excitation at the second rung with a probability determined by the two-photon state occupation

$$P_2 = \frac{|\alpha|^4}{2}\, e^{-|\alpha|^2} \tag{4.6}$$

within the external pump. We see from Fig. 4.2 that $\hbar\omega_{\text{opt}}$ is resonant only with the second rung such that we may selectively excite only that state. As a further property, we notice that the second-rung emission energy $\hbar\omega_{\text{2nd}}$ (4.2) and the optimum pump energy $\hbar\omega_{\text{opt}}$ (4.5) are generally different.

Figure 4.3 verifies the developed physical picture for the second-rung generation. Here, we analyze numerically the second-rung emission response as function of the excitation properties. Figure 4.3(a) presents the second-rung emission intensity $I(\omega_{\text{2nd}})$ as function of the pumping frequency $\omega$. The position of the lower second-rung emission frequency $\omega_{\text{2nd}}$ is indicated by the solid vertical line while the upper vacuum Rabi-peak position is given by the dashed vertical line. Indeed, we observe a sharp resonance at one optimum pumping frequency which is exactly in between the lower second-rung emission frequency and the upper vacuum Rabi peak, giving $\hbar\omega = \hbar\omega_c + \frac{g}{\sqrt{2}}$. This is in perfect agreement with Eq. (4.5) for $\Delta = 0$. Hence, we have verified the correct optimum pumping frequency.

To verify further the basic mechanism for the second-rung generation, Fig. 4.3(b) shows the second-rung emission intensity as function of the pumping field amplitude. The pump is centered at the optimum pumping frequency. Here, we observe that the second-rung emission increases with increasing pump strength, until it reaches a maximum and eventually decreases for strong excitation. In Fig. 4.3(c), we have also shown the corresponding two-photon state occupation $P_2$ in the pump pulse. Indeed, we observe that $P_2$ shows a maximum at the same optimum pumping field amplitude. *Hence, the second-rung emission is directly connected to the occupation of the two-photon state in the pump pulse.*

To illustrate further the critical dependence of the second-rung emission on the two-photon state occupation in the pump, we have shown the full photon-number distribution
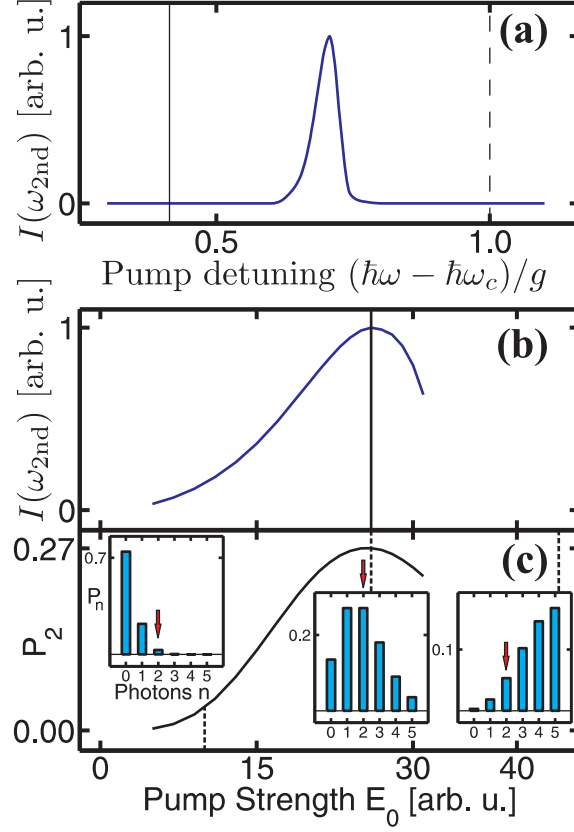
Figure 4.3: Second-rung emission properties, showing the optimum pumping frequency and optimum pumping intensity (QD-disk system, $\Delta = 0$). (a) Second-rung emission intensity as function of the pumping frequency. The lower second-rung emission frequency (upper vacuum Rabi peak) is indicated by a solid (dashed) vertical line. (b) Second-rung emission intensity as function of the pumping field amplitude. The maximum is marked by a vertical line. (c) Two-photon state occupation $P_2$ as function of the pumping field amplitude. The insets show the full photon-number distribution $P_n$ for three representative field amplitudes which are marked by the dashed vertical lines. The arrow indicates $P_2$ as a guide for the eye. According to Paper [III].

$P_n$ for three representative field amplitudes, as shown in the insets of Fig. 4.3(c). The arrow indicates $P_2$ as a guide for the eye. The first inset shows $P_n$ for a small field amplitude, the second shows it at the optimum field amplitude, and the third inset shows $P_n$ for strong excitation. We observe that $|2\rangle$ is only weakly occupied in the low intensity regime while it is maximally occupied at the optimum field amplitude. For strong excitation, the two-photon state becomes depleted and the occupations of the higher Fock states are dominating. Hence, it is important to match not only the optimum pumping frequency but also the optimum pumping intensity to guarantee a sufficient two-photon state occupation in the pump field and thus the second-rung emission. We also notice that the second-rung emission intensity scales like the square of the pumping intensity, as can be seen from Eq. (4.6) for $I \equiv |\alpha|^2$, thus

$$I(\omega_{2\text{nd}}) \sim P_2 \sim I^2 \tag{4.7}$$

holds in the low-intensity regime. The quadratic response of the second rung versus the input intensity Eq. (4.7) has already been verified experimentally with fixed atoms in high-quality cavities [25]. This experiment is discussed more thoroughly in the following.

## 4.3 Atomic Experiment

The experimental observation of the second rung has already been reported for atoms in high-quality cavities [24–26]. In Ref. [24], atoms were passing through a microcavity with a weak coherent light field injected and the atomic transition rate between the unexcited and excited state has been measured, which has shown a clear resonance at the vacuum Rabi peak and second rung. Very recently, one could demonstrate the existence of the second rung in an atom-cavity system via the direct spectroscopic measurement [25]. In this experiment, an atom has been fixed inside the cavity while an external laser has excited the coupled atom-cavity system. The transmitted emission intensity has been measured for varying cavity frequencies while fixing the laser frequency in resonance with the atomic transition energy. As a result, the experiment could demonstrate a resonance in the transmitted emission intensity at the optimum second-rung detuning frequency.

In the following, we show that we find the same second-rung pumping mechanism in the semiconductor QD and atomic systems. We apply our theory to the atom-cavity system studied in Ref. [25] by changing the cavity parameters and the dephasing conditions to the atomic system. We demonstrate that we can explain the observed experimental data.

In order to apply our developed theory to the atom-cavity system in Ref. [25], we need to change the dephasing conditions. In the atomic systems, we have the special dephasing conditions where a population decays twice as fast as a polarization. Hence, we have to include a dephasing $\gamma_f$ for the population in the equations of motion in a self-consistent manner. Analogous to a polarization, we need to damp all quantities which contain a population operator $\hat{f}_j^{cv}$ consistently, i.e. we introduce a dephasing $\gamma_f$
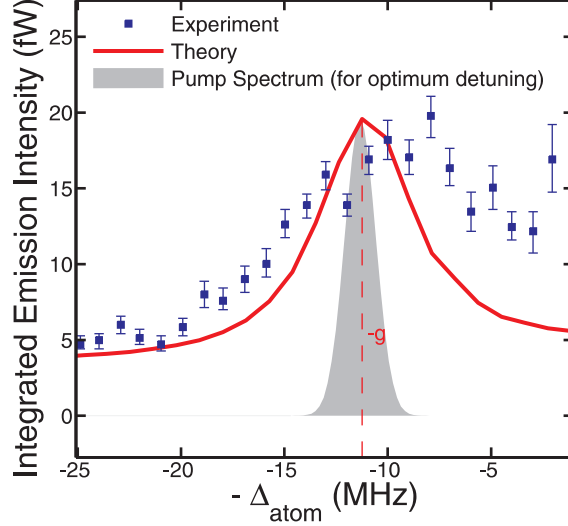
Figure 4.4: Second-rung resonance in the atomic system in the experiment and theory. The transmitted power as function of the detuning is shown. The dots with errorbars are experimental data (Ref. [25]) and the solid line is the cluster-expansion calculation at the singlet-doublet-triplet level. The theory curve is shifted upwards by 3.5 fW in order to fit the experimental data. The dashed vertical line marks the optimum second-rung detuning. The shaded area presents the mode distribution of the exciting pump pulse for the optimum detuning.

via

$$\mathrm{i}\hbar\,\frac{\partial}{\partial t}\,\langle\hat{O}\hat{f}_j^{cv}\rangle = -\mathrm{i}\gamma_f\langle\hat{O}\hat{f}_j^{cv}\rangle + \text{original terms,} \tag{4.8}$$

where $\hat{O}$ can be any operator which does not include a population operator $\hat{f}_j^{cv}$. Finally, we need to set $\gamma_f = 2\gamma_p$ for the atomic dephasing conditions with dephasing for the polarization to be $\gamma_P = 3$ MHz. The remaining relevant system parameters are the cavity half width $\gamma_{\mathrm{cav}} = 1.25$ MHz, the cavity frequency $\hbar\omega_c = 1.59$ eV, and the atomic dipole moment of $d = 1.12$ Å$e = 5.4$ D, resulting into the light-matter coupling constant $g = 11.2$ MHz.

Figure 4.4 shows the transmitted emission intensity as function of the detuning $-\Delta_{\mathrm{atom}} \equiv -(E_{\mathrm{atom}} - \hbar\omega_c)$ where $E_{\mathrm{atom}}$ denotes the atomic transition energy. The quadratic dots with errorbars are the experimental data in Ref. [25] and the solid line is our theoretical result. The shaded area presents the mode distribution of the exciting pump pulse for the optimum detuning which is marked by a dashed vertical line. The experiment shows a clear resonance in the spectrum of the transmitted light. *This experimentally observed resonance is the optimum frequency for the generation of the second-rung emission and is well reproduced by our theoretical calculation.* Thus, we can indeed explain the measured results. We notice that our numerical model includes effects up to the second rung such that the higher-rung resonances are absent in our calculation. In the experimental data, we identify such higher-rung contributions as a

weakly pronounced shoulder at the detuning $-\Delta_{\text{atom}} \approx -8$ MHz which originates from the third rung, as also explained in Ref. [25].

Concluding, we have applied our theory to the atomic system by changing the cavity and dephasing conditions. In this atomic system, it has been possible to experimentally detect the second rung directly in the intensity spectrum which reveals a clear resonance at the optimum second-rung detuning. This optimum detuning has already been identified in Sec. 4.2 and is in agreement with the QD analysis. *Hence, we find the same second-rung pumping mechanism in the semiconductor QD and atomic systems.* Furthermore, our theoretical results can indeed explain the experimental results and are in good agreement with the experimental data.

# 5 Second Rung via Two-Photon Correlations

In Chapter 4, we have identified the second-rung resonances in the intensity spectrum and the corresponding optimum excitation conditions. We have applied idealistic dephasing conditions for this analysis. However, the semiconductor QD systems contain significant dephasing originating from the QD-phonon and QD-wetting-layer coupling. In this Chapter, we therefore analyze the QD emission with realistic dephasing. We find that the realistic dephasing of the current samples washes out the second-rung resonances. In particular, the second rung is smeared out in the vacuum-Rabi background. Thus, it is difficult to observe the second rung directly in the intensity spectrum. Therefore, we have to follow another scheme. We follow the photon-statistics scheme for the observation of the second rung. We analyze the auto-correlated two-photon correlation $g_{\omega,\omega}^{(2)}$ spectrum which determines the probability of detecting two photons both having frequency $\omega$. In this Chapter, we show that the auto-correlated two-photon correlation $g_{\omega,\omega}^{(2)}$ spectrum yields a good method to observe the second rung.

Methodically, we solve again the resonance fluorescence equations and include realistic dephasing of the current samples. We apply the optimum excitation conditions and compute the intensity spectrum and also the two-photon correlation spectrum.

We find that the vacuum Rabi peaks are absent in the auto-correlated two-photon correlation $g_{\omega,\omega}^{(2)}$ spectrum. Moreover, we obtain a pronounced $g_{\omega,\omega}^{(2)} \gg 1$ resonance at the second rung. This second-rung resonance is robust enough against dephasing. We can explain this strongly enhanced $g^{(2)}$ resonance via the squeezing type field which is produced when the Fock-state $|2\rangle$ is added to the cavity. This strong bunching $g^{(2)} \gg 1$ due to the second rung has been observed experimentally in the atomic systems [26], demonstrating the feasibility of the proposed photon-statistics scheme.

*Most of the results that we discuss in this Chapter are based on Paper [II].*

## 5.1 Difficulties in Semiconductor QDs

In Chapter 3, we have discussed the relevant operator combinations and their time dynamics. We have included into the theory the dephasing which is due to the scattering processes present in the QDs. These scattering processes in QDs arise from coupling to extended continuum states of the surrounding semiconductor material as well as to phonons. In the following, we show that the discrete resonances of the second rung are clearly visible in the resonance fluorescence when scattering is low. These resonances smear out at realistic scattering levels of current QD-cavity setups. Thus, it is difficult
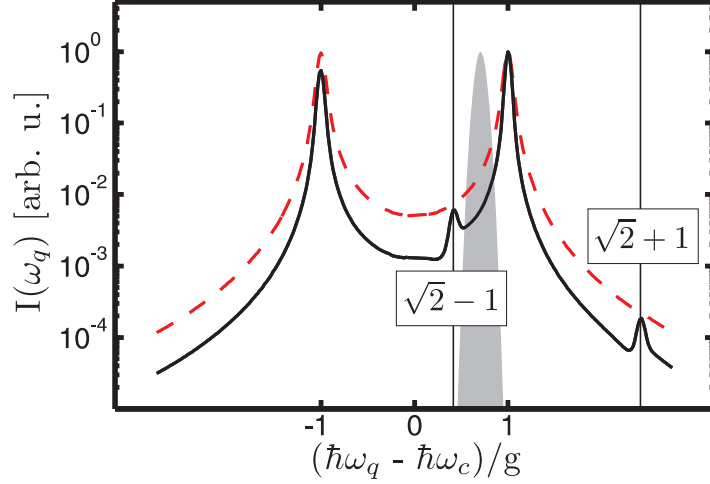
Figure 5.1: Influence of the dephasing on the resonance fluorescence spectrum (QD-disk system, $\Delta = 0$). For the optimum second-rung pumping conditions (grey shaded area), the emission spectrum is shown for the ideal low dephasing $\gamma_P = 0.06$ GHz (solid line) and elevated dephasing $\gamma_P = 0.4$ GHz (dashed line). The second-rung resonances are marked by the vertical lines. According to Paper [II].

to observe the second-rung signatures directly in the emitted spectrum of the fluorescent light. However, one can overcome this difficulty using photon-statistics spectroscopy, as demonstrated in Sec. 5.2.

Figure 5.1 shows the influence of the dephasing $\gamma_P$ on the observability of the second rung. In Fig. 5.1, the emission spectrum for the optimum second-rung pumping (grey shaded area) is presented for the ideal low dephasing (solid line) and elevated dephasing (dashed line). We observe that for the ideal case, the quantum rungs are clearly visible, i.e., the second-rung pumping induces true strong coupling effects in the QD system. However, the realistic dephasing of $\gamma_P = 0.4$ GHz washes out the most intriguing features in the standard experiments, as can be seen from the dashed line. We notice that the second rung is smeared out in the vacuum-Rabi background. To overcome this difficulty, we analyze next the possibility to observe true strong-coupling effects in the photon-correlations [69] $g^{(2)}$ and show that they can serve as more robust signatures.

## 5.2 Photon-Statistics Scheme

Following the early work of Brown and Twiss [70], the correlations between the photons of two light beams can be measured in a setup which is depicted in Fig. 5.2. In their original work [71], they have analyzed the properties of the coherent light from radio stars, but the experimental method can be applied to any light source with quantum statistics different from the coherent one. In this setup, the incident beam is converted into two beams via a beam splitter, as shown in Fig. 5.2. The two detectors for each
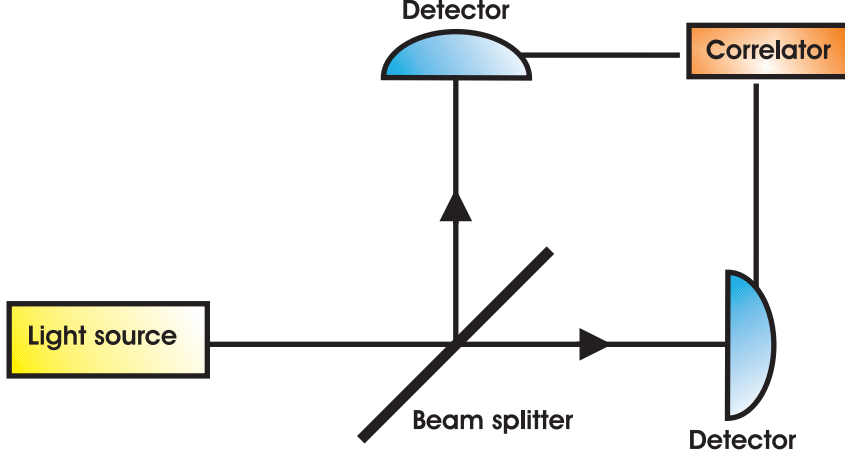
Figure 5.2: Schematic of the Hanbury-Brown-Twiss (HBT) setup for the photon-correlation measurement.

beam are measuring the intensity signal which is proportional to the number of the detected photons [72]. Finally, the intensity fluctuations of both detectors are correlated by analyzing the difference counts which yield the information about the two-photon correlations.

We can utilize the Heisenberg equations of motion, presented in Sec. 3, to compute the quantum statistics [43] $\langle [\hat{B}^\dagger]^J [\hat{B}]^K \rangle$, J and K integers, of the emitted light. Especially, we evaluate the auto-correlated two-photon correlation spectrum $g^{(2)}(\omega_q)$ which is defined by

$$g^{(2)}(\omega_q) \equiv g^{(2)}_{\omega_q, \omega_q} \equiv \frac{\langle \hat{B}^\dagger_q \hat{B}^\dagger_q \hat{B}_q \hat{B}_q \rangle}{\langle \hat{B}^\dagger_q \hat{B}_q \rangle^2}, \tag{5.1}$$

determining the probability of detecting two photons with frequency $\omega_q$ at the same time. We decompose $g^{(2)}$ into the different clusters and solve the full dynamics in the singlet-doublet-triplet approximation. We note that the formal decomposition into the clusters is discussed in more detail in Sec. 6.2 and App. B.

In order to gain some insights into the definition of the two-photon correlations, we first discuss a few simple examples in the following. We consider the case that only the cavity mode is relevant out of the many light modes, such that we may define the two-photon correlation via [68]

$$g^{(2)} \equiv \frac{\langle \hat{B}^\dagger \hat{B}^\dagger \hat{B} \hat{B} \rangle}{\langle \hat{B}^\dagger \hat{B} \rangle^2}. \tag{5.2}$$

For a better understanding of the following argumentation, we shortly review the basic results for common light sources which yield

$$g^{(2)} \begin{cases} < 1 & \text{antibunching} \\ > 1 & \text{bunching} \\ = 1 & \text{coherent state} \\ = 2 & \text{thermal light} \end{cases} . \tag{5.3}$$

In general, we have $g^{(2)} = 1$ for the coherent state and $g^{(2)} = 2$ for the thermal light. For $g^{(2)} < 1$, the light emission is *antibunched* while it is *bunched* for $g^{(2)} > 1$. The antibunching is the phenomena for which the probability to detect only one photon at a time is enhanced and has been created in the laboratory by Ref. [1] for the first time. Bunching, on the other hand, is the effect when the photon stream tends to come in clusters.

Let us now consider a light field state which is close to the vacuum state but has a finite Fock-state $|1\rangle$ occupation

$$|\psi\rangle_A = \sqrt{1 - \varepsilon^2}|0\rangle + \varepsilon|1\rangle. \tag{5.4}$$

Then, we obtain for the two-photon correlation $g^{(2)}_{|\psi\rangle_A} = 0$. In this case, the probability to detect two photons is zero. If we next consider the state which is close to the vacuum state but has finite Fock-state $|1\rangle$ and $|2\rangle$ components according to

$$|\psi\rangle_B = \sqrt{1 - \varepsilon^2 - \frac{\varepsilon^4}{2}}|0\rangle + \varepsilon|1\rangle + \frac{\varepsilon^2}{\sqrt{2}}|2\rangle, \tag{5.5}$$

we obtain $g^{(2)}_{|\psi\rangle_B} = \frac{1}{(1+\varepsilon^2)^2}$ which approaches $g^{(2)}_{|\psi\rangle_B} \to 1$ as $\varepsilon$ goes to zero. This is clear since $|\psi\rangle_B$ is almost a coherent state Eq. (4.3) when approaching the vacuum state. Otherwise, if we have a state close to the vacuum state with only a minor Fock-state $|2\rangle$ occupation as can be realized in the second-rung pumping scheme (Chapter 4)

$$|\psi\rangle_C = \sqrt{1 - \varepsilon^4}|0\rangle + \varepsilon^2|2\rangle, \tag{5.6}$$

the two-photon correlation yields $g^{(2)}_{|\psi\rangle_C} = \frac{1}{2\varepsilon^4}$ which diverges $g^{(2)}_{|\psi\rangle_C} \to \infty$ when $|\psi\rangle_C$ approaches the vacuum state. This simple example already shows that we can obtain gigantic $g^{(2)}$ values when we try to access the two-photon strong-coupling states. In the following, we further demonstrate and explain this phenomena.

In Figs. 5.3(a)-5.3(c), the solid line presents the computed $g^{(2)}(\omega_q)$ spectrum Eq. (5.1) for the different QD-cavity systems after the resonant second-rung pumping (shaded area). The energetic position of the second rung (upper vacuum-Rabi peak) is marked by the solid (dashed) vertical line. *Our results verify that all QD-cavity systems yield $g^{(2)}$ resonances with gigantic values close to $10^3$ at the second-rung energy.* This strongly enhanced $g^{(2)}$ follows from the fundamental properties of the resonant second-rung pumping which exclusively enables the Fock-state $|2\rangle$ to interact with the QD. Since the cavity initially is in the vacuum state, the addition of this Fock state essentially creates cavity light into the state $|0\rangle + \sqrt{P_2}|2\rangle$, similar to Eq. (5.6), which is a squeezed state with an appreciably small $P_2$. The same conclusion follows from Eq. (3.11) showing that the squeezing correlations $\Delta\langle \hat{B}\hat{B} \rangle$ are created in this process. It is well-known [73] that a squeezed state close to a vacuum produces a very large $g^{(2)}$ when it interacts with a fermionic system. Hence, the resonant second-rung pumping leads to the generation of squeezing which produces the gigantic $g^{(2)}$ resonance.

The large second-rung resonance in $g^{(2)}$ for small $\gamma_P$ has a critical consequence for elevated $\gamma_P$. *We show that the $g^{(2)}$ resonance remains clearly visible even for elevated*
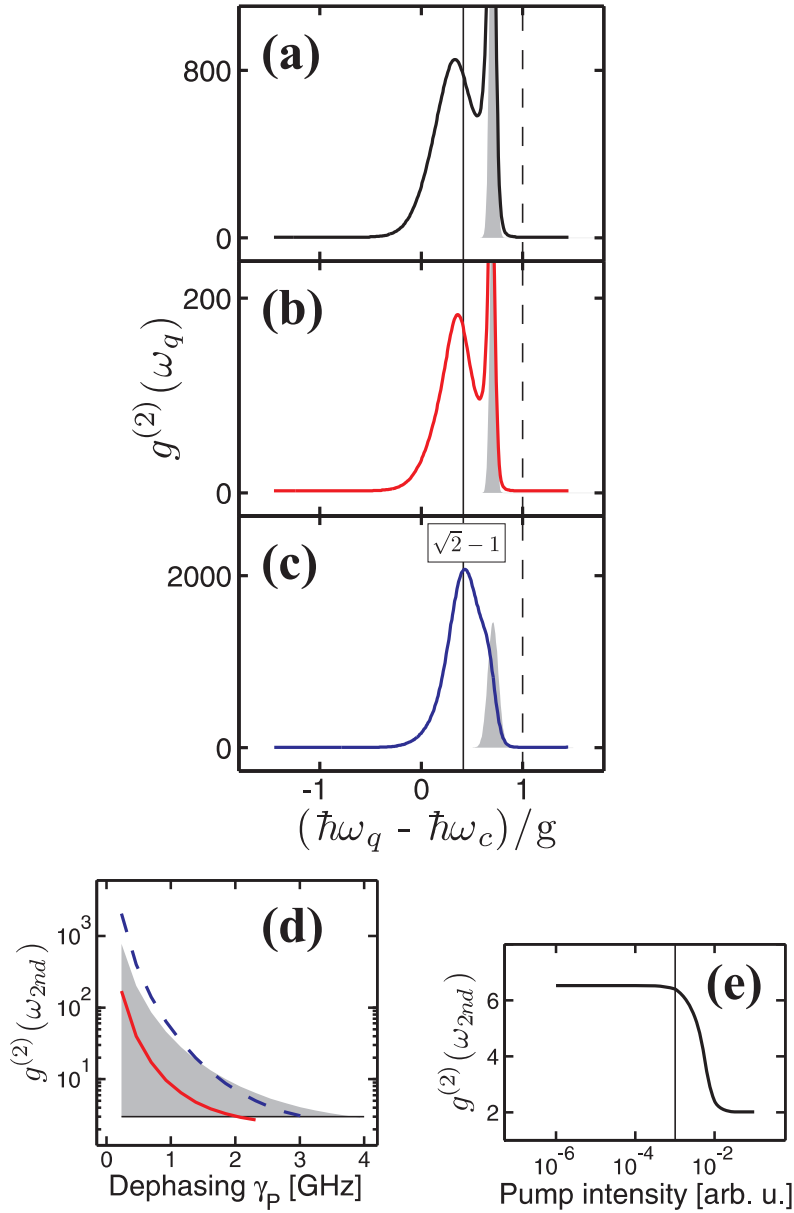
Figure 5.3: Photon correlation spectra $g^{(2)}$ for (a) QD-pillar, (b) QD-crystal, and (c) QD-disk system, at the time when the pump (shaded area) has its maximum ($\Delta = 0$ and $\gamma_P = 0.23$ GHz). (d) The corresponding $g^{(2)}$ at the second rung as function of dephasing for the QD-pillar (shaded), QD-crystal (solid), and QD-disk (dashed) systems. The horizontal line at $g^{(2)} = 3$ serves as visibility limit. (e) The pump-intensity dependence of $g^{(2)}$ at the second rung in the QD-pillar system ($\gamma_p = 2.3$ GHz). The vertical line marks the applied pump intensity for (a)-(d). According to Paper [II].

*dephasing* $\gamma_P$. Figure 5.3(d) presents for the three different QD-cavity systems the computed value of $g^{(2)}$ at the spectral position of the second rung as function of dephasing $\gamma_P$. The horizontal line at $g^{(2)} = 3$ serves as a visibility limit for the observability of the second rung. We see that for all cases, a clear resonance occurs even for dephasing values as large as $\gamma_P = 2$ GHz. This is considerably larger than the natural dot dephasing of $\gamma_P = 0.3$ GHz [74] and it is in the range of the broad cavity widths $\gamma_{\text{cav}} = 5 - 6$ GHz of the QD-pillar and QD-crystal cavity. From Figs. 5.3(a)-5.3(c), we also can see that there is no vacuum-Rabi peak in the $g^{(2)}$ spectrum. Thus, the $g^{(2)}$ spectroscopy provides a unique resonance at the second-rung position. Since the pump and the second-rung energies are different, the squeezing-generated $g^{(2)}$ feature around the pumping energy can always be distinguished from the actual second-rung peak.

Figure 5.3(e) presents the pump-intensity dependence of $g^{(2)}$ at the second rung for a large dephasing $\gamma_p = 2.3$ GHz. We notice that the $g^{(2)}$ signal remains unchanged in the low-intensity regime [26] but decreases for too strong excitation. Since the gigantic second-rung resonance in $g^{(2)}$ can be traced back to the property of a squeezed vacuum for which $g^{(2)}$ diverges as the vacuum is reached, $g^{(2)}$ gradually decreases for strong excitations. Thus, the resonant second-rung pumping has to be performed in the low-intensity regime which is defined such that $g^{(2)}(\omega_{\text{2nd}})$ approaches a constant value. The calculations in Figs. 5.3(a)-5.3(d) have been performed in this stable regime for a pump intensity which is marked by the vertical line in Fig. 5.3(e).

Hence, we could show that for the resonant second-rung pumping, the fluorescence spectrum shows intriguing strong-coupling effects which are clearly visible for small dephasing. For the realistic scattering levels, however, it is difficult to observe the second rung directly in the emitted spectrum. To analyze further the observability of the second rung, we have made use of the special structure of the Heisenberg equations of motion derived in Sec. 3. In particular, we have computed the two-photon statistics spectrum $g^{(2)}(\omega_q)$ which shows the second rung more clearly even at elevated dephasing levels, which should open a way for the experimental verification of true strong-coupling effects in the current QD-cavity systems.

# 6 Generation of Squeezing

In Chapter 5, we have seen that the auto-correlated two-photon correlations yield a more robust method than the intensity spectrum. In this Chapter, we introduce also the cross-correlated two-photon correlations and show that they yield a larger resonance than the auto correlations and provide a more favorable time dynamics. These insights are important for the experimental detection of the second-rung signal in the resonance fluorescence scheme.

We derive and present the resonance fluorescence equations for strong-coupling semiconductor quantum-dot systems. Even though we have already presented these equations in Chapter 3, we again repeat and highlight the insights focusing now on the generation of the squeezing. We follow the photoluminescence and the two-photon emission spectrum under realistic dephasing conditions.

Using the developed formalism, we also identify the origin of squeezed light in optically excited semiconductor systems. We find that the quantum statistics of matter is crucial for obtaining squeezed light. Discussing the general case of generic light-matter interaction, we conclude that the matter has to have fermionic statistics in order to generate squeezed-light emission.

To obtain detailed insights, we develop a reduced model which is compared with the full numerical calculations. We show that this simplified model yields very accurate results under typical strong-coupling conditions. We predict and analyze the appearance of the auto- and cross-correlation resonances in the two-photon emission spectrum of the fluorescent light. The auto- and cross-correlation resonances reveal the existence of the one- and two-photon strong-coupling states of Jaynes-Cummings ladder. We find that the auto-correlation resonance exists only transiently while the cross-correlation resonance can exist after the optical excitation process. Furthermore, the cross-correlation resonance is larger than the auto-correlation resonance. Hence, experimental efforts should be focused on the cross correlations which allow for a detection under steady-state conditions with an enhanced signal.

*Most of the results that we discuss in this Chapter are based on Paper [IV].*

## 6.1 Resonance Fluorescence Equations

Starting from the system Hamiltonian [60] for the strong-coupling semiconductor quantum-dot systems

$$
\begin{aligned}
\hat{H} &= E^c c_j^\dagger c_j + E^v v_j^\dagger v_j + \sum_q \hbar\omega_q \left( \hat{B}_q^\dagger \hat{B}_q + \frac{1}{2} \right) \\
&+ \sum_{qj} \left( \mathrm{i}\mathcal{F}_{q,j}^\star \hat{B}_q^\dagger \hat{P}_j - \mathrm{i}\mathcal{F}_{q,j} \hat{B}_q \hat{P}_j^\dagger \right),
\end{aligned}
\tag{6.1}
$$

we set up the Heisenberg equations of motion for the relevant operator combinations and apply the cluster-expansion approach [27–29, 43]. This way, we obtain a coupled set of integro-differential equations which, e.g., describe the quantum statistics of the fluorescent light from the strongly coupled system. In the following, we are mainly interested in the generation of squeezing under resonant-pumping conditions where the QD-cavity system is coherently excited via an external laser pump while the re-emitted light spectrum is detected.

Thus, we must evaluate the photon-number like correlations

$$
\Delta\langle \hat{B}_q^\dagger \hat{B}_{q'} \rangle \equiv \langle \hat{B}_q^\dagger \hat{B}_{q'} \rangle - \langle \hat{B}_q^\dagger \rangle \langle \hat{B}_{q'} \rangle
\tag{6.2}
$$

and the correlations in the two-photon emission

$$
\Delta\langle \hat{B}_q^\dagger \hat{B}_{q'}^\dagger \rangle \equiv \langle \hat{B}_q^\dagger \hat{B}_{q'}^\dagger \rangle - \langle \hat{B}_q^\dagger \rangle \langle \hat{B}_{q'}^\dagger \rangle.
\tag{6.3}
$$

These correlations represent the difference between the corresponding two-photon expectation value and its classical factorization. In general, $\Delta\langle \hat{B}_q^\dagger \hat{B}_{q'} \rangle$ determines the intensity of incoherent resonance fluorescence while $\Delta\langle \hat{B}_q^\dagger \hat{B}_{q'}^\dagger \rangle$ defines how much the emission is squeezed. For example, a single-mode light field with quadrature operators $\hat{x} \equiv (\hat{B} + \hat{B}^\dagger)/2$ and $\hat{y} \equiv (\hat{B} - \hat{B}^\dagger)/(2\mathrm{i})$ obeying the Heisenberg uncertainty relation $\Delta x \Delta y \geq 1/4$ shows quadrature squeezing $\Delta X$ ($\Delta Y$) [43]

$$
\Delta X^2 = \frac{1}{4} + \frac{1}{2}(\Delta\langle \hat{B}^\dagger \hat{B} \rangle + |\Delta\langle \hat{B}^\dagger \hat{B}^\dagger \rangle|),
\tag{6.4}
$$

$$
\Delta Y^2 = \frac{1}{4} + \frac{1}{2}(\Delta\langle \hat{B}^\dagger \hat{B} \rangle - |\Delta\langle \hat{B}^\dagger \hat{B}^\dagger \rangle|),
\tag{6.5}
$$

which is given by the maximum (minimum) of the quadrature fluctuation $\Delta x \equiv \sqrt{\langle \hat{x}^2 \rangle - \langle \hat{x} \rangle^2}$ ($\Delta y$). Thus, the emergent two-photon correlation $\Delta\langle \hat{B}^\dagger \hat{B}^\dagger \rangle$ is directly related to the squeezing in one quadrature direction. These correlations are typically built up in the resonance fluorescence configurations [44–46].

The dynamics of the intensity correlations follows from [28, 60] the luminescence

equations

$$i\hbar \frac{\partial}{\partial t} \Delta\langle \hat{B}_q^\dagger \hat{B}_{q'}\rangle = (\hbar\omega_{q'} - \hbar\omega_q)\,\Delta\langle \hat{B}_q^\dagger \hat{B}_{q'}\rangle + iN(\mathcal{F}_{q'}^\star \Delta\langle \hat{B}_q^\dagger \hat{P}\rangle$$
$$+ \mathcal{F}_q \Delta\langle \hat{B}_{q'}^\dagger \hat{P}\rangle^\star), \tag{6.6}$$

$$i\hbar \frac{\partial}{\partial t} \Delta\langle \hat{B}_q^\dagger \hat{P}\rangle = (E^{cv} - \hbar\omega_q - i\gamma_P)\,\Delta\langle \hat{B}_q^\dagger \hat{P}\rangle$$
$$+ \ i\mathcal{F}_q\left(f^e - |P|^2\right)$$
$$- \ \left(1 - f^e - f^h\right) i \sum_{q'} \mathcal{F}_{q'} \Delta\langle \hat{B}_q^\dagger \hat{B}_{q'}\rangle$$
$$+ \ d\langle E^{(+)}\rangle \Delta\langle \hat{B}_q^\dagger (c^\dagger c - v^\dagger v)\rangle + \Delta\langle 3\rangle, \tag{6.7}$$

while the squeezing dynamics follows from

$$i\hbar \frac{\partial}{\partial t} \Delta\langle \hat{B}_q^\dagger \hat{B}_{q'}^\dagger\rangle = -(\hbar\omega_q + \hbar\omega_{q'})\,\Delta\langle \hat{B}_q^\dagger \hat{B}_{q'}^\dagger\rangle$$
$$+ \ iN\left(\mathcal{F}_{q'}\Delta\langle \hat{B}_q^\dagger \hat{P}^\dagger\rangle + \mathcal{F}_q \Delta\langle \hat{B}_{q'}^\dagger \hat{P}^\dagger\rangle\right), \tag{6.8}$$

$$i\hbar \frac{\partial}{\partial t} \Delta\langle \hat{B}_q^\dagger \hat{P}^\dagger\rangle = -(\hbar\omega_q + E^{cv} + i\gamma_P)\,\Delta\langle \hat{B}_q^\dagger \hat{P}^\dagger\rangle$$
$$- \ i\mathcal{F}_q P^\star P^\star$$
$$- \ \left(1 - f^e - f^h\right) i \sum_{q'} \mathcal{F}_{q'}^\star \Delta\langle \hat{B}_q^\dagger \hat{B}_{q'}^\dagger\rangle + \Delta\langle 3\rangle$$
$$- \ d\langle E^{(-)}\rangle \Delta\langle \hat{B}_q^\dagger (c^\dagger c - v^\dagger v)\rangle. \tag{6.9}$$

We assume here that the QDs have an identical transition energy $E^{cv}$ which produces $N$ as the number of QDs that are optically pumped via the coherent light field $\langle E\rangle = \langle E^{(-)}\rangle + \langle E^{(+)}\rangle$. Here, we applied the rotating-wave approximation such that only the $\langle E^{(-)}\rangle \sim e^{i\omega_q t}$ part of the classical field appears in Eq. (6.9) while $\langle E^{(+)}\rangle \sim e^{-i\omega_q t}$ can be ignored due to its rapid oscillations. The appearing $\Delta\langle 3\rangle$ symbol denotes three-particle correlations. We omitted the specific QD index $j$ due to our idealizing assumption of electronically uncoupled identical dots such that the sum over the dot index $j$ just leads to a prefactor $N$. We stress that we consider the case $N = 1$ in the following investigations, i.e. we describe the experimentally relevant situation in which a *single* dot couples to a cavity resonance.

The *resonance fluorescence equations* (6.6)-(6.9) contain homogeneous parts proportional to $\hbar\omega_q$ which stem from the uncoupled light field. The coherent light $\langle E\rangle = \langle \hat{E}(r_j)\rangle = \sum_q i\mathcal{E}_q u_q(r_j)\langle \hat{B}_q\rangle + \text{c.c.}$ excites the QDs and generates polarization $P \equiv \langle v^\dagger c\rangle$, electron densities $f^e \equiv \langle c^\dagger c\rangle$, and hole densities $f^h \equiv 1 - \langle v^\dagger v\rangle$ all of which constitute sources for the spontaneous emission. We note that the spontaneous source term $f^e - |P|^2$ in the luminescence equation (6.7) can be cast into the format $f^e f^h + \Delta\langle c^\dagger v^\dagger cv\rangle$ where the two-particle correlation $C_X \equiv \Delta\langle c^\dagger v^\dagger cv\rangle$ can be exactly solved for the case of a strict two-level system, resulting into $f^e - |P|^2$. However, if electrons and holes behave independently as in carrier-capture processes, we have to solve the two-particle

correlations $C_X$ separately [29, 75]. In the resonance fluorescence equations (6.6)-(6.9), the stimulated contributions $\sum_{q'} \mathcal{F}_{q'} \Delta \langle \hat{B}_q^\dagger \hat{B}_{q'} \rangle$ together with the photon-density correlations $\Delta \langle \hat{B}_q^\dagger c^\dagger c \rangle$ and the three-particle correlations $\Delta \langle 3 \rangle$ produce the different rungs of Jaynes-Cummings ladder.

We note that the equations of motion of the photon-density correlations $\Delta \langle \hat{B}_q^\dagger c^\dagger c \rangle$ are structurally similar to the luminescence and squeezing equations (6.6)-(6.9). In the full numerical calculation at the singlet-doublet-triplet level, we compute all the correlations up to the three-particle level, i.e. the $\Delta \langle 3 \rangle$ terms are explicitly included. Furthermore, the coupling between the light field and the QDs is evaluated self-consistently via the Maxwell-Bloch equations. To account for the dissipative effect of the semiconductor wetting-layer material, we include dephasing for all polarization-dependent quantities, as can be seen from the homogeneous part of Eqs. (6.7) and (6.9) where the dephasing constant $\gamma_P$ enters.

As an example of our numerical evaluations, we present in Fig. 6.1 the photoluminescence (PL) spectrum of the strongly-coupled system after excitation with a coherent pump pulse. To obtain these results, we have numerically solved the full resonance fluorescence equations (6.6)-(6.9) at the singlet-doublet-triplet level assuming a cavity-quality factor $Q = 24000$, resonant conditions $\hbar \omega_c = E^{cv}$, light-matter coupling constant $g = 8.8$ GHz, and dephasing constant $\gamma_P = 0.6$ GHz. Figure 6.1(a) presents the $q, q'$ dependence of the intensity correlations $\Delta \langle \hat{B}_q^\dagger \hat{B}_{q'} \rangle$. The horizontal and vertical lines at $\hbar \omega_c + (\sqrt{2} - 1)g$ ($\hbar \omega_c \pm g$) indicate the second-rung (first-rung) resonances of the Jaynes-Cummings ladder. We assume that the coherent pump pulse is tuned to the optimum second-rung excitation energy $\hbar \omega_c + (1/\sqrt{2})g$ (dashed vertical line) based on our original prediction [60]. In Fig. 6.1(b), we clearly see the vacuum-Rabi splitting in the fluorescent light spectrum with two main peaks at the first-rung resonances $\hbar \omega_c \pm g$. Even though this double-peaked spectrum is consistent with the assumption of strong-coupling conditions, no additional second-rung resonances are seen in the intensity spectrum due to the assumed realistic broadening effects.

Equations (6.8) and (6.9) describing the *squeezing dynamics* show that the squeezing correlations $\Delta \langle \hat{B}_q^\dagger \hat{B}_{q'}^\dagger \rangle$ couple to the photon-polarization correlations $\Delta \langle \hat{B}_q^\dagger \hat{P}^\dagger \rangle$. These correlations are spontaneously generated via the squeezing source term $-\mathrm{i} \mathcal{F}_q P^\star P^\star$ in Eq. (6.9). To investigate the origin of the squeezing source term [76], we formally replace our composite fermionic QD-polarization operator $\hat{P}^\dagger$ by a general polarization operator denoted by $\hat{\mathcal{P}}^\dagger$ and write the general light-matter interaction Hamiltonian as

$$\hat{\mathcal{H}}_{\mathrm{int}} = \sum_q \left( \mathrm{i} \mathcal{F}_q^\star \hat{B}_q^\dagger \hat{\mathcal{P}} - \mathrm{i} \mathcal{F}_q \hat{B}_q \hat{\mathcal{P}}^\dagger \right). \tag{6.10}$$

The two-photon emission then follows from

$$\begin{aligned}
\mathrm{i} \hbar \, & \frac{\partial}{\partial t} \, \Delta \langle \hat{B}_q^\dagger \hat{B}_{q'}^\dagger \rangle \\
= \, & - \left( \hbar \omega_q + \hbar \omega_{q'} \right) \Delta \langle \hat{B}_q^\dagger \hat{B}_{q'}^\dagger \rangle \\
& + \, \mathrm{i} N \left( \mathcal{F}_{q'} \Delta \langle \hat{B}_q^\dagger \hat{\mathcal{P}}^\dagger \rangle + \mathcal{F}_q \Delta \langle \hat{B}_{q'}^\dagger \hat{\mathcal{P}}^\dagger \rangle \right),
\end{aligned} \tag{6.11}$$
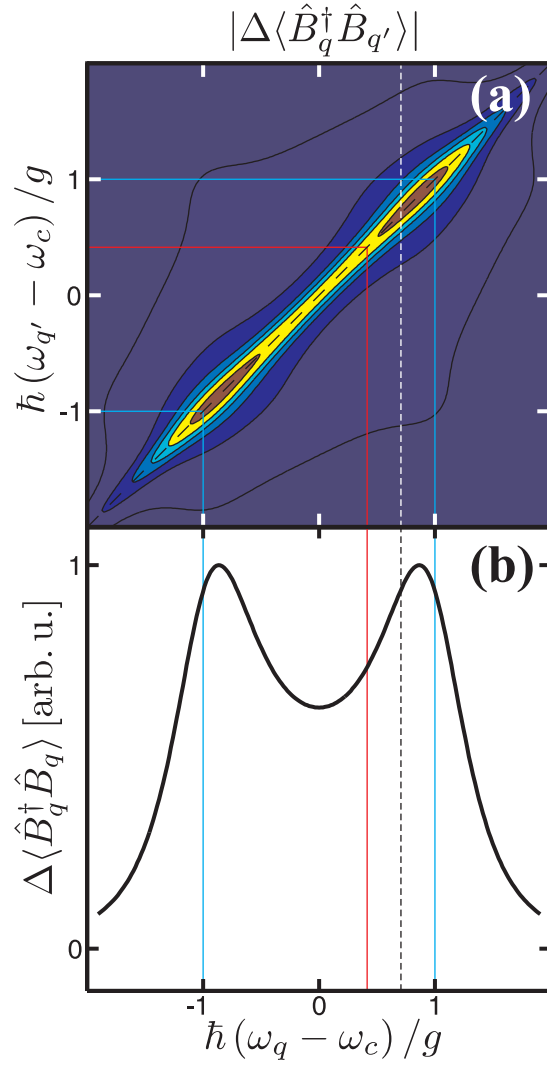
Figure 6.1: Full numerical calculation of the photoluminescence (PL) spectrum $\Delta \langle \hat{B}_q^\dagger \hat{B}_{q'} \rangle$, showing the vacuum-Rabi splitting (cavity-quality factor $Q = 24000$). (a) PL spectrum $|\Delta \langle \hat{B}_q^\dagger \hat{B}_{q'} \rangle|$ as function of $q, q'$ in a contour plot. (b) Intensity spectrum $\Delta \langle \hat{B}_q^\dagger \hat{B}_q \rangle$. In all cases, the horizontal and vertical lines at $\hbar \omega_c + (\sqrt{2} - 1)g$ $(\hbar \omega_c \pm g)$ indicate the second-rung (first-rung) resonances of the Jaynes-Cummings ladder. The pump is tuned to $\hbar \omega_c + (1/\sqrt{2})g$ as indicated by the dashed vertical line. From Paper [IV].

which is formally equivalent to Eq. (6.8). To identify the source term in the photon-polarization correlations $\Delta\langle\hat{B}_q^\dagger\hat{\mathcal{P}}^\dagger\rangle$, we evaluate the commutator between the photon operator $\hat{B}_q^\dagger$ and the general interaction Hamiltonian $\hat{\mathcal{H}}_{\mathrm{int}}$, yielding

$$
\begin{aligned}
\mathrm{i}\hbar\frac{\partial}{\partial t}\ \Delta\langle\hat{B}_q^\dagger\hat{\mathcal{P}}^\dagger\rangle\Big|_{\mathrm{int}}^{\mathrm{phot}} & \\
\equiv\ & \langle\left[\hat{B}_q^\dagger,\hat{\mathcal{H}}_{\mathrm{int}}\right]_-\hat{\mathcal{P}}^\dagger\rangle - \langle\left[\hat{B}_q^\dagger,\hat{\mathcal{H}}_{\mathrm{int}}\right]_-\rangle\langle\hat{\mathcal{P}}^\dagger\rangle \\
=\ & \mathrm{i}\mathcal{F}_q\left[\langle\hat{\mathcal{P}}^\dagger\hat{\mathcal{P}}^\dagger\rangle - \langle\hat{\mathcal{P}}^\dagger\rangle\langle\hat{\mathcal{P}}^\dagger\rangle\right].
\end{aligned}
\tag{6.12}
$$

Here, the spontaneous source term is given by $\mathrm{i}\mathcal{F}_q\left[\langle\hat{\mathcal{P}}^\dagger\hat{\mathcal{P}}^\dagger\rangle - \langle\hat{\mathcal{P}}^\dagger\rangle\langle\hat{\mathcal{P}}^\dagger\rangle\right]$ regardless of the operator properties of $\hat{\mathcal{P}}^\dagger$. If the polarization operator $\hat{\mathcal{P}}$ obeys bosonic commutation relations, we obtain

$$
\mathrm{i}\hbar\frac{\partial}{\partial t}\left[\langle\hat{\mathcal{P}}^\dagger\hat{\mathcal{P}}^\dagger\rangle - \langle\hat{\mathcal{P}}^\dagger\rangle\langle\hat{\mathcal{P}}^\dagger\rangle\right]_{\mathrm{int}}^{\mathrm{bos}} = -2\mathrm{i}\sum_q\mathcal{F}_q^\star\Delta\langle\hat{B}_q^\dagger\hat{\mathcal{P}}^\dagger\rangle.
\tag{6.13}
$$

This yields a closed set of equations which contain only two-particle correlations. Hence, the quantum statistics of light and bosonic matter are mapped onto another, but squeezed light cannot be generated from bosonic matter if squeezing is not already present initially.

This situation is very different if the matter excitations exhibit fermionic properties like the QD electrons do. As a consequence of the Pauli exclusion principle, we have

$$
\langle\hat{\mathcal{P}}^\dagger\hat{\mathcal{P}}^\dagger\rangle^{\mathrm{ferm}} = 0
\tag{6.14}
$$

such that the squeezing source simplifies into

$$
\left[\langle\hat{\mathcal{P}}^\dagger\hat{\mathcal{P}}^\dagger\rangle - \langle\hat{\mathcal{P}}^\dagger\rangle\langle\hat{\mathcal{P}}^\dagger\rangle\right]^{\mathrm{ferm}} = -\langle\hat{\mathcal{P}}^\dagger\rangle\langle\hat{\mathcal{P}}^\dagger\rangle.
\tag{6.15}
$$

The squeezing in fermionic matter systems thus follows from the nonlinear polarization source $\mathcal{P}^\star\mathcal{P}^\star$ resulting from the fermionic character of $\hat{\mathcal{P}}^\dagger$. Hence, squeezing in fermionic systems can be created spontaneously whenever a polarization is present in the system.

In the resonance fluorescence scheme, the light pulse, depicted in Fig. 6.2(a), excites the matter and produces a polarization as shown in Fig. 6.2(b). Due to the fermionic character of the polarization, we have a spontaneous source for the photon-polarization correlations. This finally leads to the generation of squeezed light Fig. 6.2(c). *In this process, the quantum statistics of matter is crucial to obtain squeezed light. If the light-matter interaction can be described via the general interaction Hamiltonian (6.10), the matter has to exhibit fermionic structure in order to generate squeezed light.*

## 6.2 Analytic Solution for Resonance Fluorescence

In App. A.1, we develop a reduced model to describe the two-photon emission spectrum. The reduced model allows us to gain deep insights and is solved analytically in App. A.2. In the following, we discuss the results obtained from this analysis.
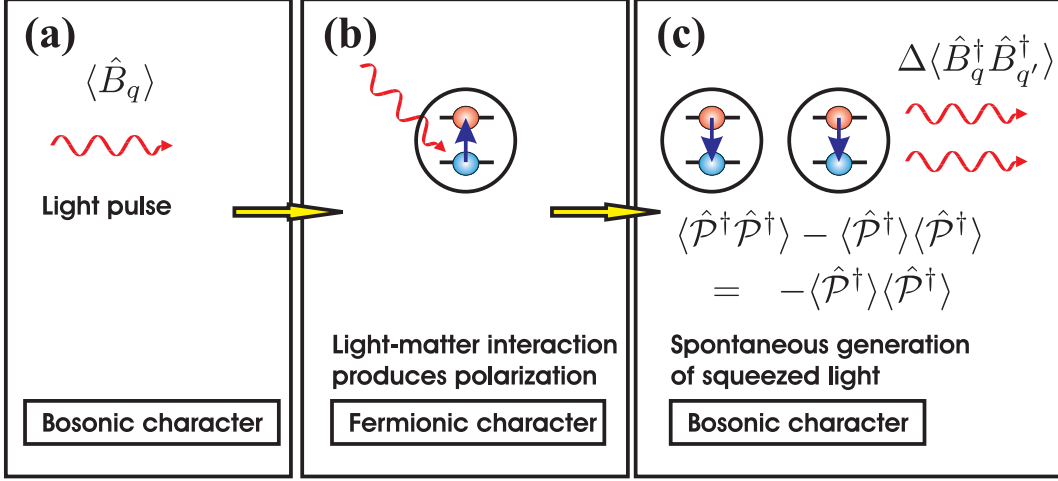
Figure 6.2: Mechanism for the generation of squeezed light. The light pulse (a) excites the matter and produces a polarization (b). The fermionic character of the polarization is a spontaneous source term for the generation of squeezed light (c). According to Ref. [76], Fig. 5.2.

Figure 6.3 presents the analytic solution of the two-photon emission $\Delta\langle\hat{B}_q^\dagger\hat{B}_{q'}^\dagger\rangle$ in the resonance fluorescence. Here, we used $\hbar\omega_c = E^{cv}$, the light-matter coupling constant $g = 8.8$ GHz, and the dephasing constant $\gamma_P = 0.6$ GHz. Figure 6.3(a) shows the generated two-photon signals (dashed, solid) after coherent excitation with a pump pulse (shaded area). In the following, we determine the auto- as well as cross-correlation signals that are defined from $\Delta\langle\hat{B}_\omega^\dagger\hat{B}_{\omega'}^\dagger\rangle$ with equal ($\omega = \omega'$) and different ($\omega \neq \omega'$) frequencies, respectively, in the correlation measurement. More specifically, we define the *auto-correlation signal* (dashed, scaled) $|\Delta\langle\hat{B}_{\hbar\omega_{2\mathrm{nd}}}^\dagger\hat{B}_{\hbar\omega_{2\mathrm{nd}}}^\dagger\rangle|$ at the second-rung to first-rung transition frequency

$$\hbar\omega_{2\mathrm{nd}} \equiv \hbar\omega_c + (\sqrt{2}-1)g. \tag{6.16}$$

Additionally, we monitor the *cross-correlation signal* (solid) $|\Delta\langle\hat{B}_{\hbar\omega_{1\mathrm{st}}}^\dagger\hat{B}_{\hbar\omega_{2\mathrm{nd}}}^\dagger\rangle|$ between the $\hbar\omega_{2\mathrm{nd}}$ energy and the first rung

$$\hbar\omega_{1\mathrm{st}} \equiv \hbar\omega_c + g. \tag{6.17}$$

In Fig. 6.4, the second-rung pumping scheme is shown together with a schematic presentation of the introduced auto- and cross-correlation signals. Here, the $|\Delta\langle\hat{B}_{\hbar\omega_{2\mathrm{nd}}}^\dagger\hat{B}_{\hbar\omega_{2\mathrm{nd}}}^\dagger\rangle|$ measures correlations between the second and first rung while $|\Delta\langle\hat{B}_{\hbar\omega_{1\mathrm{st}}}^\dagger\hat{B}_{\hbar\omega_{2\mathrm{nd}}}^\dagger\rangle|$ defines correlations between the second rung, first rung, and ground state.

In Fig. 6.3, we observe that both auto and cross correlations are built up via the pump. *While the auto correlation is smaller than the cross correlation and decays with time after the pump has been gone, the cross correlation survives and reaches a steady state. Thus, the auto correlation can be observed only transiently while the cross correlation exists also in the long-time limit.* Consequently, the auto correlation stems from modes $E_j^\pm$,
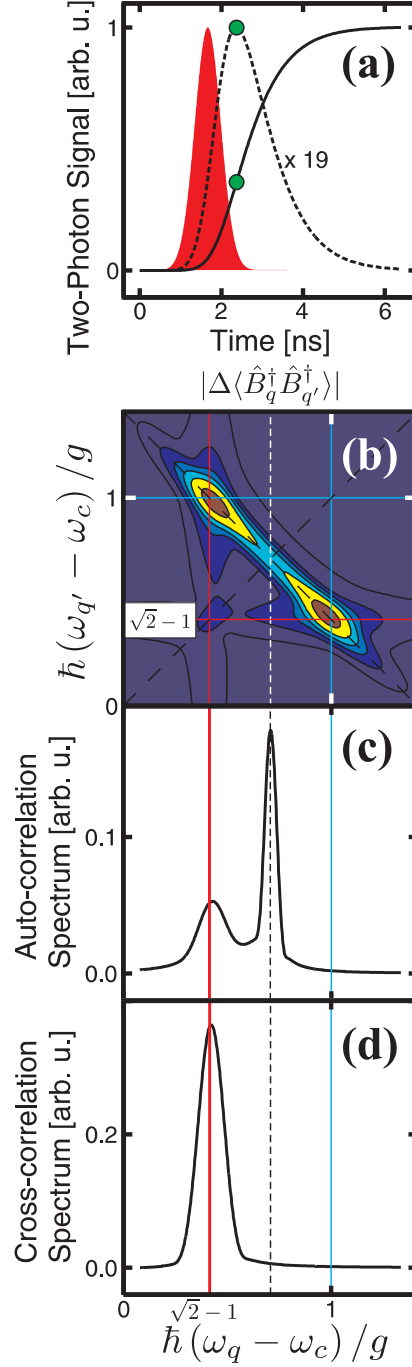
Figure 6.3: *Analytic solution* of the two-photon emission $\Delta\langle\hat{B}_q^\dagger\hat{B}_{q'}^\dagger\rangle$ in the resonance fluorescence. (a) Dynamics of auto (dashed line, scaled) and cross (solid line) correlations after coherent excitation (shaded area). The points mark the snapshot time for frames (b)-(d). (b) Full dependence of two-photon emission on $q, q'$. (c) Auto-correlation spectrum $|\Delta\langle\hat{B}_q^\dagger\hat{B}_q^\dagger\rangle|$. (d) Cross-correlation spectrum $|\Delta\langle\hat{B}_{\hbar\omega_{1\mathrm{st}}}^\dagger\hat{B}_q^\dagger\rangle|$. In all cases, the horizontal and vertical lines at $\hbar\omega_c + (\sqrt{2}-1)g$ ($\hbar\omega_c + g$) indicate the second-rung (first-rung) resonances of the Jaynes-Cummings ladder. The pump is tuned to $\hbar\omega_c + (1/\sqrt{2})g$ as indicated by the dashed vertical line. From Paper [IV].

Figure 6.4: Schematic presentation of the auto and cross correlations in the second-rung
pumping scheme.

introduced in Eqs. (A.39)-(A.43), while the cross correlation is determined by the long-
living mode $E_1$ (A.38). In the language of Ref. [77], we note that the auto correlation
can be identified as polarization-like quantity which decays on a time scale defined by
the dephasing $\gamma_P$ while the cross correlation behaves density-like and can exist after the
excitation process.

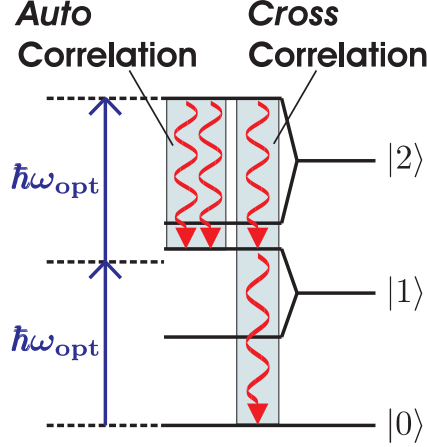Figure 6.3(b) shows the full $q, q'$ dependence of the two-photon emission $|\Delta\langle\hat{B}_q^\dagger\hat{B}_{q'}^\dagger\rangle|$
at the time $t = 2.4$ ns marked by a circle in Figure 6.3(a). The horizontal and verti-
cal lines at $\hbar\omega_{2\text{nd}}$ ($\hbar\omega_{1\text{st}}$) indicate the second-rung (first-rung) transition energies. The
coherent pump pulse excites the system at the optimum second-rung excitation energy
$\hbar\omega_c + (1/\sqrt{2})g$, as indicated by the dashed vertical line. The two-photon emission spec-
trum $|\Delta\langle\hat{B}_q^\dagger\hat{B}_{q'}^\dagger\rangle|$ Fig. 6.3(b) shows that two symmetric peaks at the cross correlations
are dominating. Additionally, a contribution at the auto correlation of second-rung
transition energy can be identified.

To clarify these observations further, Fig. 6.3(c) shows the auto-correlation spectrum
$|\Delta\langle\hat{B}_q^\dagger\hat{B}_q^\dagger\rangle|$ while Fig. 6.3(d) shows the cross-correlation spectrum $|\Delta\langle\hat{B}_{\hbar\omega_{1\text{st}}}^\dagger\hat{B}_q^\dagger\rangle|$ with
fixed energy of one photon to $\hbar\omega_{1\text{st}}$. From Fig. 6.3(c), we conclude that the auto-
correlation spectrum $|\Delta\langle\hat{B}_q^\dagger\hat{B}_q^\dagger\rangle|$ demonstrates the appearance of the second-rung at
$\hbar\omega_q = \hbar\omega_{2\text{nd}}$, marked by the lowest vertical line, and the pump peak. Unlike the emission
spectrum, see Fig. 6.1, $\Delta\langle\hat{B}_q^\dagger\hat{B}_q^\dagger\rangle$ does not contain a peak at the first rung, which allows
for a direct detection of the second rung even for an appreciable dephasing [60]. However,
the second-rung resonance in the auto-correlation spectrum is visible only transiently as
shown by the dashed line in Fig. 6.3(a).

In Fig. 6.3(d), we notice that the cross-correlation spectrum indeed displays a pro-
nounced resonance at the second-rung transition energy marked by the lowest vertical
line. Thus, the correlations $|\Delta\langle\hat{B}_{\hbar\omega_{1\text{st}}}^\dagger\hat{B}_q^\dagger\rangle|$ produce a peak only at the second-rung energy
$\hbar\omega_q = \hbar\omega_{2\text{nd}}$ which makes it even a better candidate for the unambiguous detection of
the second rung with realistic QD systems. Note that the dephasing we have used is the
same dephasing as in Fig. 6.1 and yet the second-rung resonance remains distinctively

pronounced. The second-rung resonance in the cross-correlation spectrum builds up and reaches a steady state as shown by the solid line in Fig. 6.3(a). Moreover, the second-rung resonance appearing in the cross-correlation spectrum is also clearly visible in the full $q, q'$ dependence of the two-photon emission spectrum $|\Delta\langle \hat{B}_q^\dagger \hat{B}_{q'}^\dagger \rangle|$ Fig. 6.3(b). The cross-correlation peak is also about 7 times higher than the second-rung signature in the auto correlation such that it provides us with the most sensitive feature to demonstrate true strong coupling in QD microcavities.

In App. A.3, we show that the cross-correlation peak is given by

$$|\Delta\langle \hat{B}_{\hbar\omega_{1\mathrm{st}}}^\dagger \hat{B}_{\hbar\omega_{2\mathrm{nd}}}^\dagger \rangle|(t \to \infty)$$

$$= |\mathcal{F}_{\hbar\omega_{1\mathrm{st}}} \mathcal{F}_{\hbar\omega_{2\mathrm{nd}}}| N \sqrt{\frac{4\left(\frac{g^2}{\gamma_P^2}+1\right)^2 + 2\frac{g^2}{\gamma_P^2}}{\gamma_P^2 + 4g^2}} \frac{s_0\sqrt{\pi}\Delta T}{\hbar}$$

$$\times \exp\left[-(\sqrt{2}-2\Omega_p)^2 \frac{g^2 \Delta T^2}{4\hbar^2}\right]. \tag{6.18}$$

It is interesting to note that under steady-state conditions the width of the cross-correlation peak can be controlled via the pump duration $\Delta T$ which enters the Gaussian in Eq. (6.18). A longer pump pulse thus leads to a sharper emission pattern. Moreover, we find that the peak height depends on the pump frequency $\Omega_p$, which identifies the optimum pump frequency [60] $\Omega_p^{\mathrm{opt}} = 1/\sqrt{2}$.

The two-photon emission spectrum $\Delta\langle \hat{B}_\omega^\dagger \hat{B}_{\omega'}^\dagger \rangle$ can be experimentally accessed by measuring the two-photon correlations [60, 69]

$$g_{\omega,\omega'}^{(2)} \equiv \frac{\langle \hat{B}_\omega^\dagger \hat{B}_{\omega'}^\dagger \hat{B}_{\omega'} \hat{B}_\omega \rangle}{\langle \hat{B}_\omega^\dagger \hat{B}_\omega \rangle \langle \hat{B}_{\omega'}^\dagger \hat{B}_{\omega'} \rangle}. \tag{6.19}$$

The correlations $g_{\omega,\omega'}^{(2)}$ determine the probability to detect two photons with frequency $\omega$ and $\omega'$ at the same time. Using the cluster expansion for incoherent fields, i.e. $\langle \hat{B} \rangle = 0$, we obtain an exact relation between the generation of the squeezed-light emission $\Delta\langle \hat{B}_\omega^\dagger \hat{B}_{\omega'}^\dagger \rangle$ and the two-photon correlations $g_{\omega,\omega'}^{(2)}$

$$g_{\omega,\omega'}^{(2)} = 1 + \frac{|\Delta\langle \hat{B}_\omega^\dagger \hat{B}_{\omega'}^\dagger \rangle|^2 + |\Delta\langle \hat{B}_\omega^\dagger \hat{B}_{\omega'} \rangle|^2 + \Delta\langle 4 \rangle}{\Delta\langle \hat{B}_\omega^\dagger \hat{B}_\omega \rangle \Delta\langle \hat{B}_{\omega'}^\dagger \hat{B}_{\omega'} \rangle}. \tag{6.20}$$

*For the second-rung emission, one can reach a situation where $\Delta\langle \hat{B}^\dagger \hat{B}^\dagger \rangle$ dominates over $\Delta\langle \hat{B}^\dagger \hat{B} \rangle$ and the four-photon correlations $\Delta\langle 4 \rangle$. In this case, $g^{(2)}$ displays a pronounced peak at the frequency where the squeezing is observed, i.e. at the second rung [60].*

## 6.3 Numerical Solution for Resonance Fluorescence

In order to verify the predictions of the simplified model, presented in Sec. 6.2, we numerically solve the full resonance fluorescence equations (6.6)-(6.9) at the singlet-doublet-triplet level for the cavity-quality factor $Q = 1.2 \cdot 10^5$ and otherwise same parameters
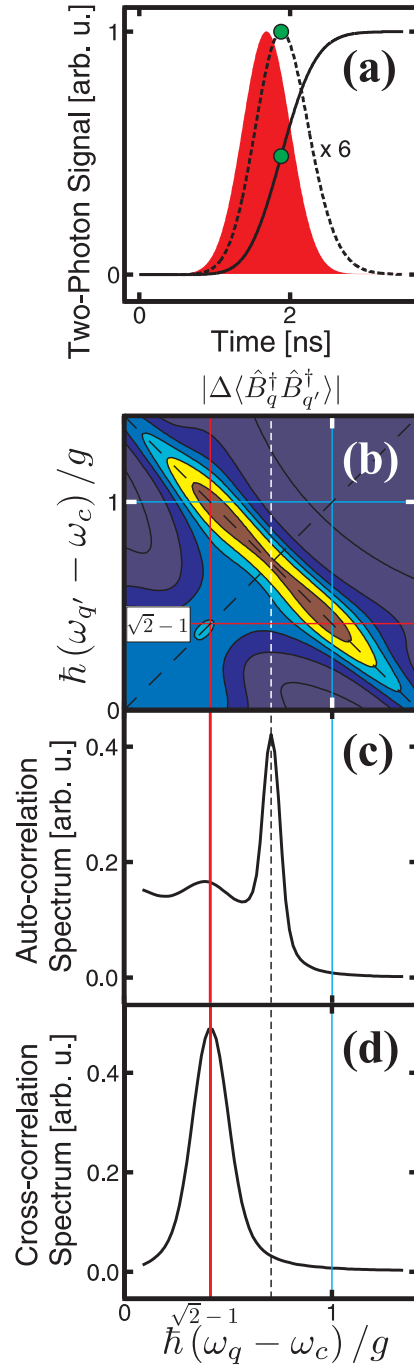
Figure 6.5: *Full numerical solution* of the two-photon emission $\Delta\langle\hat{B}_q^\dagger\hat{B}_{q'}^\dagger\rangle$ in the resonance fluorescence (cavity-quality factor $Q = 1.2 \cdot 10^5$). The same quantities are plotted as in Fig. 6.3. From Paper [IV].

used for Fig. 6.3. The solution of the two-photon emission $\Delta\langle \hat{B}_q^\dagger \hat{B}_{q'}^\dagger \rangle$ under resonance fluorescence conditions is shown in Fig. 6.5 where the same quantities are plotted as in Fig. 6.3. *We find a very good agreement between the numerical and analytical results.* In particular, Fig. 6.5 confirms all insights gained through the analytical investigations.

The detailed inspection of Fig. 6.5(a) also reveals that the decay of the auto-correlation signal (dashed) is faster than in the analytic calculation and is almost adiabatically following the pump. In addition, Figs. 6.5(b)-6.5(d) yield broader resonances, which stem from the true multimode nature of the problem.

To understand the origin of these differences, we remind ourselves that the delta-function approximation Eq. (A.12) constitutes the main simplification in the analytic model and is well fulfilled for high-quality cavities. Consequently, we attribute the deviations in Fig. 6.5 from the analytic solution Fig. 6.3 to the finite cavity lifetime $\tau_\text{cav}$ which is given by

$$\tau_\text{cav} \equiv \hbar/(2\gamma_\text{cav}) = 60 \text{ ps}. \tag{6.21}$$

Since this is much smaller than the pump duration as shown in Fig. 6.5(a) by the shaded area, we obtain an almost adiabatic following of the auto-correlation signal. Moreover, the finite cavity lifetime leads to broader resonances.

## 6.4 Conclusions

In this Chapter, we have derived the resonance fluorescence equations for strong-coupling semiconductor quantum-dot systems, based on a fully quantized multimode theory and a cluster-expansion approach. We have identified the origin of squeezed light in optically excited semiconductor systems. The quantum statistics of matter is crucial for obtaining squeezed light. Discussing the general case of generic light-matter interaction, we conclude that the matter has to have fermionic statistics in order to generate squeezed-light emission.

To obtain detailed insights, we have developed a reduced model which is compared with the full numerical calculations. We show that this simplified model yields very accurate results under typical strong-coupling conditions. We have predicted and analyzed the appearance of auto- and cross-correlation resonances in the two-photon emission spectrum of the fluorescent light. The auto- and cross-correlation resonances reveal the existence of the one- and two-photon strong-coupling states of Jaynes-Cummings ladder. We have found that the auto-correlation resonance exists only transiently while the cross-correlation resonance can exist after the optical excitation process.

These insights should be valuable for forthcoming experiments which aim at demonstrating the strong-coupling regime with true quantum characteristics. We have shown that the photon-correlation measurement provides a robust method to detect the two-photon strong-coupling states of the Jaynes-Cummings ladder in the current QD microcavities. *Our results suggest that experimental efforts should be focused on the cross-correlation measurement which shows a larger resonance than in the auto-correlation measurement and which allows for a detection under steady-state conditions.*

# 7 Conclusion and Outlook

In this Thesis, we have developed a fully quantized theory to study the resonance fluorescence from semiconductor nanostructures. Here, the matter system is coherently excited via an external laser pump while the re-emitted light spectrum is detected. We have analyzed the appearance of the second rung of the Jaynes-Cummings ladder in the strong-coupling semiconductor quantum dots (QDs) and proposed feasible experimental schemes to detect these signatures. We have pointed out that the second rung is a truly quantum-optical effect. We have applied the theory to the current QD systems which have shown the semiclassical vacuum-Rabi splitting. Moreover, we have theoretically analyzed experimental results obtained from an atomic system which has revealed the second rung in the intensity spectrum. For the QD systems, our results are still predictive because the experimental work is still in progress, while our theoretical results for the atomic system are in good agreement with the experiment.

To obtain these results, we have set up a fully quantized model which describes the interaction between many QDs inside a cavity and many quantized light modes. This model turns out to be very convenient because it allows us to describe, e.g., the propagation of the light and the light-matter coupling without phenomenological parameters. For this, we solve the light-mode functions for a given resonator model by evaluating the Helmholtz equation via a transfer-matrix method. The experimental parameters, like the quality of the cavity and the vacuum Rabi splitting, are adjusted to the specific experimental configurations.

As a next step, we have followed the Heisenberg equation-of-motion technique to evaluate the relevant operator combinations. We have encountered a hierarchy problem which stems from the quantized interaction Hamiltonian. To truncate this hierarchy, we have applied the cluster-expansion approach which produces consistent approximations. This approach allows us to include all correlations up to a desired order. We have thoroughly analyzed the accuracy of the obtained equations by comparing the corresponding numerical results with the exact solutions for the case of one single QD and one single light mode. These investigations are presented in more detail in the Appendices. We have found that the second rung in the intensity spectrum is well described at the three-particle level while the second rung in the squeezing spectrum is already well described at the two-particle level. Hence, we have justified that we can use a theory which includes all correlations up to the three-particle level. The resulting equations are called Maxwell-Bloch equations, luminescence equations, squeezing equations, and triplet equations.

Applying the theory, we have found that the second-rung emission is determined by the two-photon state occupation in the pump pulse. In this connection, we have identified the optimum excitation conditions which lead to the re-emission from the

second rung. We have analyzed a recent atomic experiment which has demonstrated the second rung directly in the intensity spectrum. Our theory shows good agreement with the experimental results. Moreover, we have shown that we obtain the same second-rung pumping mechanism in the atomic and semiconductor QD systems.

Since the realistic dephasing of the current QD samples washes out the most interesting effects in the intensity spectrum, we have suggested to use the two-photon correlation measurement. In contrast to the intensity spectrum, we find that the vacuum Rabi peaks are absent in the two-photon correlation spectrum, which eliminates the large background contributions. Moreover, we find an enhanced resonance at the second-rung emission frequency which we trace back to the squeezing type field which is generated in the second-rung pumping process. We have demonstrated that this enhanced resonance is robust enough against dephasing. Since this large two-photon correlation resonance at the second rung has already been observed in a separate atomic experiment only shortly after our proposal, we are convinced that this method should be applicable also in the QD systems.

Extending our discussions, we have also introduced the cross-correlated two-photon correlations. We have suggested that the experimental efforts should be focused on the cross correlations because they can be detected under steady-state conditions and lead to a larger resonance than via the auto correlations. We have confirmed all insights by a reduced model which we have solved analytically. The derivation of the analytical solution is worked out in detail in the Appendix. We have shown that the reduced model yields very accurate results under typical strong-coupling conditions. In particular, we have obtained a very good agreement between the numerics and analytics.

We have used the developed formalism to explain the physical origin of the squeezed-light emission. Following the general case of generic light-matter coupling, we have concluded that the matter has to have fermionic statistics in order to produce the squeezed light. Finally, we have also presented an exact relation between the generated squeezing and the two-photon correlations.

As an outlook, I will finish the remaining Papers which are still in preparation, see 'Author's Contributions' at the beginning of the Thesis. In particular, the entanglement analysis, the theoretical proposal for the exciton-biexciton pumping for CdSe-based QDs in Zeno-logic applications, and the atomic vs. quantum-dot strong coupling will be summarized in Papers.

# A Analytics for Generation of Squeezing

In Chapter 6, we have presented the results which cover the buildup of resonances in the two-photon emission spectrum. In App. A, we provide the corresponding analytics. In App. A.1, we develop a reduced model which describes the two-photon emission spectrum and which we solve analytically in App. A.2. Finally, we derive a steady-state formula in App. A.3.

*Most of the results that we discuss in App. A have been published in Ref. [78]. The argumentation is therefore kept close to this paper.*

## A.1 Reduced Model

We notice that the resonance fluorescence equations (6.6)-(6.9) introduce coupling between different $q$-modes via the stimulated terms $\sum_{q'} \mathcal{F}_{q'} \Delta \langle \hat{B}_q^\dagger \hat{B}_{q'} \rangle$ and $\sum_{q'} \mathcal{F}_{q'}^\star \Delta \langle \hat{B}_q^\dagger \hat{B}_{q'}^\dagger \rangle$. In order to treat these contributions, it is convenient to define a Boson operator for an *effective cavity mode*

$$\hat{B}_c \equiv \mathcal{N} \sum_q \mathcal{F}_q \hat{B}_q. \tag{A.1}$$

The norm

$$\mathcal{N}^{-1} = \sqrt{\sum_q |\mathcal{F}_q|^2} \equiv g_1 \tag{A.2}$$

ensures that the cavity mode is bosonic and properly related to the light-matter coupling constant $g_1$ for one QD. Here, we define the light-matter coupling constant $g_N$ for $N$ QDs by

$$g_N \equiv \sqrt{N} g_1 \tag{A.3}$$
$$\equiv g, \tag{A.4}$$

where we also use the abbreviation $g$ for $g_N$. The stimulated contributions can then be expressed in terms of the photon-cavity correlations $\Delta \langle \hat{B}_q^\dagger \hat{B}_c^{(\dagger)} \rangle$

$$\sum_{q'} \mathcal{F}_{q'} \Delta \langle \hat{B}_q^\dagger \hat{B}_{q'} \rangle = g_1 \Delta \langle \hat{B}_q^\dagger \hat{B}_c \rangle, \tag{A.5}$$

$$\sum_{q'} \mathcal{F}_{q'}^\star \Delta \langle \hat{B}_q^\dagger \hat{B}_{q'}^\dagger \rangle = g_1 \Delta \langle \hat{B}_q^\dagger \hat{B}_c^\dagger \rangle. \tag{A.6}$$

## A Analytics for Generation of Squeezing

We also introduce *scaled photon operators* $\hat{b}_q$ which are connected to the original photon operators $\hat{B}_q$ via

$$\hat{B}_q = \frac{\mathcal{F}_q^\star}{g_1}\hat{b}_q. \tag{A.7}$$

Using the transformation rules (A.1) and (A.7), the resonance fluorescence equations (6.6)-(6.9) can be rewritten. For the luminescence equations, we obtain

$$i\hbar\frac{\partial}{\partial t}\Delta\langle\hat{b}_q^\dagger\hat{b}_{q'}\rangle = (\hbar\omega_{q'} - \hbar\omega_q)\Delta\langle\hat{b}_q^\dagger\hat{b}_{q'}\rangle$$
$$+\ iNg_1\left(\Delta\langle\hat{b}_q^\dagger\hat{P}\rangle + \Delta\langle\hat{b}_{q'}^\dagger\hat{P}\rangle^\star\right), \tag{A.8}$$

$$i\hbar\frac{\partial}{\partial t}\Delta\langle\hat{b}_q^\dagger\hat{P}\rangle = (E^{cv} - \hbar\omega_q - i\gamma_P)\Delta\langle\hat{b}_q^\dagger\hat{P}\rangle$$
$$-\ ig_1\left(1 - f^e - f^h\right)\Delta\langle\hat{b}_q^\dagger\hat{B}_c\rangle$$
$$+\ ig_1\left(f^e - |P|^2\right) + \Delta\langle 3\rangle$$
$$+\ d\langle E^{(+)}\rangle\Delta\langle\hat{b}_q^\dagger(c^\dagger c - v^\dagger v)\rangle, \tag{A.9}$$

and the squeezing dynamics follow from

$$i\hbar\frac{\partial}{\partial t}\Delta\langle\hat{b}_q^\dagger\hat{b}_{q'}^\dagger\rangle = -(\hbar\omega_q + \hbar\omega_{q'})\Delta\langle\hat{b}_q^\dagger\hat{b}_{q'}^\dagger\rangle$$
$$+\ iNg_1\left(\Delta\langle\hat{b}_q^\dagger\hat{P}^\dagger\rangle + \Delta\langle\hat{b}_{q'}^\dagger\hat{P}^\dagger\rangle\right), \tag{A.10}$$

$$i\hbar\frac{\partial}{\partial t}\Delta\langle\hat{b}_q^\dagger\hat{P}^\dagger\rangle = -(\hbar\omega_q + E^{cv} + i\gamma_P)\Delta\langle\hat{b}_q^\dagger\hat{P}^\dagger\rangle$$
$$-\ ig_1\left(1 - f^e - f^h\right)\Delta\langle\hat{b}_q^\dagger\hat{B}_c^\dagger\rangle - ig_1 P^\star P^\star$$
$$-\ d\langle E^{(-)}\rangle\Delta\langle\hat{b}_q^\dagger(c^\dagger c - v^\dagger v)\rangle + \Delta\langle 3\rangle. \tag{A.11}$$

In Sec. 2, we have seen that the light-mode function proportional to $|\mathcal{F}_q|^2$ describes a Lorentzian centered around the cavity frequency $\omega_c$. For high-quality cavities, this Lorentzian essentially reduces the spectrum to the cavity mode. In the reduced model, we thus apply the *delta-function approximation*

$$\sum_{q'}|\mathcal{F}_{q'}|^2\hbar\omega_{q'}\Delta\langle\hat{B}_q^\dagger\hat{B}_{q'}^\dagger\rangle \approx \hbar\omega_c\sum_{q'}|\mathcal{F}_{q'}|^2\Delta\langle\hat{B}_q^\dagger\hat{B}_{q'}^\dagger\rangle, \tag{A.12}$$

which allows us to set up equations of motion for the photon-cavity correlations $\Delta\langle\hat{b}_q^\dagger\hat{B}_c^\dagger\rangle$ that follow from

$$i\hbar\frac{\partial}{\partial t}\Delta\langle\hat{b}_q^\dagger\hat{B}_c^\dagger\rangle = \mathcal{N}^2\sum_{q'}|\mathcal{F}_{q'}|^2\left[i\hbar\frac{\partial}{\partial t}\Delta\langle\hat{b}_q^\dagger\hat{b}_{q'}^\dagger\rangle\right]. \tag{A.13}$$

For instance, using the delta-function approximation (A.12) and the equation of mo-

tion (A.8), we obtain for the homogeneous part

$$
\begin{aligned}
i\hbar \frac{\partial}{\partial t} \Delta\langle \hat{b}_q^\dagger \hat{B}_c \rangle|_{\text{hom}} &= \mathcal{N}^2 \sum_{q'} |\mathcal{F}_{q'}|^2 \left[ i\hbar \frac{\partial}{\partial t} \Delta\langle \hat{b}_q^\dagger \hat{b}_{q'} \rangle \right]|_{\text{hom}} \\
&= \mathcal{N}^2 \sum_{q'} |\mathcal{F}_{q'}|^2 \left( \hbar\omega_{q'} - \hbar\omega_q \right) \Delta\langle \hat{b}_q^\dagger \hat{b}_{q'} \rangle \\
&\approx \left( \hbar\omega_c - \hbar\omega_q \right) \mathcal{N}^2 \sum_{q'} |\mathcal{F}_{q'}|^2 \Delta\langle \hat{b}_q^\dagger \hat{b}_{q'} \rangle \\
&= \left( \hbar\omega_c - \hbar\omega_q \right) \Delta\langle \hat{b}_q^\dagger \hat{B}_c \rangle.
\end{aligned}
\tag{A.14}
$$

We observe that photon-cavity correlations appear again on the right hand side such that the set of equations is closed. Similarly, the dynamics of cavity-cavity correlations $\Delta\langle \hat{B}_c^\dagger \hat{B}_c^\dagger \rangle$ and cavity-polarization correlations $\Delta\langle \hat{B}_c^\dagger \hat{P}^\dagger \rangle$ can be derived to become

$$
\begin{aligned}
i\hbar \frac{\partial}{\partial t} \Delta\langle \hat{B}_c^\dagger \hat{B}_c^\dagger \rangle &= (-2\hbar\omega_c) \, \Delta\langle \hat{B}_c^\dagger \hat{B}_c^\dagger \rangle \\
&\quad + 2iNg_1 \Delta\langle \hat{B}_c^\dagger \hat{P}^\dagger \rangle,
\end{aligned}
\tag{A.15}
$$

$$
\begin{aligned}
i\hbar \frac{\partial}{\partial t} \Delta\langle \hat{B}_c^\dagger \hat{P}^\dagger \rangle &= -\left( \hbar\omega_c + E^{cv} + i\gamma_P \right) \Delta\langle \hat{B}_c^\dagger \hat{P}^\dagger \rangle \\
&\quad - ig_1 \left( 1 - f^e - f^h \right) \Delta\langle \hat{B}_c^\dagger \hat{B}_c^\dagger \rangle - ig_1 P^\star P^\star \\
&\quad - d\langle E^{(-)} \rangle \Delta\langle \hat{B}_c^\dagger \left( c^\dagger c - v^\dagger v \right) \rangle + \Delta\langle 3 \rangle,
\end{aligned}
\tag{A.16}
$$

where we can again make use of Eq. (A.12) and identification (A.2) multiple times.

In this reduced model, we further simplify the resonance fluorescence equations (A.8)-(A.11) by focusing on the *low-excitation regime*. In this limit, only minor electron densities will be generated via optical pumping such that $f^e, f^h \ll 1$. Moreover, spontaneous source terms proportional to the QD polarization and the QD densities dominate in this regime over the photon-density correlations $\Delta\langle \hat{b}_q^\dagger (c^\dagger c - v^\dagger v) \rangle$ which we therefore omit in the reduced model. We also neglect the coupling to the three-particle correlations $\Delta\langle 3 \rangle$ and assume resonant conditions $E^{cv} = \hbar\omega_c$.

In the next step, we identify all correlations which couple to the two-photon emission $\Delta\langle \hat{b}_q^\dagger \hat{b}_{q'}^\dagger \rangle$ and summarize them into a squeezing vector $\Delta\boldsymbol{S}(t)$ defined by

$$
\begin{aligned}
\Delta\boldsymbol{S}(t) \equiv \big( & \Delta\langle \hat{B}_c^\dagger \hat{B}_c^\dagger \rangle, \Delta\langle \hat{B}_c^\dagger \hat{P}^\dagger \rangle, \Delta\langle \hat{b}_q^\dagger \hat{B}_c^\dagger \rangle, \Delta\langle \hat{b}_q^\dagger \hat{P}^\dagger \rangle, \\
& \Delta\langle \hat{b}_{q'}^\dagger \hat{B}_c^\dagger \rangle, \Delta\langle \hat{b}_{q'}^\dagger \hat{P}^\dagger \rangle, \Delta\langle \hat{b}_q^\dagger \hat{b}_{q'}^\dagger \rangle \big)(t).
\end{aligned}
\tag{A.17}
$$

Using Eqs. (A.13), (A.15), and (A.16), we explicitly evaluate the dynamics of the squeezing vector $\Delta\boldsymbol{S}(t)$ to obtain

$$
i\hbar \frac{\partial}{\partial t} \Delta\langle \hat{B}_c^\dagger \hat{B}_c^\dagger \rangle = 2iNg_1 \Delta\langle \hat{B}_c^\dagger \hat{P}^\dagger \rangle,
\tag{A.18}
$$

$$
\begin{aligned}
i\hbar \frac{\partial}{\partial t} \Delta\langle \hat{B}_c^\dagger \hat{P}^\dagger \rangle &= -i\gamma_P \Delta\langle \hat{B}_c^\dagger \hat{P}^\dagger \rangle - ig_1 \Delta\langle \hat{B}_c^\dagger \hat{B}_c^\dagger \rangle \\
&\quad - ig_1 P^\star P^\star,
\end{aligned}
\tag{A.19}
$$

## A Analytics for Generation of Squeezing

$$i\hbar \frac{\partial}{\partial t} \Delta \langle \hat{b}_q^\dagger \hat{B}_c^\dagger \rangle = -(\hbar\omega_q - \hbar\omega_c) \Delta \langle \hat{b}_q^\dagger \hat{B}_c^\dagger \rangle$$
$$+ iNg_1 \left( \Delta \langle \hat{b}_q^\dagger \hat{P}^\dagger \rangle + \Delta \langle \hat{B}_c^\dagger \hat{P}^\dagger \rangle \right), \tag{A.20}$$

$$i\hbar \frac{\partial}{\partial t} \Delta \langle \hat{b}_q^\dagger \hat{P}^\dagger \rangle = -(\hbar\omega_q - \hbar\omega_c + i\gamma_P) \Delta \langle \hat{b}_q^\dagger \hat{P}^\dagger \rangle$$
$$- ig_1 \Delta \langle \hat{b}_q^\dagger \hat{B}_c^\dagger \rangle - ig_1 P^\star P^\star, \tag{A.21}$$

$$i\hbar \frac{\partial}{\partial t} \Delta \langle \hat{b}_{q'}^\dagger \hat{B}_c^\dagger \rangle = -(\hbar\omega_{q'} - \hbar\omega_c) \Delta \langle \hat{b}_{q'}^\dagger \hat{B}_c^\dagger \rangle$$
$$+ iNg_1 \left( \Delta \langle \hat{b}_{q'}^\dagger \hat{P}^\dagger \rangle + \Delta \langle \hat{B}_c^\dagger \hat{P}^\dagger \rangle \right), \tag{A.22}$$

$$i\hbar \frac{\partial}{\partial t} \Delta \langle \hat{b}_{q'}^\dagger \hat{P}^\dagger \rangle = -(\hbar\omega_{q'} - \hbar\omega_c + i\gamma_P) \Delta \langle \hat{b}_{q'}^\dagger \hat{P}^\dagger \rangle$$
$$- ig_1 \Delta \langle \hat{b}_{q'}^\dagger \hat{B}_c^\dagger \rangle - ig_1 P^\star P^\star, \tag{A.23}$$

$$i\hbar \frac{\partial}{\partial t} \Delta \langle \hat{b}_q^\dagger \hat{b}_{q'}^\dagger \rangle = -(\hbar\omega_q + \hbar\omega_{q'} - 2\hbar\omega_c) \Delta \langle \hat{b}_q^\dagger \hat{b}_{q'}^\dagger \rangle$$
$$+ iNg_1 \left( \Delta \langle \hat{b}_q^\dagger \hat{P}^\dagger \rangle + \Delta \langle \hat{b}_{q'}^\dagger \hat{P}^\dagger \rangle \right), \tag{A.24}$$

where the rotating frame $\langle E \rangle \sim e^{-iE^{cv}\frac{t}{\hbar}}$ has been used. It is convenient to define the constant source vector

$$\boldsymbol{D}_0 \equiv (0, 1, 0, 1, 0, 1, 0), \tag{A.25}$$

the time-dependent driving term

$$s(t) \equiv -ig_1 P^\star(t) P^\star(t), \tag{A.26}$$

and the corresponding time-dependent driving vector

$$\boldsymbol{D}(t) \equiv \boldsymbol{D}_0 s(t) \tag{A.27}$$

to rewrite Eqs. (A.18)-(A.24). This leads to the more compact notation

$$i\hbar \frac{\partial}{\partial t} \Delta S_j(t) = -\sum_k M_{jk} \Delta S_k(t) + D_j(t). \tag{A.28}$$

We notice again that the squeezing is driven by the nonlinear source term $P^\star P^\star(t)$ Eq. (A.26), as already discussed in Sec. 6.1. The homogeneous part of Eq. (A.28) is

determined by the (static) matrix $\boldsymbol{M}$ defined as

$$
\boldsymbol{M} = \begin{pmatrix}
\boxed{\begin{matrix} 0 & -2\mathrm{i}Ng_1 \\ \mathrm{i}g_1 & \mathrm{i}\gamma_P \end{matrix}} & 0 & 0 & 0 & 0 & 0 \\[4pt]
\begin{matrix} 0 & -\mathrm{i}Ng_1 \\ 0 & 0 \end{matrix} & \boxed{\begin{matrix} g_N\Omega_q & -\mathrm{i}Ng_1 \\ \mathrm{i}g_1 & (g_N\Omega_q+\mathrm{i}\gamma_P) \end{matrix}} & 0 & 0 & 0 & 0 \\[4pt]
\begin{matrix} 0 & -\mathrm{i}Ng_1 \\ 0 & 0 \end{matrix} & 0 & 0 & \boxed{\begin{matrix} g_N\Omega_{q'} & -\mathrm{i}Ng_1 \\ \mathrm{i}g_1 & (g_N\Omega_{q'}+\mathrm{i}\gamma_P) \end{matrix}} & 0 \\[4pt]
\begin{matrix} 0 & 0 \end{matrix} & 0 & -\mathrm{i}Ng_1 & 0 & -\mathrm{i}Ng_1 & \boxed{g_N(\Omega_q+\Omega_{q'})}
\end{pmatrix},
$$

$$(\text{A.29})$$

with the reduced photon energy $\Omega_q \equiv \hbar(\omega_q-\omega_c)/g_N$. We observe that Eq. (A.28) is linear if the source terms are treated independently from the correlations. Furthermore, we notice that the momenta $q, q'$ only parametrically enter the equations of motion. Hence, we can solve the full spectral dependence of the two-photon correlations. In analogy to the two-photon emission, we may also rewrite the photon-number like correlations $\Delta\langle \hat{b}_q^\dagger \hat{b}_{q'}\rangle$ of Eqs. (A.8)-(A.9). These correlations determine the intensity of the incoherent photoluminescence (PL) via the linear equation

$$
\mathrm{i}\hbar\frac{\partial}{\partial t}PL_j(t) = -\sum_k M_{jk}^{PL}PL_k(t) + D_j^{PL}(t), \tag{A.30}
$$

with an appropriate luminescence vector $\boldsymbol{PL}$, homogeneous matrix $\boldsymbol{M^{PL}}$, and driving vector $\boldsymbol{D^{PL}}$.

## A.2 Analytic Solution for Resonance Fluorescence

We can analytically solve the linear set of equations (A.28) if we diagonalize the static homogeneous matrix $\boldsymbol{M}$. The eigenstates $\boldsymbol{\phi}_\lambda$ of the homogeneous part $\boldsymbol{M}$ are given by

$$
\boldsymbol{M}\boldsymbol{\phi}_\lambda = E_\lambda\boldsymbol{\phi}_\lambda \tag{A.31}
$$

with the eigenvalues $E_\lambda$ and index number $\lambda$. Since the eigenstates $\{\boldsymbol{\phi}_\lambda\}$ form a complete basis, we can express the source vector $\boldsymbol{D}_0$ in terms of the eigenstates

$$
\boldsymbol{D}_0 = \sum_\lambda D_\lambda\boldsymbol{\phi}_\lambda, \tag{A.32}
$$

where the expansion coefficients $D_\lambda$ have been introduced. We can formally integrate Eq. (A.28) for initially vanishing correlations $\Delta\boldsymbol{S}(t=0)=\boldsymbol{0}$ to obtain

$$
\Delta\boldsymbol{S}(t) = \frac{1}{\mathrm{i}\hbar}\int_0^t \mathrm{e}^{\frac{\mathrm{i}}{\hbar}\boldsymbol{M}(t-u)}\boldsymbol{D}(u)\,\mathrm{d}u. \tag{A.33}
$$

Using $\boldsymbol{D}(t) = \boldsymbol{D}_0 s(t)$ together with Eq. (A.32) and the relation

$$
\mathrm{e}^{\frac{\mathrm{i}}{\hbar}\boldsymbol{M}(t-u)}\boldsymbol{\phi}_\lambda = \mathrm{e}^{\frac{\mathrm{i}}{\hbar}E_\lambda(t-u)}\boldsymbol{\phi}_\lambda, \tag{A.34}
$$

## A Analytics for Generation of Squeezing

we end up with the general solution of the squeezing vector

$$\Delta \boldsymbol{S}(t) = \sum_\lambda D_\lambda \boldsymbol{\phi}_\lambda \frac{1}{\mathrm{i}\hbar} \int_0^t \mathrm{e}^{\frac{\mathrm{i}}{\hbar} E_\lambda (t-u)} s(u) \, \mathrm{d}u. \tag{A.35}$$

Especially, the correlations in the two-photon emission $\Delta \langle \hat{b}_q^\dagger \hat{b}_{q'}^\dagger \rangle (t)$ follow from

$$\Delta \langle \hat{b}_q^\dagger \hat{b}_{q'}^\dagger \rangle (t) = \Delta S_{j=7}(t). \tag{A.36}$$

At this point, we again note that the $q, q'$ dependence only enters parametrically via the static matrix $\boldsymbol{M}$, the static eigenvectors $\boldsymbol{\phi}_\lambda$ and eigenvalues $E_\lambda$, and the constant source coefficients $D_\lambda$. Hence, we can obtain the full multimode dependence of the resonance fluorescence.

We observe that the matrix $\boldsymbol{M}$ in Eq. (A.29) casts into the form

$$\boldsymbol{M} = \begin{pmatrix} \boxed{\boldsymbol{M_1}} & \boldsymbol{0} \\ \boldsymbol{M_2} & \boxed{\boldsymbol{M_3}} \end{pmatrix}, \tag{A.37}$$

i.e. it consists of four submatrices and has zero entries in the upper right corner. Since $\mathrm{Det}(\boldsymbol{M}) = \mathrm{Det}(\boldsymbol{M_1}) \cdot \mathrm{Det}(\boldsymbol{M_3})$ holds according to the theorem on the determinants of block matrices, we find compact eigensolutions with eigenvalues following from

$$E_1 = g(\Omega_q + \Omega_{q'}), \tag{A.38}$$

$$E_2^\pm = g\left( \Omega_q \pm \sqrt{1 - \frac{\gamma_P^2}{4g^2}} + \mathrm{i}\frac{\gamma_P}{2g} \right) \tag{A.39}$$

$$= g(\Omega_q \pm 1) \text{ for } \gamma_P = 0, \tag{A.40}$$

$$E_3^\pm = g\left( \Omega_{q'} \pm \sqrt{1 - \frac{\gamma_P^2}{4g^2}} + \mathrm{i}\frac{\gamma_P}{2g} \right) \tag{A.41}$$

$$= g(\Omega_{q'} \pm 1) \text{ for } \gamma_P = 0, \tag{A.42}$$

$$E_4^\pm = g\left( \pm \sqrt{2 - \frac{\gamma_P^2}{4g^2}} + \mathrm{i}\frac{\gamma_P}{2g} \right) \tag{A.43}$$

$$= g(\pm\sqrt{2}) \text{ for } \gamma_P = 0, \tag{A.44}$$

$$\Omega_q \equiv \hbar(\omega_q - \omega_c)/g,$$

where we have repeated the definition of the reduced photon energy $\Omega_q$ in the last line. Equations (A.40), (A.42), and (A.44) simplify the obtained expressions for vanishing dephasing. However, we fully include dephasing $\gamma_P$ in the analytic solution, i.e. we use Eqs. (A.38), (A.39), (A.41), and (A.43). We notice that the $E_1$ eigenmode can exist in the long-time limit while the other modes decay with the rate $\gamma_P/2$ after their generation. Thus, the $E_1$ mode survives while $E_j^\pm$ are present only transiently.

## A.3 Analytic Steady-State Solution

We can derive a steady-state solution of the squeezing vector $\Delta \boldsymbol{S}$ if we make use of the general solution Eq. (A.35). The squeezing source is given by polarization $P^2$ which is built up by the classical light field $\langle E \rangle(t)$ for which we make the Ansatz

$$\langle E \rangle(t) = \frac{E_0}{2} e^{-\frac{i}{\hbar}\Omega_p g t} e^{-\frac{(t-t_0^{\text{pump}})^2}{2\Delta T^2}} \tag{A.45}$$

with pump amplitude $E_0$, pump frequency

$$\Omega_p \equiv \hbar(\omega_p - \omega_c)/g, \tag{A.46}$$

pump duration $\Delta T$ and pump delay time $t_0^{\text{pump}}$. Since the polarization is proportional to the classical light field $P(t) \sim \langle E \rangle(t)$ according to the Maxwell-Bloch equations [28, 65] and the squeezing source $s(t) = -ig_1 P^\star P^\star(t)$ is connected to the polarization, we find

$$s(t) = s_0 \, e^{2\frac{i}{\hbar}\Omega_p g t} e^{-\frac{\left(t-t_0^{\text{pump}}\right)^2}{\Delta T^2}}, \tag{A.47}$$

with unitless pump strength $s_0$. In the long-time limit $\Delta \boldsymbol{S}(t \to \infty)$, the squeezing generation Eq. (A.35) can be obtained from the long-living mode $\boldsymbol{\phi}_{\lambda=1}$

$$
\begin{aligned}
\Delta \boldsymbol{S}(t \to \infty) \;=\;& D_{\lambda=1} \boldsymbol{\phi}_{\lambda=1} \frac{s_0 \sqrt{\pi} \Delta T}{i\hbar} e^{\frac{i}{\hbar}E_1(t-t_0^{\text{pump}})} \\
\times\;& e^{\frac{i}{\hbar}2\Omega_p g t_0^{\text{pump}}} e^{-(E_1-2\Omega_p g)^2 \frac{\Delta T^2}{4\hbar^2}}, 
\end{aligned}
\tag{A.48}
$$

where we have used Eq. (A.47). Especially, we find for the cross correlation in steady state

$$
\begin{aligned}
& |\Delta \langle \hat{B}^\dagger_{\hbar\omega_{1\text{st}}} \hat{B}^\dagger_{\hbar\omega_{2\text{nd}}} \rangle|(t \to \infty) \\
=\;& |\mathcal{F}_{\hbar\omega_{1\text{st}}} \mathcal{F}_{\hbar\omega_{2\text{nd}}}| N \sqrt{\frac{4\left(\frac{g^2}{\gamma_P^2}+1\right)^2 + 2\frac{g^2}{\gamma_P^2}}{\gamma_P^2 + 4g^2}} \frac{s_0 \sqrt{\pi} \Delta T}{\hbar} \\
\times\;& \exp\left[-(\sqrt{2} - 2\Omega_p)^2 \frac{g^2 \Delta T^2}{4\hbar^2}\right]. 
\end{aligned}
\tag{A.49}
$$

# B Analytical Model for Second-Rung Generation

Appendix B provides very nice analytical derivations and numerical tests of our theory. In particular, we show that the equations of motion in Chapter 3 yield good results when we compare with the exact analytical expressions. These analytical expressions are obtained within the original Jaynes-Cummings model which includes only one QD and one cavity mode. We use the analytical model to study the quantum statistics of the re-emitted light in the resonance fluorescence scheme.

Methodically, we apply the exactly solvable Jaynes-Cummings model to calculate the quantum statistics of the fluorescent light. Here, we are mainly interested in the intensity spectrum, squeezing spectrum, and two-photon correlations $g^{(2)}$ after the excitation with a coherent light field. In App. C, we also study the excitation with a thermal light field and investigate the role of different clusters. To compare with the numerical results, we solve the equations of motion in Chapter 3 for one QD and one cavity mode.

We find that the second rung is well described via the cluster expansion and verify that we obtain the same spectra in the numerics and analytics. Especially, the emission spectrum, squeezing spectrum, and also the two-photon correlations $g^{(2)}$ are well described within the developed theory. We also find that the analytical model predicts gigantic $g^{(2)} \gg 1$ values if the coherent light field contains less than one photon on average.

## B.1 Eigensolutions

We can approximate the full dot problem presented in Chapter 2 if we consider only one dot and one strong confining cavity mode. In this situation, we can reduce the system Hamiltonian (2.2) to the well-known Jaynes-Cummings Hamiltonian [16] which reads

$$
\begin{aligned}
\hat{H}_{\mathrm{JC}} &= \left( E^c \hat{c}^\dagger \hat{c} + E^v \hat{v}^\dagger \hat{v} \right) + \hbar\omega_c \left( \hat{B}^\dagger \hat{B} + \frac{1}{2} \right) \\
&+ g \left( \hat{B}^\dagger \hat{P} + \hat{B} \hat{P}^\dagger \right),
\end{aligned} \tag{B.1}
$$

where the polarization operator is again defined by $\hat{P} \equiv \hat{v}^\dagger \hat{c}$. Another representation, often used in the atomic strong-coupling situations which are well described by the single-mode Jaynes-Cummings Hamiltonian, is given by [16, 68]

$$
\hat{H}_{\mathrm{JC}} = E^{cv}\sigma_z + \hbar\omega_c(\hat{B}_c^\dagger \hat{B}_c + 1/2) + g(\hat{B}_c^\dagger \sigma_- + \hat{B}_c \sigma_+), \tag{B.2}
$$

where $E^{cv}$ denotes the transition energy of the atom, $\sigma_z, \sigma_-, \sigma_+$ are the usual Pauli sigma matrices, $\hat{B}_c$ ($\hat{B}_c^\dagger$) is the cavity photon annihilation (creation) operator with energy $\hbar\omega_c$, and $g$ is the light-matter coupling constant. The $\sigma_z$ part of Eq. (B.2) is the free Hamiltonian of the uncoupled atom and the $\hat{B}_c^\dagger\hat{B}_c$ part describes the energy of the uncoupled light field. The light-matter coupling stems from $g$-dependent contributions in Eq. (B.2) where $\hat{B}_c^\dagger\sigma_-$ lowers the two-level system from the excited to ground state by emitting a photon - the opposite process $\hat{B}_c\sigma_+$ excites the two-level system via photon absorption.

This model predicts the Jaynes-Cummings ladder Fig. 1.1 where the eigen states are explicitly given by [68, 79]

$$\begin{aligned}
\hat{H}_{\text{JC}}|\psi_0\rangle &= E_{0,0}|\psi_0\rangle, & \text{(B.3)} \\
\hat{H}_{\text{JC}}|\psi_{n\pm}\rangle &= E_{n\pm}|\psi_{n\pm}\rangle, n = 1, 2, \ldots, & \text{(B.4)}
\end{aligned}$$

with eigenenergies

$$E_{0,0} = -\Delta/2, \ E_{n\pm} = \hbar\omega_c n \pm \sqrt{\Delta^2/4 + g^2 n}, \tag{B.5}$$

where have introduced the finite atom-cavity detuning $\Delta \equiv E^{cv} - \hbar\omega_c$. Equation (B.5) produces the Jaynes-Cummings ladder where the excited states $|\psi_{n\pm}\rangle$ show a photon-number dependent splitting of $2\sqrt{\Delta^2/4 + g^2 n}$. Especially, the second rung is obtained for $n = 2$ with the splitting $2\sqrt{\Delta^2/4 + 2g^2}$ or $2\sqrt{2}g$ for the zero-detuning case. We use this exactly solvable model to set up the analytical formulae for the second-rung generation. Furthermore, we show that we can reproduce the second rung within the cluster-expansion approach.

## B.2 Quantum Statistics

To obtain more insights into the second-rung generation, we consider an unexcited dot ($|\text{down}\rangle$) which interacts with a generic light field which can be described via the density matrix

$$\hat{\rho}_{\text{field}} = \sum_{n,n'=0}^{\infty} |n\rangle C_{n,n'}\langle n'| \tag{B.6}$$

in the Fock basis $\{|n\rangle\}_{n=0,1,2,\ldots}$. The total initial density matrix is then given by

$$\hat{\rho}(t = 0) = |\text{down}\rangle\langle\text{down}|\hat{\otimes}\rho_{\text{field}} \tag{B.7}$$

and the time evolution follows from

$$\hat{\rho}(t) = \exp(-\mathrm{i}\hat{H}_{\text{JC}}t/\hbar)\hat{\rho}(t = 0)\exp(\mathrm{i}\hat{H}_{\text{JC}}t/\hbar). \tag{B.8}$$

Since the quantum statistics of the emitted light can be described [43] by pure photon expectation values

$$I_K^J \equiv \langle[\hat{B}^\dagger]^J[\hat{B}]^K\rangle, \ \text{J and K integers} \geq 0, \tag{B.9}$$

it is useful to compute the partial trace

$$\hat{\rho}_B(t) \equiv \text{Tr}_{\text{dot}}[\hat{\rho}(t)] = \langle \text{down}|\hat{\rho}(t)|\text{down}\rangle + \langle \text{up}|\hat{\rho}(t)|\text{up}\rangle, \tag{B.10}$$

given explicitly in Ref. [80]. With the help of the reduced density matrix $\hat{\rho}_B(t)$, we obtain the pure photon expectation values

$$I_K^J = \text{Tr}_B[\hat{\rho}_B(t)[\hat{B}^\dagger]^J[\hat{B}]^K] \equiv \sum_{n=0}^{\infty} \langle n|\hat{\rho}_B(t)[\hat{B}^\dagger]^J[\hat{B}]^K|n\rangle \tag{B.11}$$

which for the resonant condition $\Delta = 0$ explicitly read

$$\begin{aligned}
I_K^J(t) = \sum_{n=K}^{\infty} &\frac{\sqrt{n!}\sqrt{(n-K+J)!}}{(n-K)!} \exp(-i\omega_c(K-J)t) \\
&\times \Big[ C_{n+1,n-K+J+1} \sin(\sqrt{n+1}\frac{gt}{\hbar}) \sin(\sqrt{n-K+J+1}\frac{gt}{\hbar}) \\
&\quad + C_{n,n-K+J} \cos(\sqrt{n}\frac{gt}{\hbar}) \cos(\sqrt{n-K+J}\frac{gt}{\hbar}) \Big].
\end{aligned} \tag{B.12}$$

In the following, we are interested in the excitation with a coherent light field, i.e. $\hat{\rho}_{\text{field}} = |\alpha\rangle\langle\alpha|$ with the coherent state $|\alpha\rangle = \sum_{n=0}^{\infty} Q_n|n\rangle$, $Q_n \equiv \alpha^n/\sqrt{n!}\exp[-|\alpha|^2/2]$, such that $C_{n,n'} = Q_n Q_{n'}^\star$ holds. For $n = n'$, we obtain the usual photon-number distribution $P_n = C_{n,n}$.

# B.3  Second-Rung Generation

To follow the emission properties of the coupled system for the coherent excitation, we consider again the correlated quantities

$$\begin{aligned}
\Delta\langle \hat{B}^\dagger \hat{B}\rangle &\equiv \langle \hat{B}^\dagger \hat{B}\rangle - |\langle \hat{B}\rangle|^2, \tag{B.13} \\
\Delta\langle \hat{B}^\dagger \hat{B}^\dagger\rangle &\equiv \langle \hat{B}^\dagger \hat{B}^\dagger\rangle - (\langle \hat{B}\rangle^\star)^2, \tag{B.14}
\end{aligned}$$

where the photon-number like correlation $\Delta\langle \hat{B}^\dagger \hat{B}\rangle$ defines the emission intensity while $\Delta\langle \hat{B}^\dagger \hat{B}^\dagger\rangle$ describes the squeezing. The time evolutions of these quantities are determined via Eq. (B.12) and are presented in Figs. B.1(a)-B.1(b), for the initial average photon number $I \equiv \langle \hat{B}^\dagger \hat{B}\rangle(t=0) = |\alpha|^2 = 0.01$; the inset of Fig. B.1(c) shows the corresponding photon-number distribution $P_n$. In Figs. B.1(a)-B.1(b), the shaded area is the exact analytical solution, according to Eq. (B.12), the dashed line is the singlet-doublet (sd), the solid line is the singlet-doublet-triplet (sdt), and the dotted line is the singlet-doublet-triplet-quadrupolet (sdtq) approximation. The single-mode numerics at the different approximation levels (sd, sdt, sdtq) is obtained by reducing the general equations of motion of the full dot-cavity problem, given in Chapter 3 and App. D, to one dot and one single cavity mode according to Eq. (B.1).

In Fig. B.1(a), we observe that the sd numerics (dashed) does not fully reproduce the exact emission dynamics (shaded). However, we can see that the sdt approximation
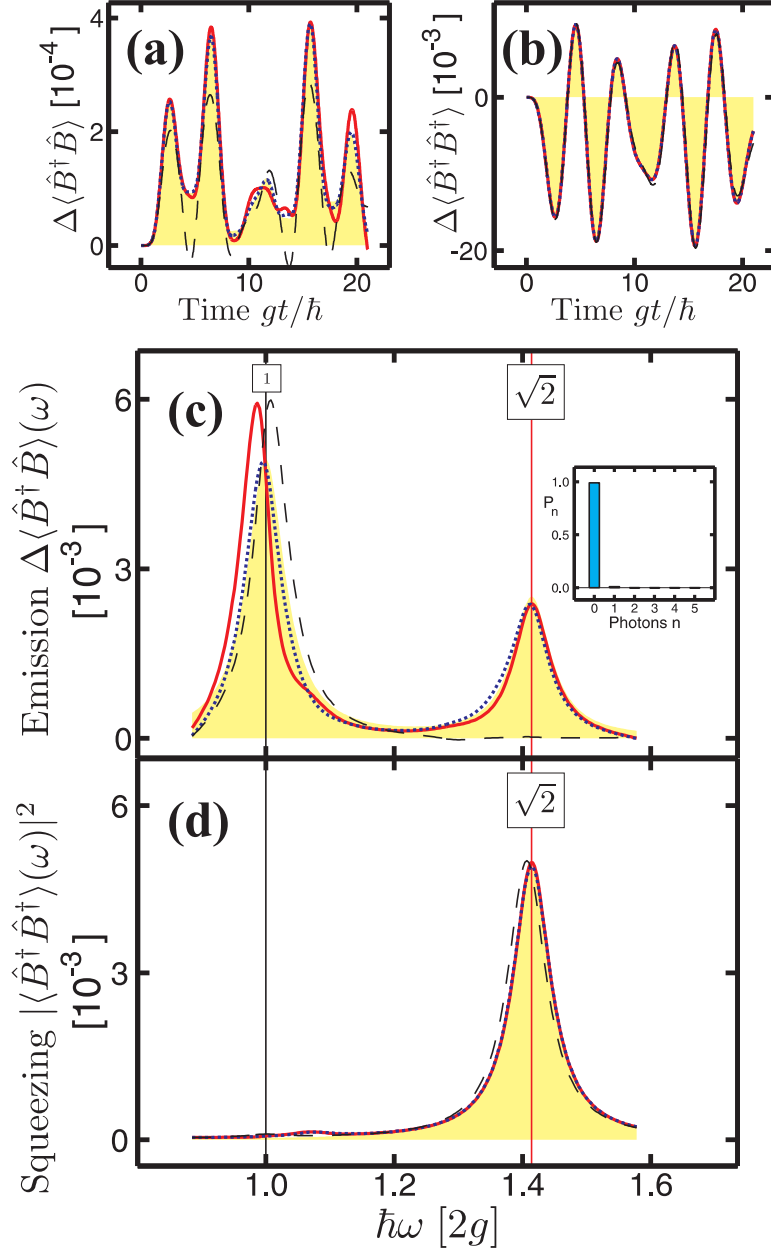
Figure B.1: Cluster-expansion approach reproduces the second rung. In all frames: The shaded area is the analytical solution, the dashed line is the singlet-doublet (sd), the solid line is the singlet-doublet-triplet (sdt), and the dotted line is the singlet-doublet-triplet-quadrupolet (sdtq) approximation. (a) Time evolution of the emission intensity $\Delta\langle\hat{B}^{\dagger}\hat{B}\rangle$. (b) Time evolution of the squeezing $\Delta\langle\hat{B}^{\dagger}\hat{B}^{\dagger}\rangle$. (c) Emission spectrum $\Delta\langle\hat{B}^{\dagger}\hat{B}\rangle(\omega)$. The second rung (vacuum Rabi peak) is marked by a vertical line and labeled $\sqrt{2}(1)$. Dephasing constant is $\gamma_{\mathrm{FT}} = 0.072\,g$. The inset shows the photon-number distribution with the average photon number $I = 0.01$. (d) Squeezing spectrum $|\langle\hat{B}^{\dagger}\hat{B}^{\dagger}\rangle(\omega)|^2$.

(solid) produces a very good agreement between the analytics and numerics. Including also the quadrupolets (dotted) changes the results only marginally. In Fig. B.1(b), we see that the squeezing dynamics is already well described at the sd level.

To determine the resonances in the system, we Fourier transform the presented time dynamics Figs. B.1(a)-B.1(b). For this purpose, we use a Fourier cosine transform defined by

$$f(\omega) \equiv 2\text{Re}\left[\int_0^\infty f(t) \exp\left(i\omega t\right) \exp\left(-\frac{\gamma_{\text{FT}} t}{\hbar}\right) dt\right], \tag{B.15}$$

where a dephasing constant $\gamma_{\text{FT}}$ has been introduced which ensures the numerical convergence of the integral and which results from the electron-electron and electron-phonon coupling in the dot-cavity system. Here, we again find analytical expressions for the spectra. In particular, the emission spectrum for the coherent excitation is determined by [79]

$$
\begin{aligned}
(\Delta\langle\hat{B}^\dagger\hat{B}\rangle &- \Delta\langle\hat{B}^\dagger\hat{B}\rangle_{\text{stat}})(\omega) \\
&= \frac{P_1\left(1-P_0\right)}{2}\frac{\hbar\gamma_{\text{FT}}}{\left(\hbar\omega-2g\right)^2+(\gamma_{\text{FT}})^2} \\
&+ \frac{P_2}{2}\frac{\hbar\gamma_{\text{FT}}}{\left(\hbar\omega-2g\sqrt{2}\right)^2+(\gamma_{\text{FT}})^2},
\end{aligned} \tag{B.16}
$$

where $\Delta\langle\hat{B}^\dagger\hat{B}\rangle_{\text{stat}}$ is the stationary part of $\Delta\langle\hat{B}^\dagger\hat{B}\rangle(t)$, explicitly given by

$$
\begin{aligned}
\Delta\langle\hat{B}^\dagger\hat{B}\rangle_{\text{stat}} \\
\equiv \langle\hat{B}^\dagger\hat{B}\rangle(t=0) + \frac{1}{2}\left(P_0-1\right) - \frac{1}{2}P_0P_1.
\end{aligned} \tag{B.17}
$$

The first term in Eq. (B.16) represents the vacuum Rabi peak, centered at $\hbar\omega/(2g) = 1$, and the second term is the second rung of the Jaynes-Cummings ladder, centered at $\hbar\omega/(2g) = \sqrt{2}$. Formally, one also obtains emission from the higher quantum rungs, but they have been neglected in Eq. (B.16). In Eq. (B.16), we indeed observe that the second rung scales like $P_2$ in the emission spectrum; a property which we have already verified numerically in Chapter 4. A similar expression can be obtained for the squeezing spectrum for the coherent excitation

$$|\langle\hat{B}^\dagger\hat{B}^\dagger\rangle|^2(\omega) = P_0P_2\frac{\hbar\gamma_{\text{FT}}}{\left(\hbar\omega-2g\sqrt{2}\right)^2+(\gamma_{\text{FT}})^2}, \tag{B.18}$$

where we have taken the full expectation value $\langle\hat{B}^\dagger\hat{B}^\dagger\rangle(t)$ for simplicity. Here, we find that there is only the second rung at $\hbar\omega/(2g) = \sqrt{2}$ which appears as a first contribution to the squeezing spectrum. In contrast to the emission intensity, the second-rung squeezing signal $|\langle\hat{B}^\dagger\hat{B}^\dagger\rangle|$ scales like $\sqrt{P_0P_2}$.

In Figs. B.1(c)-B.1(d), the emission and squeezing spectra are presented. The shaded area is again the exact analytical solution, according to Eqs. (B.16) and (B.18), the

dashed line is the sd, the solid line is the sdt, and the dotted line is the sdtq approximation. The position of the vacuum Rabi peak and second rung are marked by the vertical lines and labeled 1 and $\sqrt{2}$, respectively. Indeed, we see that both the vacuum Rabi peak and second rung are present in the emission, while only the second rung is present in the squeezing. In Fig. B.1(c), we find that the sd approximation (dashed line) is not accurate enough to reproduce the second rung in the emission spectrum; we have already found this property in Fig. 4.1 which shows that there are no quantum rungs in the emission spectrum in the singlet-doublet approximation, as indicated by the grey shaded area in Fig. 4.1. *Figure B.1(c) shows that the sdt approximation (solid line) indeed reproduces the second-rung very well.* Moreover, the higher-order correlations may be neglected as can be seen from the sdtq-level results. *In Fig. B.1(d), we notice again that already the sd level (dashed line) accurately reproduces the second rung in the squeezing spectrum.*

In summary, we have verified with these single-mode analyses that the generic singlet-doublet-triplet equations describe the second rung very well and constitute a profound basis for the investigation of true quantum-optical effects in the dot-cavity systems.

## B.4 Two-Photon Correlations

We analyze next the two-photon correlations $g^{(2)}$ which determine the probability of detecting two photons at the same time. Similarly to Eq. (5.1), we define

$$g^{(2)} \equiv \frac{\langle \hat{B}^\dagger \hat{B}^\dagger \hat{B} \hat{B} \rangle}{\langle \hat{B}^\dagger \hat{B} \rangle^2}. \tag{B.19}$$

We can evaluate the exact solution of $g^{(2)}(t)$ if we use Eq. (B.12) which defines the full quantum statistics. Furthermore, we can investigate the role of the different cluster to the exact solution. For this, it is convenient to expand the $g^{(2)}$ formula into the clusters

$$
\begin{aligned}
g^{(2)} &= \Big[ |\langle \hat{B} \rangle|^4 + 4\Delta\langle \hat{B}^\dagger \hat{B} \rangle |\langle \hat{B} \rangle|^2 + 2\mathrm{Re}[\Delta\langle \hat{B}^\dagger \hat{B}^\dagger \rangle \langle \hat{B} \rangle^2] \\
&\quad + 2\Delta\langle \hat{B}^\dagger \hat{B} \rangle^2 + |\Delta\langle \hat{B}^\dagger \hat{B}^\dagger \rangle|^2 + 4\mathrm{Re}[\langle \hat{B} \rangle \Delta\langle \hat{B}^\dagger \hat{B}^\dagger \hat{B} \rangle] \\
&\quad + \Delta\langle \hat{B}^\dagger \hat{B}^\dagger \hat{B} \hat{B} \rangle \Big] \Big/ (|\langle \hat{B} \rangle|^2 + \Delta\langle \hat{B}^\dagger \hat{B} \rangle)^2.
\end{aligned}
\tag{B.20}
$$

The correlated two-photon quantities $\Delta\langle \hat{B}^\dagger \hat{B} \rangle$ and $\Delta\langle \hat{B}^\dagger \hat{B}^\dagger \rangle$ are defined in Eqs. (B.13) and (B.14). For completeness, the three-photon and four-photon correlations can be recursively obtained via

$$
\begin{aligned}
\Delta\langle \hat{B}^\dagger \hat{B}^\dagger \hat{B} \rangle &\equiv \langle \hat{B}^\dagger \hat{B}^\dagger \hat{B} \rangle - (\langle \hat{B} \rangle^\star)^2 \langle \hat{B} \rangle \\
&\quad - 2\langle \hat{B} \rangle^\star \Delta\langle \hat{B}^\dagger \hat{B} \rangle - \langle \hat{B} \rangle \Delta\langle \hat{B}^\dagger \hat{B}^\dagger \rangle, \\
\Delta\langle \hat{B}^\dagger \hat{B}^\dagger \hat{B} \hat{B} \rangle &\equiv \langle \hat{B}^\dagger \hat{B}^\dagger \hat{B} \hat{B} \rangle - |\langle \hat{B} \rangle|^4 - 4\Delta\langle \hat{B}^\dagger \hat{B} \rangle |\langle \hat{B} \rangle|^2 \\
&\quad - \Delta\langle \hat{B}^\dagger \hat{B}^\dagger \rangle^\star (\langle \hat{B} \rangle^\star)^2 - \Delta\langle \hat{B}^\dagger \hat{B}^\dagger \rangle \langle \hat{B} \rangle^2 \\
&\quad - 2\langle \hat{B} \rangle^\star \Delta\langle \hat{B}^\dagger \hat{B}^\dagger \hat{B} \rangle^\star - 2\langle \hat{B} \rangle \Delta\langle \hat{B}^\dagger \hat{B}^\dagger \hat{B} \rangle \\
&\quad - 2\Delta\langle \hat{B}^\dagger \hat{B} \rangle^2 - |\Delta\langle \hat{B}^\dagger \hat{B}^\dagger \rangle|^2.
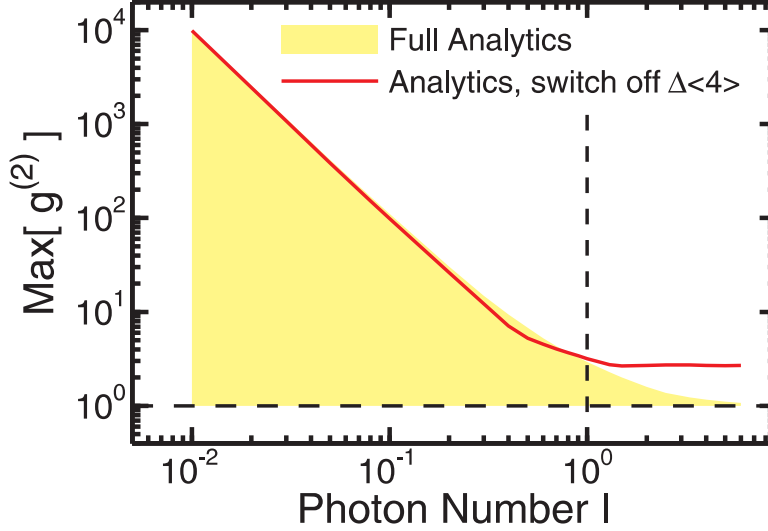\end{aligned}
\tag{B.21, B.22}
$$

Figure B.2: Maximum of $g^{(2)}$ as function of the average photon number for the coherent excitation. The shaded area presents the exact analytical solution and the solid line presents the analytical solution without the quadrupolets $\Delta\langle 4\rangle \equiv \Delta\langle \hat{B}^\dagger \hat{B}^\dagger \hat{B}\hat{B}\rangle$. The maximum of $g^{(2)}(t)$ is computed for $gt/\hbar \in [0, 20]$. Vertical and horizontal lines at 1 are guides for the eyes.

The cluster-expansion version Eq. (B.20) of $g^{(2)}$ is useful to analyze the importance of the quadrupolets $\Delta\langle \hat{B}^\dagger \hat{B}^\dagger \hat{B}\hat{B}\rangle$ which enter the nominator and which can be easily switched off.

Figure B.2 shows $g^{(2)}$ Eq. (B.19) as function of the average photon number $I$ for the coherent excitation. For convenience, we have determined the maximum $g^{(2)}$ value during the time evolution. The shaded area presents the exact analytical solution, according to Eqs. (B.12) and (B.19), while the solid line presents the analytical solution without the quadrupolets $\Delta\langle \hat{B}^\dagger \hat{B}^\dagger \hat{B}\hat{B}\rangle$. *We nicely see that $g^{(2)}$ dramatically increases if we approach the vacuum.* Furthermore, in the low-intensity regime with average photon number $I < 1$, there is an excellent agreement between the full and approximated analytical solution. *This demonstrates that we can neglect the quadrupolets in the high-$g^{(2)}$ regime for the coherent excitation. Hence, it is justified to use a singlet-doublet-triplet calculation for the analysis of the two-photon correlations, as has been done in Chapter 5.* If we approach the regime $I \geq 1$, the exact $g^{(2)}$ tends to the coherent-state value $g^{(2)} = 1$ while the approximated solution converges to a higher value close to $g^{(2)} = 3$. We thus learn that the quadrupolets become more dominant and ensure the physical consistency in the high-intensity regime. This is clear since the higher-order clusters are generated for increasing light-field intensities.

In summary, we conclude that the omission of the quadrupolets is justified in the regime with average photon number less than one. Another interesting finding is that also this simple analytical model predicts the gigantic $g^{(2)}$ values which we have found in the more demanding QD calculation in Chapter 5.

# C Thermal Excitation - Role of Correlations

We consider the single-mode Jaynes-Cummings model discussed in App. B and focus on the excitation with the thermal light. Even though we have not used the thermal excitation in this Thesis, the following results are essential if one wants to extend the presented theory to study also the thermal light. For this reason, we append here our fundamental insights which we have gained through a simple analysis.

Our main interest is to analyze the quantum statistics of the fluorescent light and the role of the different clusters. We show that for the incoherent excitation, the so-called X- (exciton) and X-photon correlations become crucial for a correct description of the quantum statistics. In particular, we demonstrate that these correlations play a major role for a consistent description of the emission in the incoherent regime, as also shown in Ref. [29] in a more demanding QD calculation. Finally, we show that the two-photon correlation $g^{(2)}$ is dominated by the four-particle correlations and reaches gigantic values for average photon number less than one.

## C.1 Extended Equations of Motion

We consider the single-mode Hamiltonian

$$
\begin{aligned}
\hat{H} &= \left( E^c \hat{c}^\dagger \hat{c} + E^v \hat{v}^\dagger \hat{v} \right) + \hbar \omega_c \left( \hat{B}^\dagger \hat{B} + \frac{1}{2} \right) \\
&\quad + \left( \mathcal{F}^\star \hat{B}^\dagger \hat{P} + \text{h.c.} \right)
\end{aligned}
\tag{C.1}
$$

and develop the necessary equations of motion for the thermal excitation. In the incoherent regime, no polarization and classical light field are present [35] such that we have $P = 0$ and $\langle \hat{B} \rangle = 0$. By studying the equation structure at the singlet-doublet-triplet-quadrupolet level, we find that only the photon-assisted polarization $\Delta \langle \hat{B}^\dagger \hat{P} \rangle$ and the four-particle correlation $\Delta \langle \hat{B}^\dagger \hat{B}^\dagger \hat{B} \hat{P} \rangle$ couple to the X- and X-photon correlation, defined by

$$
\text{X correlation} \equiv \Delta \langle \hat{P}^\dagger \hat{P} \rangle,
\tag{C.2}
$$

and

$$
\text{X-photon correlation} \equiv \Delta \langle \hat{B}^\dagger \hat{B} \hat{P}^\dagger \hat{P} \rangle.
\tag{C.3}
$$

## C Thermal Excitation - Role of Correlations

To analyze also the incoherent regime, we therefore extend the equations of motion of the correlations $\Delta\langle\hat{B}^\dagger\hat{P}\rangle$ and $\Delta\langle\hat{B}^\dagger\hat{B}^\dagger\hat{B}\hat{P}\rangle$ [79] and obtain

$$
\begin{aligned}
i\hbar\frac{\partial}{\partial t}\Delta\langle\hat{B}^\dagger\hat{P}\rangle &= i\hbar\frac{\partial}{\partial t}\Pi = (E^{cv} - \hbar\omega_c)\Pi - \mathcal{F}\left(f^c f^h + \Delta\langle\hat{P}^\dagger\hat{P}\rangle\right) \\
&\quad - \mathcal{F}\Delta\langle\hat{B}^\dagger\hat{B}\rangle\left(f^c + f^h - 1\right) - \mathcal{F}\langle\hat{B}\rangle\Delta\langle\hat{B}^\dagger\hat{f}^{cv}\rangle \\
&\quad - \mathcal{F}\Delta\langle\hat{B}^\dagger\hat{B}\hat{f}^{cv}\rangle,
\end{aligned}
\tag{C.4}
$$

$$
\begin{aligned}
i\hbar\frac{\partial}{\partial t}\Delta\langle\hat{B}^\dagger\hat{B}^\dagger\hat{B}\hat{P}\rangle &= i\hbar\frac{\partial}{\partial t}\Delta\langle\hat{B}^\dagger\hat{B}^\dagger\hat{B}\hat{P}\rangle_{\text{no X, X-photon correlations}} \\
&\quad - 2\mathcal{F}\Delta\langle\hat{B}^\dagger\hat{B}\hat{P}^\dagger\hat{P}\rangle.
\end{aligned}
\tag{C.5}
$$

The additional X- and X-photon correlations are solved directly with the Pauli exclusion principle

$$
\langle a^\dagger a^\dagger cc\rangle = \langle a^\dagger a^\dagger vv\rangle = \langle a^\dagger a^\dagger cv\rangle = 0,
\tag{C.6}
$$

where $a = c, v$ denotes the fermionic carrier operator of conduction, valence electron, respectively. We find for the dynamics of X correlation

$$
\begin{aligned}
\Delta\langle\hat{P}^\dagger\hat{P}\rangle &= \langle\hat{P}^\dagger\hat{P}\rangle - \langle\hat{P}^\dagger\hat{P}\rangle_{\text{Hartree Fock}} \\
&= f^c - |P|^2 - f^c f^h,
\end{aligned}
\tag{C.7}
$$

which reads in the incoherent regime (inc)

$$
\Delta\langle\hat{P}^\dagger\hat{P}\rangle_{\text{inc}} = f^c - f^c f^h.
\tag{C.8}
$$

Analogously, we solve the X-photon correlation which reads

$$
\begin{aligned}
\Delta\langle\hat{B}^\dagger\hat{B}\hat{P}^\dagger\hat{P}\rangle &= \left(-\frac{1}{2}\right)\left(f^c + f^h - 1\right)\Delta\langle\hat{B}^\dagger\hat{B}\hat{f}^{cv}\rangle - P^\star\Delta\langle\hat{B}^\dagger\hat{B}\hat{P}\rangle \\
&\quad - P\Delta\langle\hat{B}^\dagger\hat{B}\hat{P}\rangle^\star - \frac{1}{2}|\Delta\langle\hat{B}^\dagger\hat{f}^{cv}\rangle|^2 - |\Pi|^2 - |\Delta\langle\hat{B}^\dagger\hat{P}^\dagger\rangle|^2,
\end{aligned}
\tag{C.9}
$$

and reduces in the incoherent regime to

$$
\Delta\langle\hat{B}^\dagger\hat{B}\hat{P}^\dagger\hat{P}\rangle_{\text{inc}} = \frac{1}{2}\Delta\langle\hat{B}^\dagger\hat{B}\hat{f}^{cv}\rangle - |\Pi|^2 - \frac{1}{2}\left(f^c + f^h\right)\Delta\langle\hat{B}^\dagger\hat{B}\hat{f}^{cv}\rangle.
\tag{C.10}
$$

The extended equation of motion for the four-particle correlation $\Delta\langle\hat{B}^\dagger\hat{B}^\dagger\hat{B}\hat{P}\rangle$ in the incoherent regime then reads

$$
\begin{aligned}
i\hbar\frac{\partial}{\partial t}\Delta\langle\hat{B}^\dagger\hat{B}^\dagger\hat{B}\hat{P}\rangle_{\text{inc}} &= (E^{cv} - \hbar\omega_c)\Delta\langle\hat{B}^\dagger\hat{B}^\dagger\hat{B}\hat{P}\rangle \\
&\quad - \mathcal{F}\Big[\Delta\langle\hat{B}^\dagger\hat{B}\hat{f}^{cv}\rangle\left(1 + 2\Delta\langle\hat{B}^\dagger\hat{B}\rangle\right) - 2|\Pi|^2 \\
&\quad + \Delta\langle\hat{B}^\dagger\hat{B}^\dagger\hat{B}\hat{B}\rangle\left(f^c + f^h - 1\right)\Big] - 2\mathcal{F}^\star\Pi^2.
\end{aligned}
\tag{C.11}
$$

To summarize, the extended equations of motion in the incoherent regime consist of Eqs. (C.4) and (C.11).
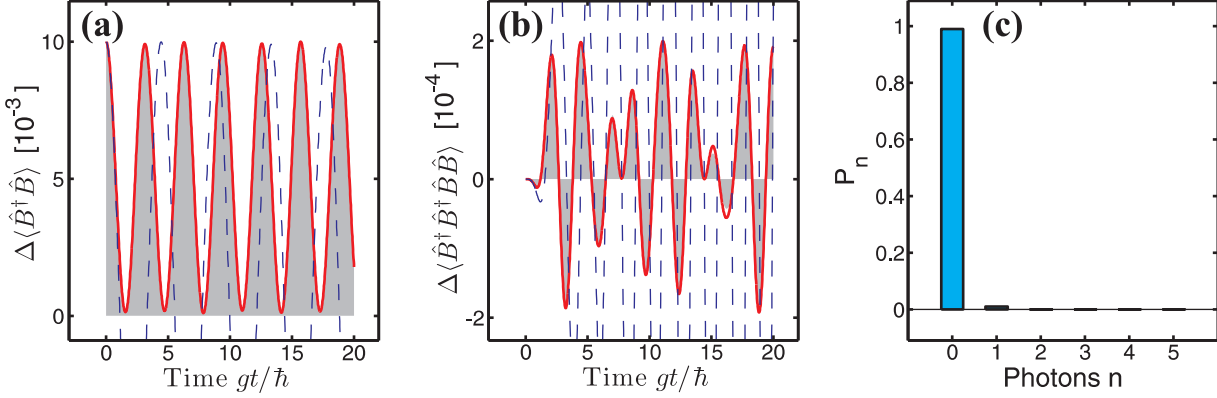
Figure C.1: Time dynamics of the emission (a) and of the four-photon correlation (b) for the thermal excitation. The shaded area is the exact analytical solution, the solid line is the fully consistent sdtq approximation, and the dashed line is the sdtq approximation where the X- and X-photon correlations are switched off. The average photon number is $I = 0.01$, the light-matter coupling constant is $g = 22$ GHz. (c) Photon-number distribution $P_n$.

## C.2 Role of Clusters

Figure C.1 shows a part of the quantum statistics of the fluorescent light for the thermal excitation. Figure C.1(a) presents the time dynamics of the emission intensity $\Delta\langle\hat{B}^\dagger\hat{B}\rangle$ and Fig. C.1(b) presents the time dynamics of the four-photon correlation $\Delta\langle\hat{B}^\dagger\hat{B}^\dagger\hat{B}\hat{B}\rangle$. The shaded area denotes the exact analytical solution according to Eq. (B.12), the solid line is the numerically calculated sdtq (singlet-doublet-triplet-quadrupolet) approximation with X- and X-photon correlations included, denoted by *fully consistent sdtq approximation* in the following, and the dashed line is the numerically calculated sdtq approximation without the X- and X-photon correlations. Figure C.1(c) shows the corresponding photon-number distribution $P_n$ for the used thermal excitation. *We observe that the two-particle and four-photon correlations presented in Fig. C.1 are well reproduced via the fully consistent sdtq approximation.* In contrast, the sdtq approximation without the X- and X-photon correlations shows negative emission intensity $\Delta\langle\hat{B}^\dagger\hat{B}\rangle$ [29]. Furthermore, the approximation does not follow the exact solution, neither in the emission intensity Fig. C.1(a) nor in the four-photon correlation Fig. C.1(b). *It is thus crucial to include the X- and X-photon correlations in the incoherent regime to obtain a physically consistent solution.*

To demonstrate further the reliability of the fully consistent sdtq approximation, we show that we can correctly describe the second rung in the higher-order expectation values. Figure C.2 presents the Fourier transform of the four-photon expectation value $\langle\hat{B}^\dagger\hat{B}^\dagger\hat{B}\hat{B}\rangle$. The shaded area is the exact solution, according to Eq. (B.12), which explicitly reads

$$\langle\hat{B}^\dagger\hat{B}^\dagger\hat{B}\hat{B}\rangle(\omega)_{\text{inc}} = P_2 \frac{\hbar\gamma_{\text{FT}}}{\left(\hbar\omega - 2g\sqrt{2}\right)^2 + (\gamma_{\text{FT}})^2}, \tag{C.12}$$
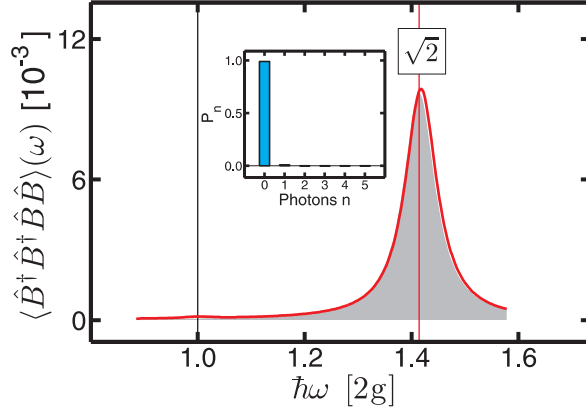
Figure C.2: Spectrum of the four-photon expectation value $\langle \hat{B}^\dagger \hat{B}^\dagger \hat{B} \hat{B} \rangle$ for the thermal excitation. The vertical lines mark the energetic position of the vacuum Rabi peak and the second rung labeled by '$\sqrt{2}$'. The shaded area is the exact analytical solution and the solid line is the fully consistent sdtq approximation. The average photon number is $I = 0.01$, the light-matter coupling constant is $g = 22$ GHz and the dephasing constant in the Fourier transform is $\gamma_{\text{FT}} = 0.072\,g$. The inset shows the photon-number distribution $P_n$.

and the solid line is the fully consistent sdtq approximation. The vertical lines mark the energetic position of the vacuum Rabi peak and the second rung which is also labeled by '$\sqrt{2}$'. The inset shows again the photon-number distribution $P_n$. Indeed, we obtain a very good agreement between the analytics and numerics. The second-rung resonance in the spectrum Fig. C.2 is well reproduced via the numerics. This shows that the fully consistent sdtq approximation accurately describes the higher-order expectation values up to four particles.

## C.3 Two-Photon Correlations

Figure C.3 shows the two-photon correlation $g^{(2)}$ as function of the average photon number $I$ for the thermal excitation. The shaded area (dotted line) is the exact solution of the maximum (minimum) $g^{(2)}(t)$ value for $gt/\hbar \in [0, 20]$, and the solid line presents the analytical solution without the quadrupolets. The dashed vertical line at $I = 1$ is a guide for the eye. *We observe that $g^{(2)}$ dramatically increases for decreasing photon numbers $I \leq 1$ and takes values up to $g^{(2)} \sim 10^3$.* The minimum value of $g^{(2)}$ converges to zero for decreasing photon numbers. For large $I > 1$, we notice that both the maximum and minimum of $g^{(2)}$ tend towards the thermal-light value of $g^{(2)} = 2$. From the solid line, we can see that we obtain a constant value of $g^{(2)} = 2$ if we switch off the quadrupolet terms $\Delta\langle 4 \rangle$. This is in extreme contrast to the exact behavior of $g^{(2)}$ which takes gigantic values in the low-intensity regime. *Thus, the four-particle correlations are essential for a consistent description of the two-photon correlation $g^{(2)}$ in the incoherent regime [81].*
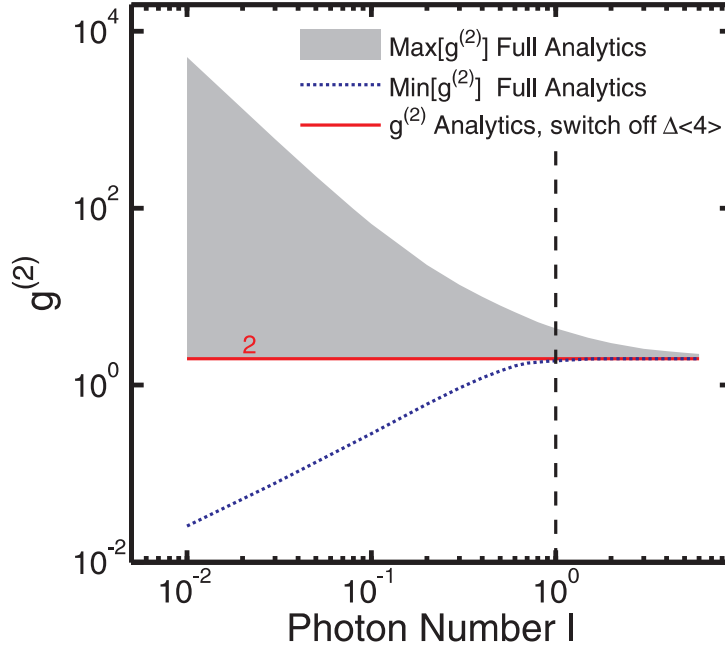
Figure C.3: Two-photon correlation $g^{(2)}$ as function of the average photon number $I$ for the thermal excitation and influence of the quadrupolet terms $\Delta\langle 4\rangle$. The shaded area (dotted line) is the full analytical solution of the maximum (minimum) of $g^{(2)}(t)$ for $gt/\hbar \in [0, 20]$. The solid line presents the analytical solution without the quadrupolets, resulting in a constant value of $g^{(2)} = 2$. The light-matter coupling constant is $g = 22$ GHz. The dashed vertical line at $I = 1$ is a guide for the eye.

# D Triplet Equations

In Chapter 3, we have applied the Heisenberg equation-of-motion technique and the cluster-expansion approach. We have set up a consistent set of singlet-doublet-triplet equations and we have discussed one of the triplet equations. In App. D, we present also the remaining triplet equations [79] for the system Hamiltonian (2.2) to close the full set of singlet-doublet-triplet equations. In particular, we obtain the photon-photon-carrier correlations and photon-photon-photon correlations.

Starting with the photon-photon-carrier correlations, the photon-photon-density correlations follow from

$$
\begin{aligned}
i\hbar \frac{\partial}{\partial t} &\Delta\langle \hat{B}_q \hat{B}_{q'} \hat{f}_j^{cv}\rangle \\
=\ & \hbar\left(\omega_q + \omega_{q'}\right)\Delta\langle \hat{B}_q \hat{B}_{q'}\hat{f}_j^{cv}\rangle \\
& + 2\sum_{q''}\Big[\mathcal{F}_{q''}\Pi_{qj}^{\star}\Delta\langle \hat{B}_{q'}\hat{B}_{q''}\rangle + \mathcal{F}_{q''}\Pi_{q'j}^{\star}\Delta\langle \hat{B}_q\hat{B}_{q''}\rangle \\
& - \mathcal{F}_{q''}^{\star}\Delta\langle \hat{B}_q\hat{P}_j\rangle\Delta\langle \hat{B}_{q''}^{\dagger}\hat{B}_{q'}\rangle - \mathcal{F}_{q''}^{\star}\Delta\langle \hat{B}_{q'}\hat{P}_j\rangle\Delta\langle \hat{B}_{q''}^{\dagger}\hat{B}_q\rangle \\
& + \mathcal{F}_{q''}P_j^{\star}\Delta\langle \hat{B}_q\hat{B}_{q'}\hat{B}_{q''}\rangle - \mathcal{F}_{q''}^{\star}P_j\Delta\langle \hat{B}_{q''}^{\dagger}\hat{B}_q\hat{B}_{q'}\rangle\Big] \\
& - 2\Omega_j\Delta\langle \hat{B}_q\hat{B}_{q'}\hat{P}_j^{\dagger}\rangle + 2\Omega_j^{\star}\Delta\langle \hat{B}_q\hat{B}_{q'}\hat{P}_j\rangle \\
& - \left(f_j^c + f_j^h\right)\left(\mathcal{F}_q^{\star}\Delta\langle \hat{B}_{q'}\hat{P}_j\rangle + \mathcal{F}_{q'}^{\star}\Delta\langle \hat{B}_q\hat{P}_j\rangle\right) \\
& + 2\sum_{q''}\mathcal{F}_{q''}\Delta\langle \hat{B}_q^{\dagger}\hat{B}_{q'}^{\dagger}\hat{B}_{q''}^{\dagger}\hat{P}_j\rangle^{\star} - 2\sum_{q''}\mathcal{F}_{q''}^{\star}\Delta\langle \hat{B}_q^{\dagger}\hat{B}_{q'}^{\dagger}\hat{B}_{q''}\hat{P}_j^{\dagger}\rangle^{\star} \\
& - P_j\left(\mathcal{F}_q^{\star}\Delta\langle \hat{B}_{q'}\hat{f}_j^{cv}\rangle + \mathcal{F}_{q'}^{\star}\Delta\langle \hat{B}_q\hat{f}_j^{cv}\rangle\right).
\end{aligned}
\tag{D.1}
$$

As further sets which contain the carrier operators, we have the photon-photon-polarization correlations which are determined by

$$i\hbar \frac{\partial}{\partial t} \Delta\langle \hat{B}_q^\dagger \hat{B}_{q'} \hat{P}_j \rangle$$

$$= (E^{cv} + \hbar\omega_{q'} - \hbar\omega_q - i\gamma_P) \Delta\langle \hat{B}_q^\dagger \hat{B}_{q'} \hat{P}_j \rangle$$

$$- \sum_{q''} \Big[ \mathcal{F}_{q''} \Delta\langle \hat{B}_q \hat{f}_j^{cv} \rangle^\star \Delta\langle \hat{B}_{q'} \hat{B}_{q''} \rangle + \mathcal{F}_{q''} \Delta\langle \hat{B}_{q'} \hat{f}_j^{cv} \rangle \Delta\langle \hat{B}_q^\dagger \hat{B}_{q''} \rangle$$

$$+ \mathcal{F}_{q''} \left( f_j^c + f_j^h - 1 \right) \Delta\langle \hat{B}_q^\dagger \hat{B}_{q'} \hat{B}_{q''} \rangle \Big]$$

$$+ \Omega_j \Delta\langle \hat{B}_q^\dagger \hat{B}_{q'} \hat{f}_j^{cv} \rangle$$

$$- \frac{1}{2} \mathcal{F}_q \left( f_j^c + f_j^h \right) \Delta\langle \hat{B}_{q'} \hat{f}_j^{cv} \rangle - 2\mathcal{F}_{q'}^\star P_j \Pi_{qj}$$

$$- \sum_{q''} \mathcal{F}_{q''} \Delta\langle \hat{B}_{q''}^\dagger \hat{B}_{q'}^\dagger \hat{B}_q \hat{f}_j^{cv} \rangle^\star, \tag{D.2}$$

$$i\hbar \frac{\partial}{\partial t} \Delta\langle \hat{B}_q \hat{B}_{q'} \hat{P}_j^\dagger \rangle$$

$$= (-E^{cv} + \hbar\omega_q + \hbar\omega_{q'} - i\gamma_P) \Delta\langle \hat{B}_q \hat{B}_{q'} \hat{P}_j^\dagger \rangle$$

$$+ \sum_{q''} \Big[ \mathcal{F}_{q''}^\star \Delta\langle \hat{B}_q \hat{f}_j^{cv} \rangle \Delta\langle \hat{B}_{q''}^\dagger \hat{B}_{q'} \rangle + \mathcal{F}_{q''}^\star \Delta\langle \hat{B}_{q'} \hat{f}_j^{cv} \rangle \Delta\langle \hat{B}_{q''}^\dagger \hat{B}_q \rangle$$

$$+ \mathcal{F}_{q''}^\star \left( f_j^c + f_j^h - 1 \right) \Delta\langle \hat{B}_{q''}^\dagger \hat{B}_q \hat{B}_{q'} \rangle \Big]$$

$$- \Omega_j^\star \Delta\langle \hat{B}_q \hat{B}_{q'} \hat{f}_j^{cv} \rangle$$

$$+ \frac{1}{2} \left( f_j^c + f_j^h \right) \left( \mathcal{F}_q^\star \Delta\langle \hat{B}_{q'} \hat{f}_j^{cv} \rangle + \mathcal{F}_{q'}^\star \Delta\langle \hat{B}_q \hat{f}_j^{cv} \rangle \right)$$

$$+ \sum_{q''} \mathcal{F}_{q''}^\star \Delta\langle \hat{B}_q^\dagger \hat{B}_{q'}^\dagger \hat{B}_{q''} \hat{f}_j^{cv} \rangle^\star, \tag{D.3}$$

$$i\hbar \frac{\partial}{\partial t} \Delta\langle \hat{B}_q \hat{B}_{q'} \hat{P}_j \rangle$$

$$= (E^{cv} + \hbar\omega_q + \hbar\omega_{q'} - i\gamma_P) \Delta\langle \hat{B}_q \hat{B}_{q'} \hat{P}_j \rangle$$

$$- \sum_{q''} \Big[ \mathcal{F}_{q''} \Delta\langle \hat{B}_q \hat{f}_j^{cv} \rangle \Delta\langle \hat{B}_{q'} \hat{B}_{q''} \rangle + \mathcal{F}_{q''} \Delta\langle \hat{B}_{q'} \hat{f}_j^{cv} \rangle \Delta\langle \hat{B}_q \hat{B}_{q''} \rangle$$

$$+ \mathcal{F}_{q''} \left( f_j^c + f_j^h - 1 \right) \Delta\langle \hat{B}_q \hat{B}_{q'} \hat{B}_{q''} \rangle \Big]$$

$$+ \Omega_j \Delta\langle \hat{B}_q \hat{B}_{q'} \hat{f}_j^{cv} \rangle$$

$$- 2P_j \left( \mathcal{F}_q^\star \Delta\langle \hat{B}_{q'} \hat{P}_j \rangle + \mathcal{F}_{q'}^\star \Delta\langle \hat{B}_q \hat{P}_j \rangle \right)$$

$$- \sum_{q''} \mathcal{F}_{q''} \Delta\langle \hat{B}_q^\dagger \hat{B}_{q'}^\dagger \hat{B}_{q''}^\dagger \hat{f}_j^{cv} \rangle^\star. \tag{D.4}$$

Finally, the photon-photon-photon correlations which contain only the photon operators follow from

$$
\begin{aligned}
i\hbar \frac{\partial}{\partial t} &\Delta\langle \hat{B}_q \hat{B}_{q'} \hat{B}_{q''} \rangle \\
&= \hbar\left(\omega_q + \omega_{q'} + \omega_{q''}\right)\Delta\langle \hat{B}_q \hat{B}_{q'} \hat{B}_{q''} \rangle \\
&+ \sum_j \left[ \mathcal{F}_q^\star \Delta\langle \hat{B}_{q'} \hat{B}_{q''} \hat{P}_j \rangle + \mathcal{F}_{q'}^\star \Delta\langle \hat{B}_q \hat{B}_{q''} \hat{P}_j \rangle \right. \\
&+ \left. \mathcal{F}_{q''}^\star \Delta\langle \hat{B}_q \hat{B}_{q'} \hat{P}_j \rangle \right],
\end{aligned}
\tag{D.5}
$$

$$
\begin{aligned}
i\hbar \frac{\partial}{\partial t} &\Delta\langle \hat{B}_q^\dagger \hat{B}_{q'} \hat{B}_{q''} \rangle \\
&= \hbar\left(\omega_{q''} + \omega_{q'} - \omega_q\right)\Delta\langle \hat{B}_q^\dagger \hat{B}_{q'} \hat{B}_{q''} \rangle \\
&+ \sum_j \left[ \mathcal{F}_{q''}^\star \Delta\langle \hat{B}_q^\dagger \hat{B}_{q'} \hat{P}_j \rangle + \mathcal{F}_{q'}^\star \Delta\langle \hat{B}_q^\dagger \hat{B}_{q''} \hat{P}_j \rangle \right. \\
&- \left. \mathcal{F}_q \Delta\langle \hat{B}_{q''} \hat{B}_{q'} \hat{P}_j^\dagger \rangle \right].
\end{aligned}
\tag{D.6}
$$

# Bibliography

[1] Kimble, H. J., Dagenais, M., and Mandel, L. (1977) Photon antibunching in resonance fluorescence. *Phys. Rev. Lett.*, **39**, 691.

[2] Slusher, R. E. et al. (1985) Observation of squeezed states generated by four-wave mixing in an optical cavity. *Phys. Rev. Lett.*, **55**, 2409.

[3] Anderson, M. H., Ensher, J. R., Matthews, M. R., Wieman, C. E., and Cornell, E. A. (1995) Observation of bose-einstein condensation in a dilute atomic vapor. *Science*, **269**, 198–201.

[4] Bouwmeester, D., Pan, J. W., Mattle, K., Eibl, M., Weinfurter, H., and Zeilinger, A. (1997) Experimental quantum teleportation. *Nature*, **390**, 575–579.

[5] Stolz, H., Kira, M., and Koch, S. W. (2008) Quantenoptik in halbleitern. *Physik Journal*, **7**, 37.

[6] Michler, P. et al. (2000) A quantum dot single-photon turnstile device. *Science*, **290**, 2282.

[7] Santori, C. et al. (2001) Triggered single photons from a quantum dot. *Phys. Rev. Lett.*, **86**, 1502.

[8] Zwiller, V. et al. (2001) Single quantum dots emit single photons at a time: Antibunching experiments. *Appl. Phys. Lett.*, **78**, 2476.

[9] Hafenbrak, R., Ulrich, S. M., Michler, P., Wang, L., Rastelli, A., and Schmidt, O. G. (2007) Triggered polarization-entangled photon pairs from a single quantum dot up to 30k. *New J. Phys.*, **9**, 315.

[10] Akopian, N., Lindner, N. H., Poem, E., Berlatzky, Y., Avron, J., Gershoni, D., Gerardot, B. D., and Petroff, P. M. (2006) Entangled photon pairs from semiconductor quantum dots. *Phys. Rev. Lett.*, **96**, 130501.

[11] Stevenson, R. M. et al. (2006) A semiconductor source of triggered entangled photon pairs. *Nature*, **439**, 179.

[12] Varcoe, B. T. H., Brattke, S., Weidinger, M., and Walther, H. (2000) Preparing pure photon number states of the radiation field. *Nature*, **403**, 743–746.

[13] Englund, D., Faraon, A., Fushman, I., Stoltz, N., Petroff, P., and Vuckovic, J. (2007) Controlling cavity reflectivity with a single quantum dot. *Nature*, **450**, 857–861.

*Bibliography*

[14] Zeilinger, A. (1999) Experiment and the foundations of quantum physics. *Rev. Mod. Phys.*, **71**, S288–S297.

[15] Braunstein, S. L. and van Loock, P. (2005) Quantum information with continuous variables. *Rev. Mod. Phys.*, **77**, 513–577.

[16] Jaynes, E. and Cummings, F. (1963) *Proc. IEEE*, **51**, 89.

[17] Reithmaier, J. P. et al. (2004) Strong coupling in a single quantum dot-semiconductor microcavity system. *Nature (London)*, **432**, 197–200.

[18] Yoshie, T. et al. (2004) Vacuum rabi splitting with a single quantum dot in a photonic crystal nanocavity. *Nature (London)*, **432**, 200.

[19] Peter, E. et al. (2005) Exciton-photon strong-coupling regime for a single quantum dot embedded in a microcavity. *Phys. Rev. Lett.*, **95**, 067401.

[20] Hennessy, K. et al. (2007) Quantum nature of a strongly coupled single quantum dot-cavity system. *Nature (London)*, **445**, 896.

[21] Khitrova, G., Gibbs, H. M., Kira, M., Koch, S. W., and Scherer, A. (2006) Vacuum rabi splitting in semiconductors. *Nature Physics*, **2**, 81–90.

[22] Thompson, R. J., Rempe, G., and Kimble, H. J. (1992) Observation of normal-mode splitting for an atom in an optical cavity. *Phys. Rev. Lett.*, **68**, 1132.

[23] Boca, A. et al. (2004) Observation of the vacuum rabi spectrum for one trapped atom. *Phys. Rev. Lett.*, **93**, 233603.

[24] Brune, M. et al. (1996) Quantum rabi oscillation: A direct test of field quantization in a cavity. *Phys. Rev. Lett.*, **76**, 1800.

[25] Schuster, I. et al. (2008) Nonlinear spectroscopy of photons bound to one atom. *Nature Phys.*, **4**, 382.

[26] Kubanek, A., Ourjoumtsev, A., Schuster, I., Koch, M., Pinkse, P. W. H., Murr, K., and Rempe, G. (2008) Two-Photon Gateway in One-Atom Cavity Quantum Electrodynamics. *Phys. Rev. Lett.*, **101**, 203602.

[27] Wyld, H. W. and Fried, B. D. (1963) Quantum mechanical kinetic equations. *Ann. Phys.*, **23**, 374.

[28] Kira, M. and Koch, S. W. (2006) Many-body correlations and excitonic effects in semiconductor spectroscopy. *Prog. Quantum Electron.*, **30**, 155.

[29] Feldtmann, T. et al. (2006) Quantum theory of light emission from a semiconductor quantum dot. *Phys. Rev. B*, **73**, 155319.

72

[30] Fricke, J. (1996) Transport equations including many-particle correlations for an arbitrary quantum system: A general formalism. *Ann. Phys. (N. Y.)*, **252**, 479.

[31] Hoyer, W., Kira, M., and Koch, S. W. (2004) *Cluster Expansion in Semiconductor Quantum Optics*. Nonequilibrium Physics at Short Time Scales, Springer, Berlin.

[32] Kira, M., Hoyer, W., Koch, S. W., Brick, P., Ell, C., Hubner, M., Khitrova, G., and Gibbs, H. M. (2003) Quantum correlations in semiconductor microcavities. *Semicond. Sci. Technol.*, **18**, S405–S410.

[33] Koch, S. W. and Kira, M. (2004) *Excitons in semiconductors*, vol. 146 of *Optics of Semiconductors and their Nanostructures - Springer Series in Solid-State Sciences*. Springer, Berlin.

[34] Kira, M., Hoyer, W., Stroucken, T., and Koch, S. W. (2001) Exciton formation in semiconductors and the influence of a photonic environment. *Phys. Rev. Lett.*, **87**, 176401.

[35] Kira, M. et al. (1999) Quantum theory of spontaneous emission and coherent effects in semiconductor microstructures. *Prog. Quantum Electron.*, **23**, 189.

[36] Koch, S. W., Kira, M., Khitrova, G., and Gibbs, H. M. (2006) Semiconductor excitons in new light. *Nature Mater.*, **5**, 523–531.

[37] Kira, M. and Koch, S. W. (2005) Microscopic theory of optical excitations, photoluminescence, and terahertz response in semiconductors. *Eur. Phys. J. D*, **36**, 143.

[38] Fetter, A. and Walecka, J. (2003) *Quantum Theory of Many-Particle Systems*. Dover Publications.

[39] Gross, E. K. U. and Dreizler, R. M. (1991) *Density Function Theory*. Springer.

[40] Metropolis, N., Rosenbluth, A. W., Rosenbluth, M. N., Teller, A. H., and Teller, E. (1953) Equation of state calculations by fast computing machines. *J. Chem. Phys.*, **21**, 1087–1092.

[41] Hillery, M., O'Connell, R. F., Scully, M. O., and Wigner, E. P. (1984) Distribution-functions in physics - fundamentals. *Phys. Rep.*, **106**, 121–167.

[42] Wigner, E. (1932) On the quantum correction for thermodynamic equilibrium. *Phys. Rev.*, **40**, 0749–0759.

[43] Kira, M. and Koch, S. W. (2008) Cluster-expansion representation in quantum optics. *Phys. Rev. A*, **78**, 022102.

[44] Kira, M., Jahnke, F., and Koch, S. W. (1999) Quantum theory of secondary emission in optically excited semiconductor quantum wells. *Phys. Rev. Lett.*, **82**, 3544–3547.

*Bibliography*

[45] Carmichael, H. J. (1985) Photon antibunching and squeezing for a single atom in a resonant cavity. *Phys. Rev. Lett.*, **55**, 2790–2793.

[46] Carmichael, H. J. and Walls, D. F. (1976) Proposal for measurement of resonant stark effect by photon correlation techniques. *J. Phys. B*, **9**, L43–L46.

[47] Sudarshan, E. C. G. (1963) Equivalence of semiclassical and quantum mechanical descriptions of statistical light beams. *Phys. Rev. Lett.*, **10**, 277.

[48] Glauber, R. J. (1963) Coherent and incoherent states of the radiation field. *Phys. Rev.*, **131**, 2766.

[49] Glauber, R. J. (1963) The quantum theory of optical coherence. *Phys. Rev.*, **130**, 2529.

[50] Cahill, K. E. and Glauber, R. J. (1969) Ordered expansions in boson amplitude operators. *Phys. Rev.*, **177**, 1857.

[51] Jackson, J. D. (1998) *Classical Electrodynamics*. Wiley & Sons.

[52] Khitrova, G., Gibbs, H. M., Jahnke, F., Kira, M., and Koch, S. W. (1999) Nonlinear optics of normal-mode-coupling semiconductor microcavities. *Rev. Mod. Phys.*, **71**, 1591–1639.

[53] Schaefer, M. (2008) *Microscopic Theory of Coherent and Incoherent Optical Properties of Semiconductor Heterostructures*. Ph.D. thesis, Philipps-University Marburg.

[54] Feldtmann, T. (2009) *Influence of Phonons on Semiconductor Quantum Emission*. Ph.D. thesis, Philipps-University Marburg.

[55] Brasken, M. et al. (2000) Full configuration interaction calculations of electron-hole correlation effects in strain-induced quantum dots. *Phys. Rev. B*, **61**, 7652.

[56] Baer, N., Gartner, P., and Jahnke, F. (2004) Coulomb effects in semiconductor quantum dots. *Eur. Phys. J. B*, **42**, 231.

[57] Wojs, A. et al. (1996) Electronic structure and magento-optics of self-assembled quantum dots. *Phys. Rev. B*, **54**, 5604.

[58] Cohen-Tannoudji, C., Dupont-Roc, J., and Grynberg, G. (1997) *Photons and Atoms: Introduction to Quantum Electrodynamics*. Wiley-VCH.

[59] Schneebeli, L., Kira, M., and Koch, S. W. (2009) Characterization of strong light-matter coupling in semiconductor quantum-dot microcavities. *Proceedings of the International Workshop NOEKS-9*, vol. 6, pp. 407–410, Phys. Status Solidi C.

[60] Schneebeli, L., Kira, M., and Koch, S. W. (2008) Characterization of strong light-matter coupling in semiconductor quantum-dot microcavities via photon-statistics spectroscopy. *Phys. Rev. Lett.*, **101**, 097401.

74

[61] Löffler, A. et al. (2005) Semiconductor quantum dot microcavity pillars with high-quality factors and enlarged dot dimensions. *Appl. Phys. Lett.*, **86**, 111105.

[62] Srinivasan, K. and Painter, O. (2007) Mode coupling and cavity-quantum-dot interactions in a fiber-coupled microdisk cavity. *Phys. Rev. A*, **75**, 023814.

[63] Cohen-Tannoudji, C., Diu, B., and Laloe, F. (1999) *Quantenmechanik 1*. Walter de Gruyter.

[64] Stoer, J. and Bulirsch, R. (2000) *Numerische Mathematik 2*. Springer.

[65] Allen, L. and Eberly, J. H. (1987) *Optical Resonance and Two-Level Atoms*. Dover Publications Inc.

[66] Tian, L. and Carmichael, H. J. (1992) Incoherent excitation of the jaynes-cummings system. *Quantum Opt.*, **4**, 131.

[67] Löffler, M., Meyer, G. M., and Walther, H. (1997) Spectral properties of the one-atom laser. *Phys. Rev. A*, **55**, 3923.

[68] Walls, D. F. and Milburn, G. J. (1995) *Quantum Optics*. Springer.

[69] Carmichael, H. J., Kochan, P., and Sanders, B. C. (1996) Photon correlation spectroscopy. *Phys. Rev. Lett.*, **77**, 631.

[70] Brown, R. H. and Twiss, R. Q. (1956) Correlation between photons in two coherent beams of light. *Nature*, **177**, 27–29.

[71] Brown, R. H. and Twiss, R. Q. (1954) A new type of interferometer for use in radio astronomy. *Philos. Mag.*, **45**, 663–682.

[72] Kira, M. Quantum optics, lecture notes, summer term 2008.

[73] Mattinson, F., Kira, M., and Stenholm, S. (2002) Photon statistics anomalies in adiabatic transfer between two cavity modes. *J. Mod. Opt.*, **49**, 1649.

[74] Bayer, M. and Forchel, A. (2002) Temperature dependence of the exciton homogeneous linewidth in $in_{0.60}ga_{0.40}as/gaas$ self-assembled quantum dots. *Phys. Rev. B*, **65**, 041308(R).

[75] Nielsen, T. R., Gartner, P., and Jahnke, F. (2004) Many-body theory of carrier capture and relaxation in semiconductor quantum-dot lasers. *Phys. Rev. B*, **69**, 235314.

[76] Fleischhaker, R. (2005) *Origin of Squeezing in Optically Excited Semiconductor Systems*. Master's thesis, Philipps-University Marburg.

[77] Kira, M. and Koch, S. W. (2006) Quantum-optical spectroscopy of semiconductors. *Phys. Rev. A*, **73**, 013813.

*Bibliography*

[78] Schneebeli, L., Kira, M., and Koch, S. W. (2009) Microscopic theory of squeezed-light emission in strong-coupling semiconductor quantum-dot systems. *Phys. Rev. A*, **80**, 033843.

[79] Schneebeli, L. (2006) *Jaynes-Cummings Ladder in Quantum-Dot Microcavities*. Master's thesis, Philipps-University Marburg.

[80] Kira, M. and Koch, S. W. (2009) Quantum-optical spectroscopy. *Proceedings of the International Workshop NOEKS-9*, vol. 6, pp. 385–388, Phys. Status Solidi C.

[81] Gies, C., Wiersig, J., Lorke, M., and Jahnke, F. (2007) Semiconductor model for quantum-dot-based microcavity lasers. *Phys. Rev. A*, **75**, 013803.

# Wissenschaftlicher Werdegang

| | |
|---|---|
| Name | Lukas Schneebeli |
| Geburtsdatum | 18. März 1982 |
| Geburtsort | Marburg (Wehrda) |
| | |
| 06/2001 | Erlangung der Allgemeinen Hochschulreife an der Wilhelm-von-Oranien Schule Dillenburg (WVO) |
| 09/2001 bis 09/2006 | Studium der Physik (Diplomstudiengang) an der Philipps-Universität Marburg |
| 10/2003 | Diplom-Vorprüfung in Physik mit Nebenfach Informatik |
| 01/2006 bis 09/2006 | Diplomarbeit zum Thema "Jaynes-Cummings Ladder in Quantum-Dot Microcavities" bei Prof. Dr. Mackillo Kira und Prof. Dr. Stephan W. Koch in der Arbeitsgruppe "Theoretische Halbleiterphysik" |
| 09/2006 | Diplomprüfung in Physik mit Nebenfach Mathematik |
| seit 11/2006 | wissenschaftlicher Mitarbeiter in der Arbeitsgruppe "Theoretische Halbleiterphysik", Philipps-Universität Marburg |